# Atomic Data: their role in interpreting observations of the solar corona / TR

Giulio Del Zanna

Senior Research Associate
DAMTP, CMS
University of Cambridge

Science & Technology Facilities Council



UNIVERSITY OF CAMBRIDGE

# Further readings

Spectroscopic diagnostics (X-rays, EUV):

- Living Review in Solar Physics (Del Zanna & Mason, 2018)
- CHIANTI user guide (Del Zanna+)
- More advanced level: Part-III lectures (Del Zanna, in prep.)

- Phillips, Feldman, Landi, 2008, Ultraviolet and X-ray Spectroscopy of the Solar Atmosphere (Cambridge University press)
- Gabriel & Mason,1982, in Applied Atomic Collision Physics, Atmospheric Physics and Chemistry, Massey, Bates eds.
- Dere & Mason, 1981,in Solar Active Regions: A Monograph from Skylab Solar Workshop III, eds. F. Q. Orrall
- Mariska, 1992 (The solar transition region, Cambridge University Press)

- Mason & Monsignori Fossi, 1994, A&A Rev., 6, 123

- Del Zanna (PhD thesis, 1999)
- Del Zanna, Landini & Mason, 2002, A&A, 385,968
- Del Zanna & Mason, The Sun as a star, Springer 2012

# Solar corona

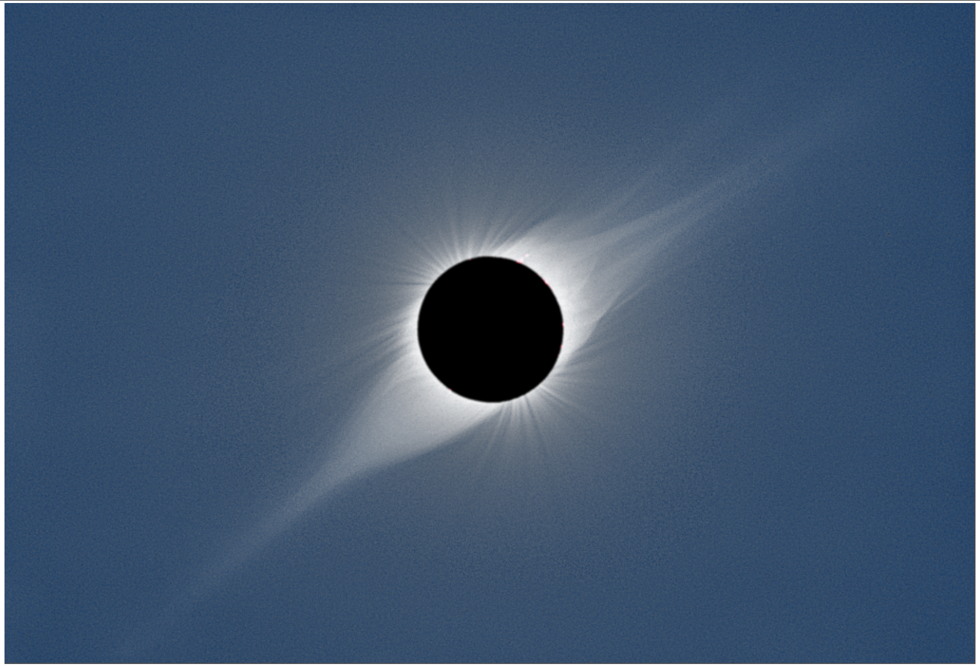

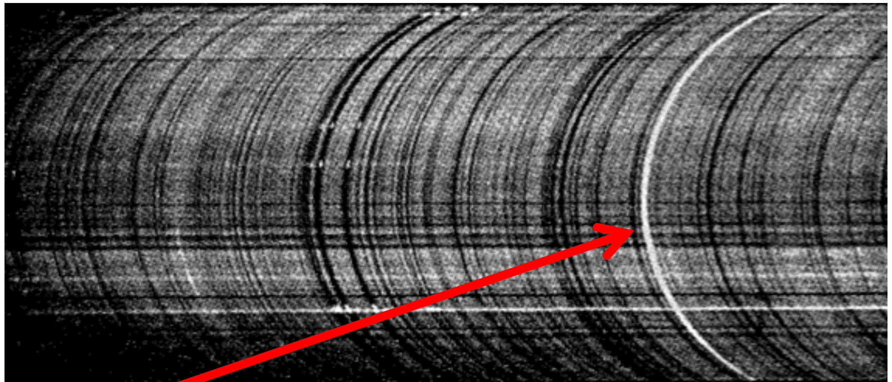

Spectrum of the solar corona from Lyot

'Coronium' green emission line first observed in 1869 by Young and Harkness at 5303 A. Red line observed later at 6374.6 A

# Fe X

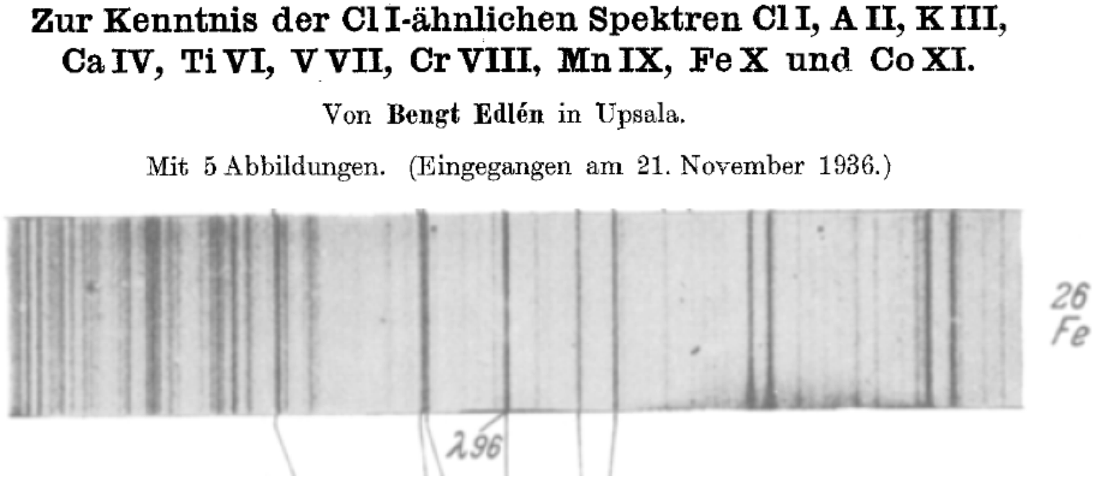
Zur Kenntnis der Cl I-ähnlichen Spektren Cl I, A II, K III, Ca IV, Ti VI, V VII, Cr VIII, Mn IX, Fe X und Co XI.

Von Bengt Edlén in Upsala.

Mit 5 Abbildungen. (Eingegangen am 21. November 1936.)



Grotrian (1939) suggested that the red line was due to Fe X, based on Edlen X-ray work.

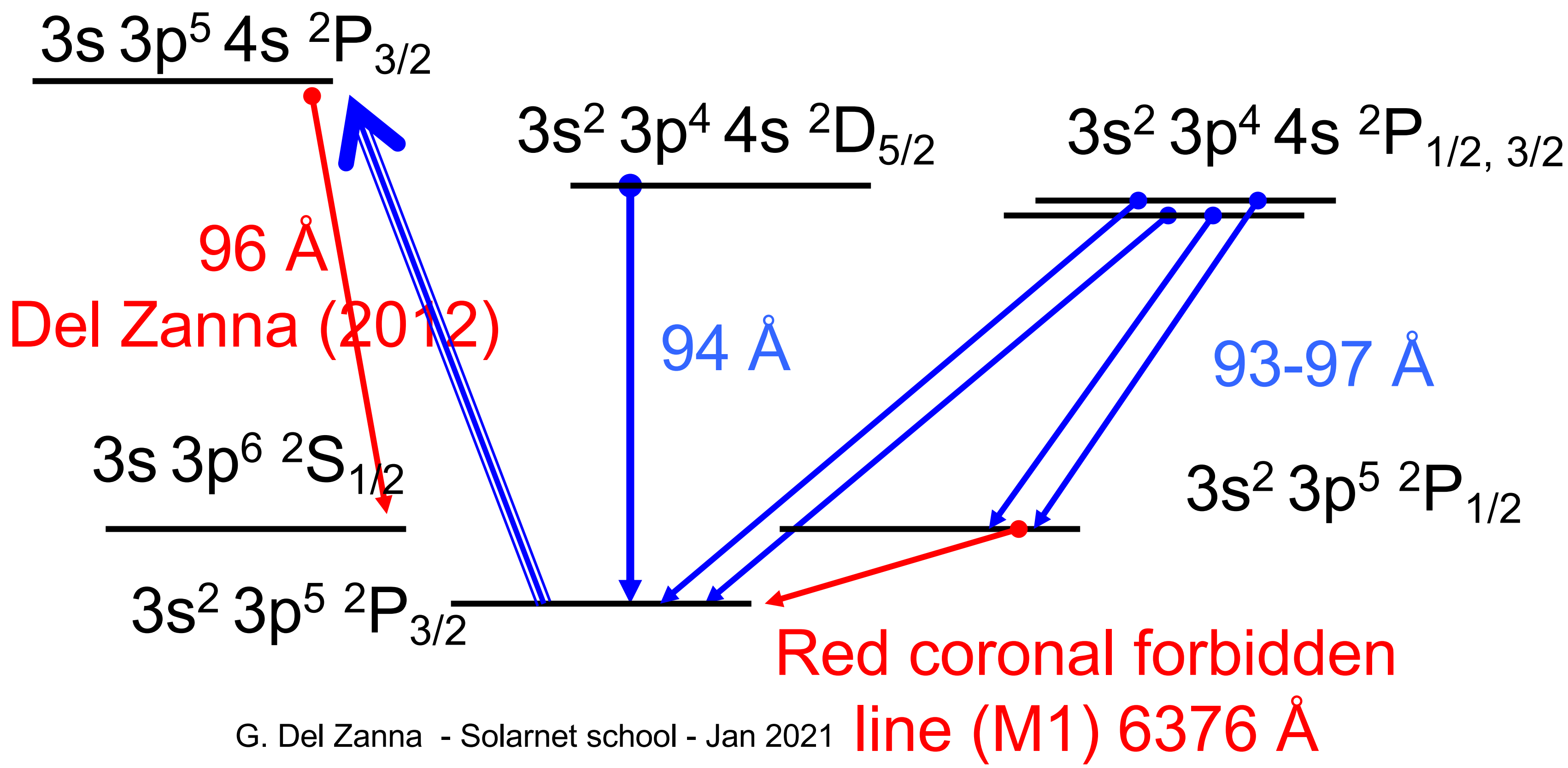

# Solar corona in the EUV

1958: First EUV spectra of the Sun (Violett & Rense) using rockets. First identifications only in 1965

comparison of fusion machines (ZETA) with solar spectra

Sun

ZETA

iron spark

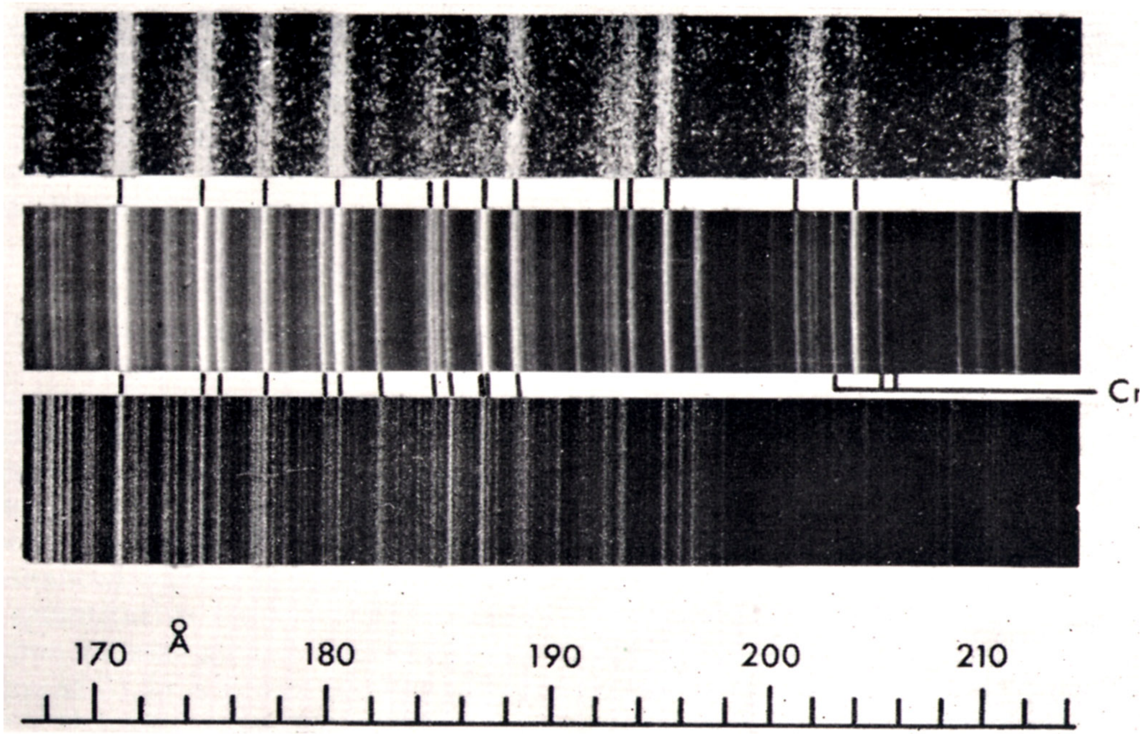


Brian Fawcett, Alan Gabriel and Carole Jordan (1965)

$3p^n - 3p^{n-1}3d$ transitions in Fe IX to Fe XIV

# Line identifications are still on-going..

See Del Zanna `benchmarking' papers

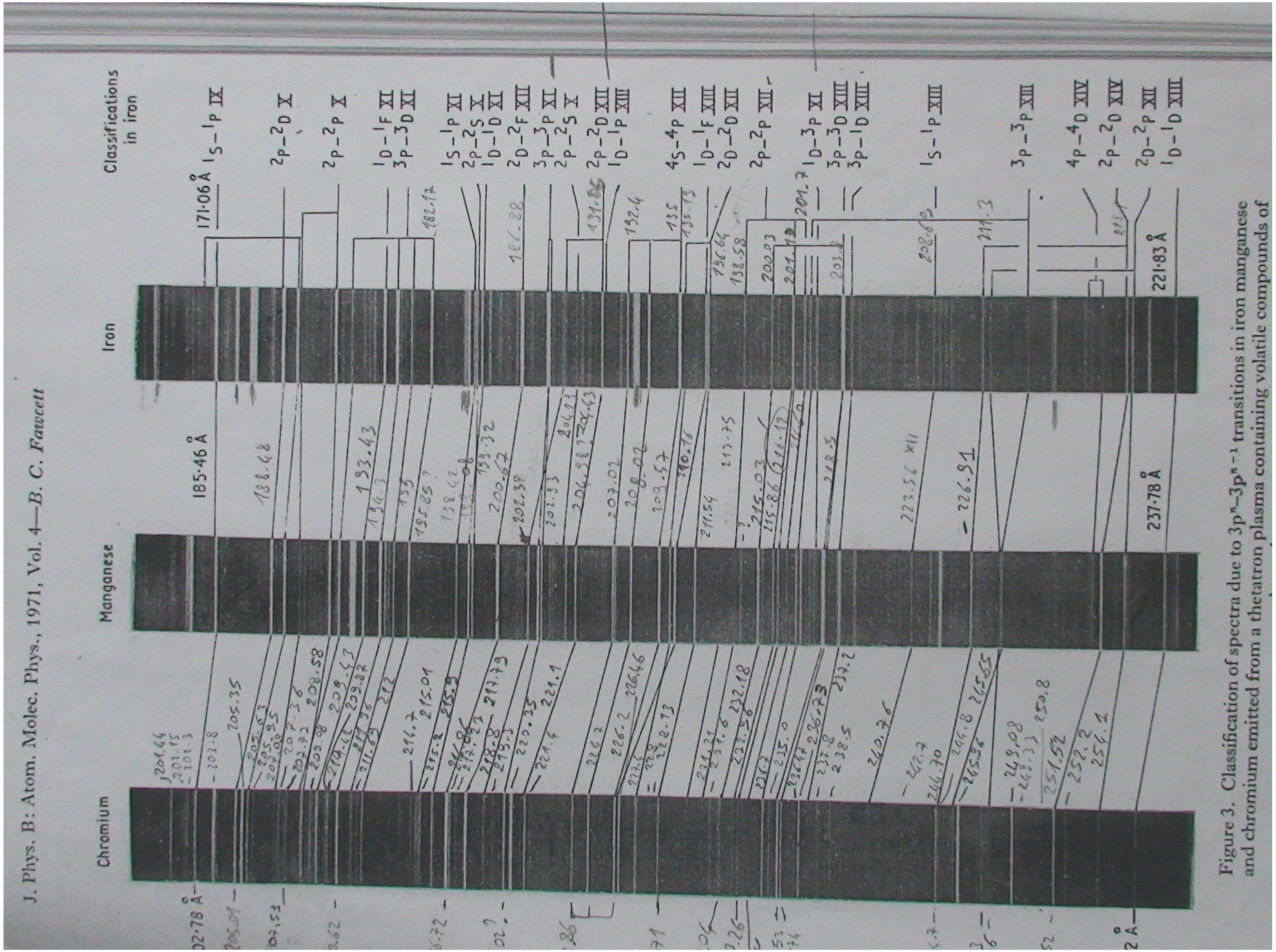

# The EUV

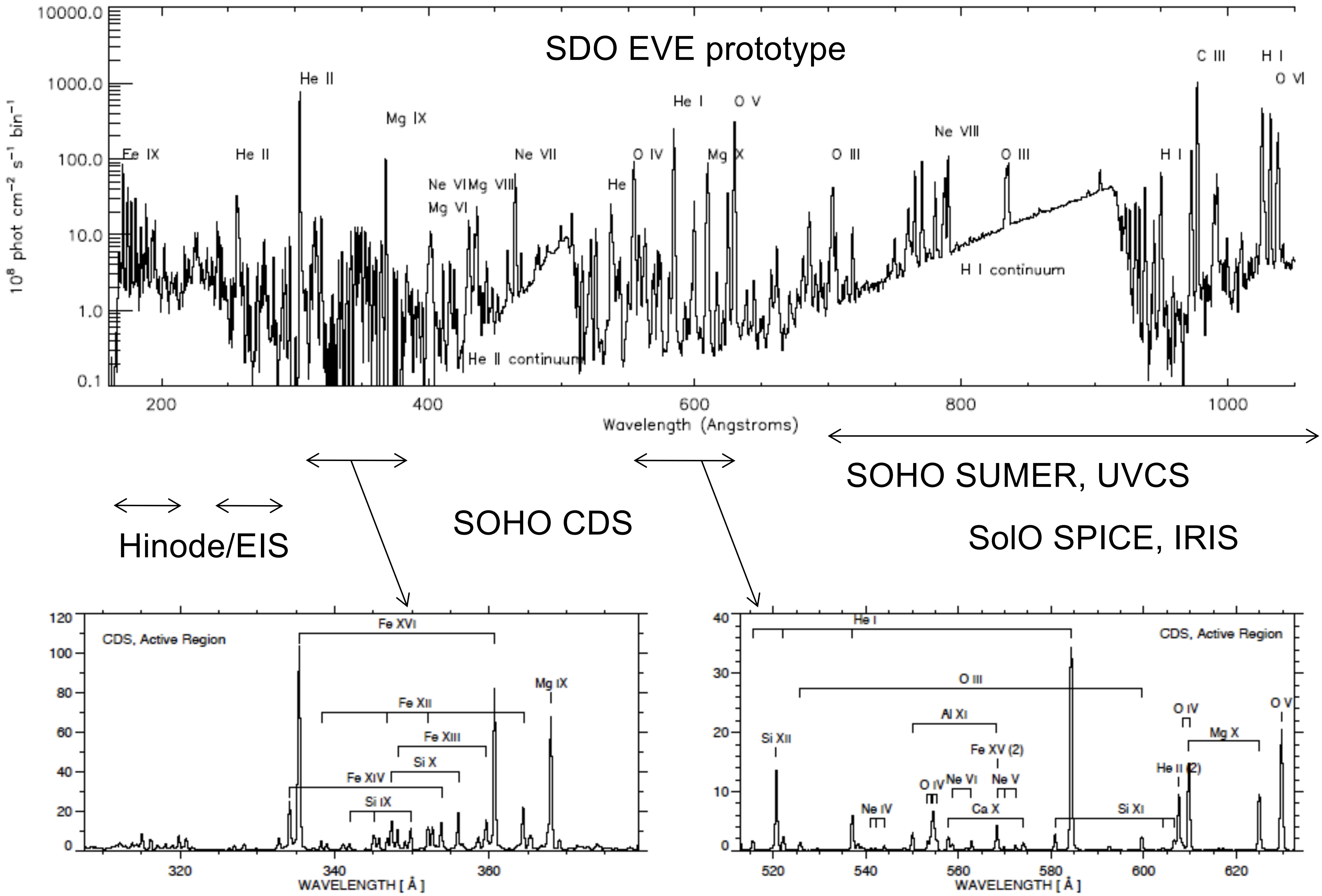
SDO EVE prototype
10000.0
1000.0
100.0
10.0
1.0
0.1
$10^8$ phot cm$^{-2}$ s$^{-1}$ bin$^{-1}$
Fe IX
He II
He II
Mg IX
Ne VI
Mg VI
Mg VIII
Ne VII
He II continuum
He
O IV
He I
Mg X
O V
O III
Ne VIII
O III
H I continuum
H I
C III
H I
O VI
200
400
600
800
1000
Wavelength (Angstroms)
SOHO SUMER, UVCS
SOHO CDS
SolO SPICE, IRIS
Hinode/EIS
CDS, Active Region
Fe XVI
Fe XII
Fe XIII
Si X
Fe XIV
Si IX
Mg IX
120
100
80
60
40
20
0
320
340
360
WAVELENGTH [ Å ]
CDS, Active Region
He I
O III
Al XI
Si XII
Fe XV (2)
O IV
Ne VI
Ne V
Ne IV
Ca X
Si XI
He II (2)
O IV
Mg X
O V
40
30
20
10
0
520
540
560
580
600
620
WAVELENGTH [ Å ]

# IRIS FUV2: TR Lines

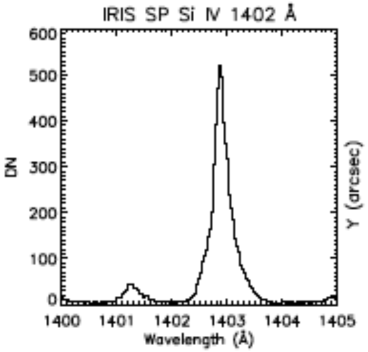


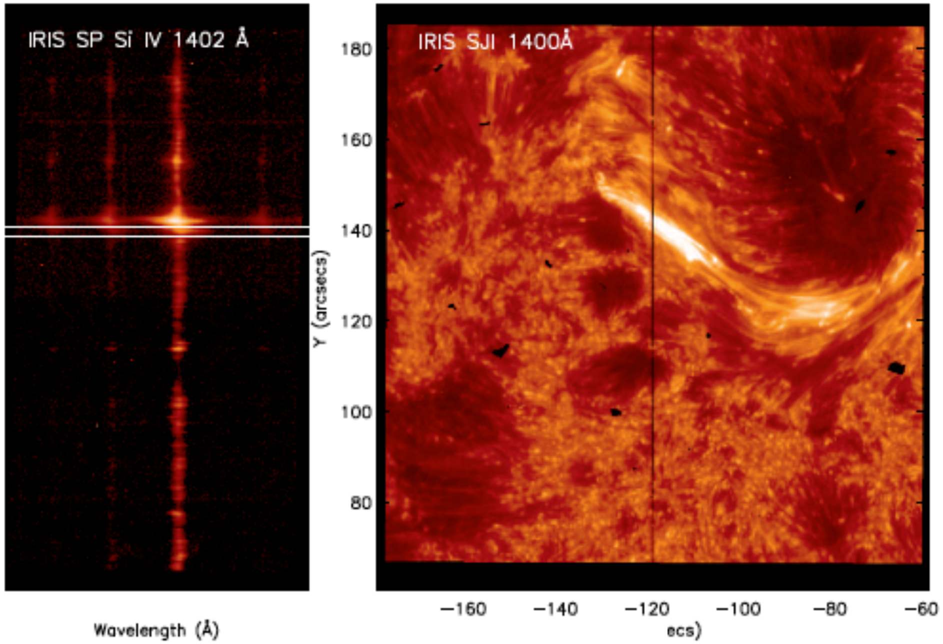


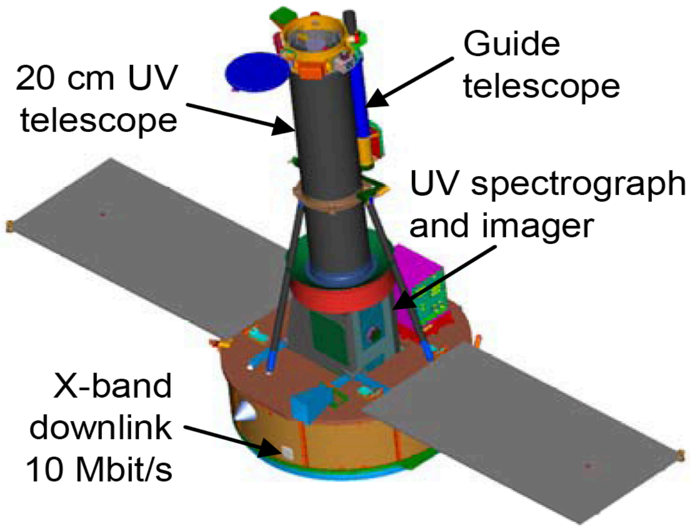


Also in the FUV1 C I, O I, C II formed in the photosphere / chromosphere

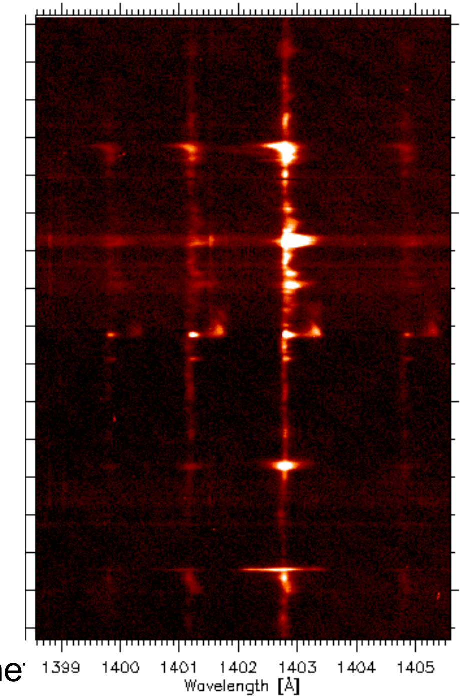


| ion | $\lambda$ [A] | transition | levels |
|---|---|---|---|
| Si IV | 1393.76 | $3s\ ^2S_{1/2} - 3p\ ^2P_{3/2}$ | $1-3$ |
| Si IV | 1402.77 | $3s\ ^2S_{1/2} - 3p\ ^2P_{1/2}$ | $1-2$ |
| O IV | 1397.20 | $2s^22p\ ^2P_{1/2} - 2s2p^2\ ^4P_{3/2}$ | $1-4$ |
| O IV | 1399.77 | $2s^22p\ ^2P_{1/2} - 2s2p^2\ ^4P_{1/2}$ | $1-3$ |
| O IV | 1401.16 | $2s^22p\ ^2P_{3/2} - 2s2p^2\ ^4P_{5/2}$ | $2-5$ |
| O IV | 1404.78 | $2s^22p\ ^2P_{3/2} - 2s2p^2\ ^4P_{3/2}$ | $2-4$ |
| S IV | 1398.04 | $3s^23p\ ^2P_{1/2} - 3s3p^2\ ^4P_{3/2}$ | $1-4$ |
| S IV | 1404.81 | $3s^23p\ ^2P_{1/2} - 3s3p^2\ ^4P_{1/2}$ | $1-3$ |
| S IV | 1406.02 | $3s^23p\ ^2P_{3/2} - 3s3p^2\ ^4P_{5/2}$ | $2-5$ |

# Solar Orbiter SPICE wavelengths

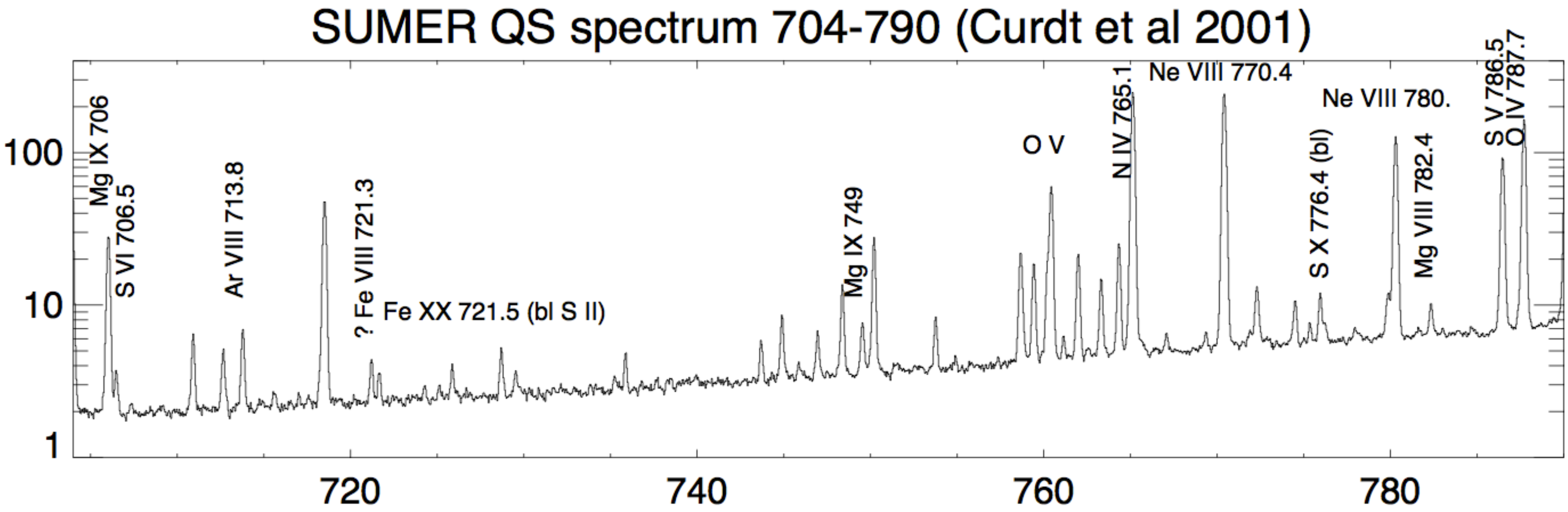


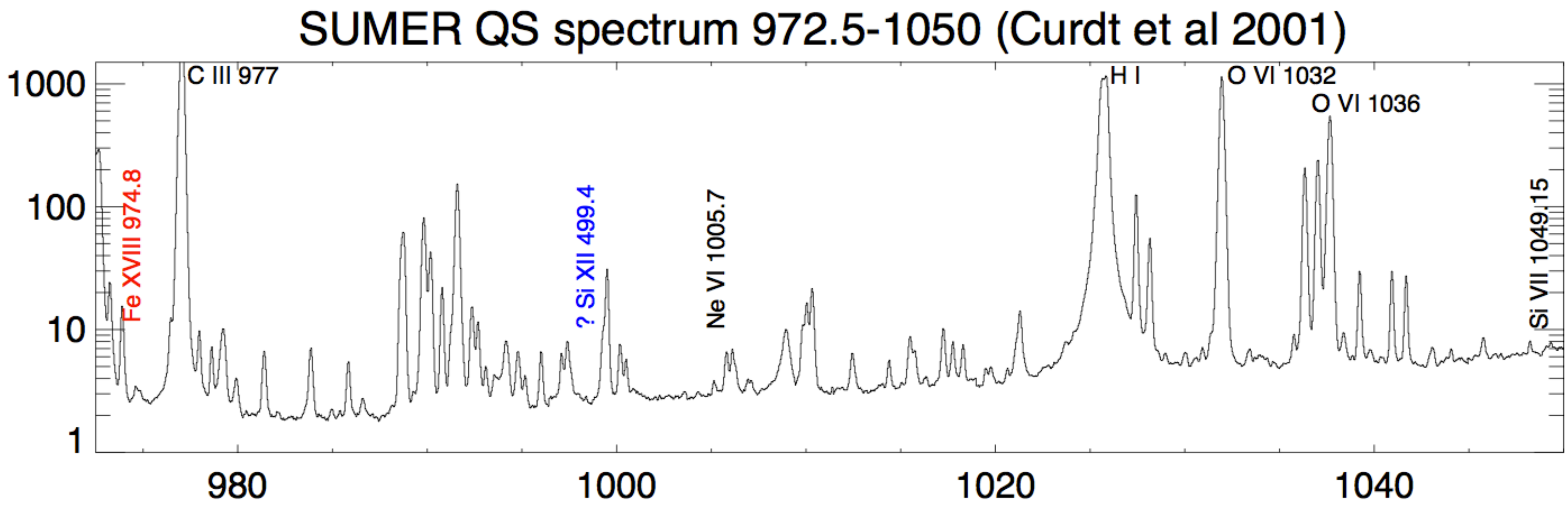

# SPICE data (first light)

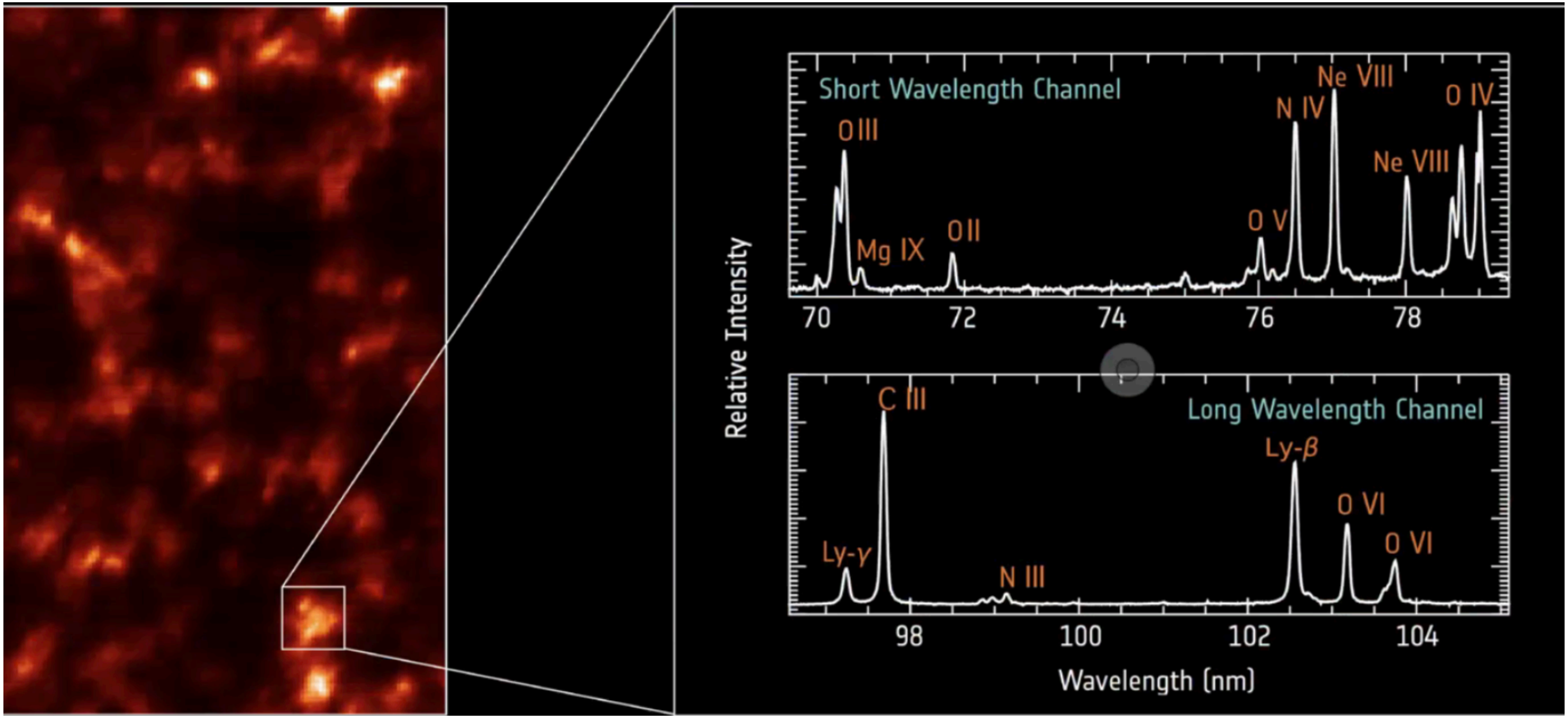

# Hinode EUV imaging spectrometer (EIS)

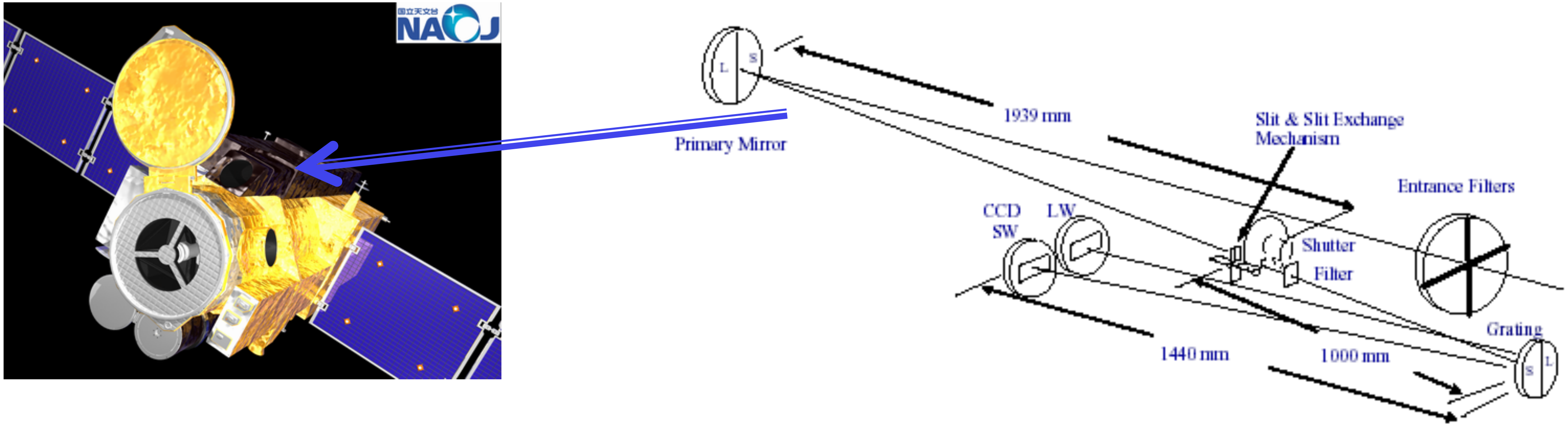


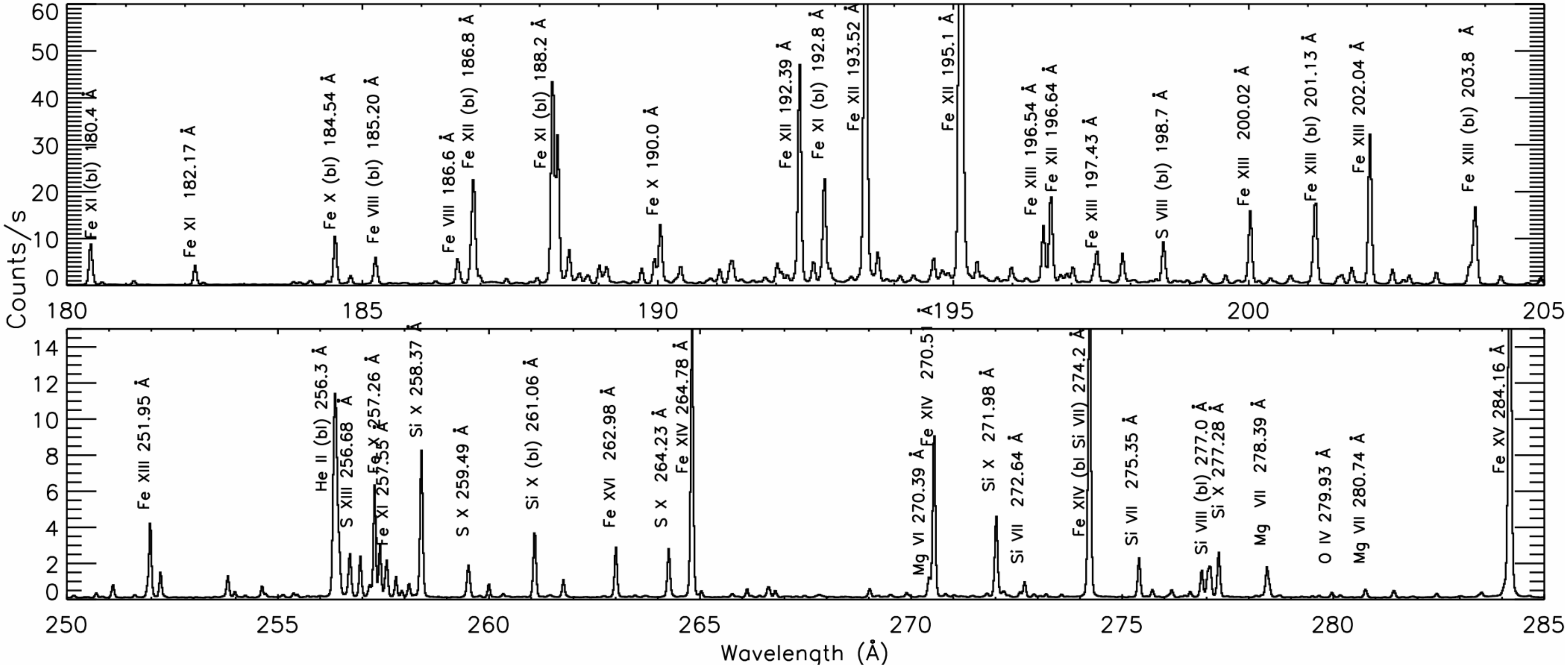

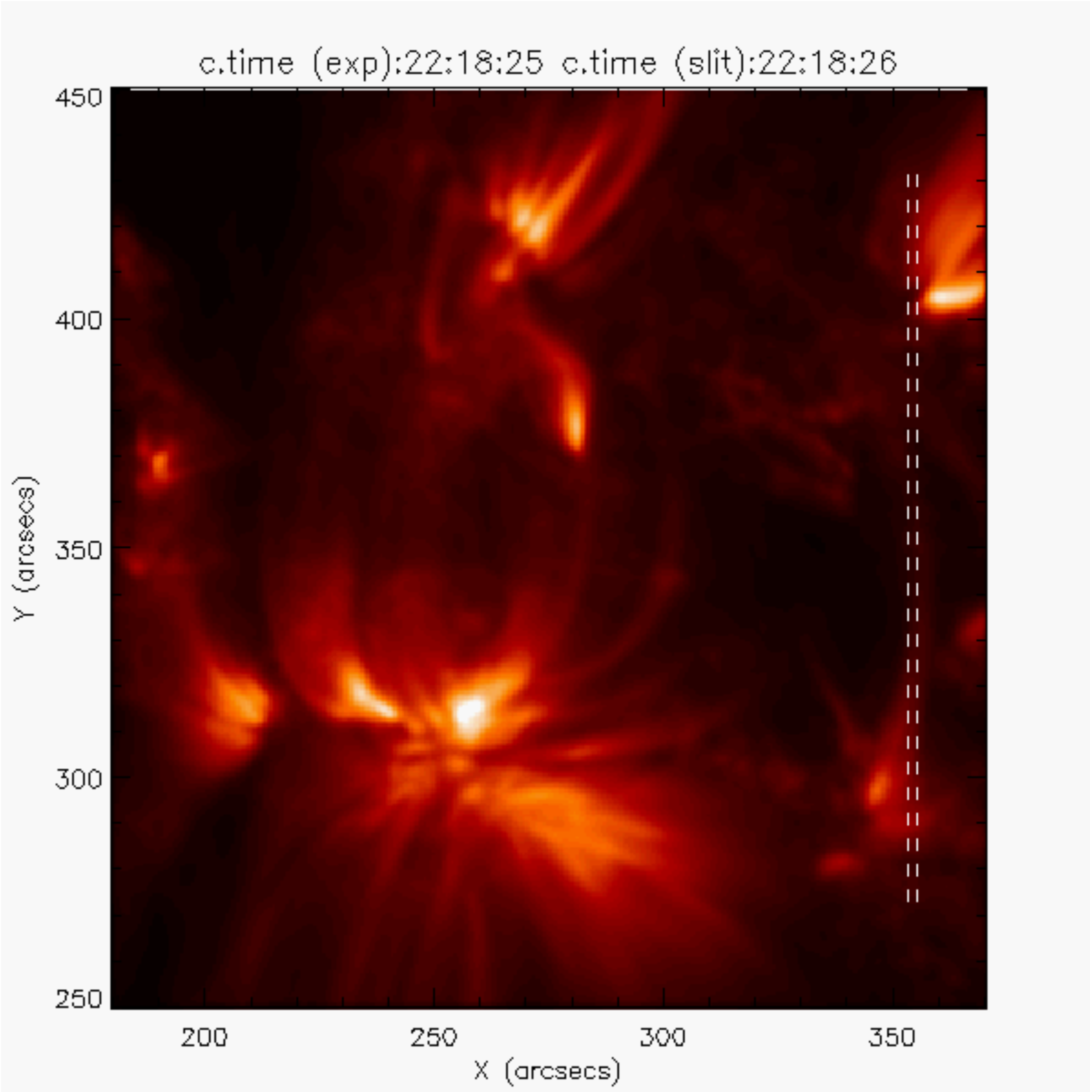


SDO/AIA vs. Hinode/EIS
Del Zanna et al. (2011)

# SDO AIA 193

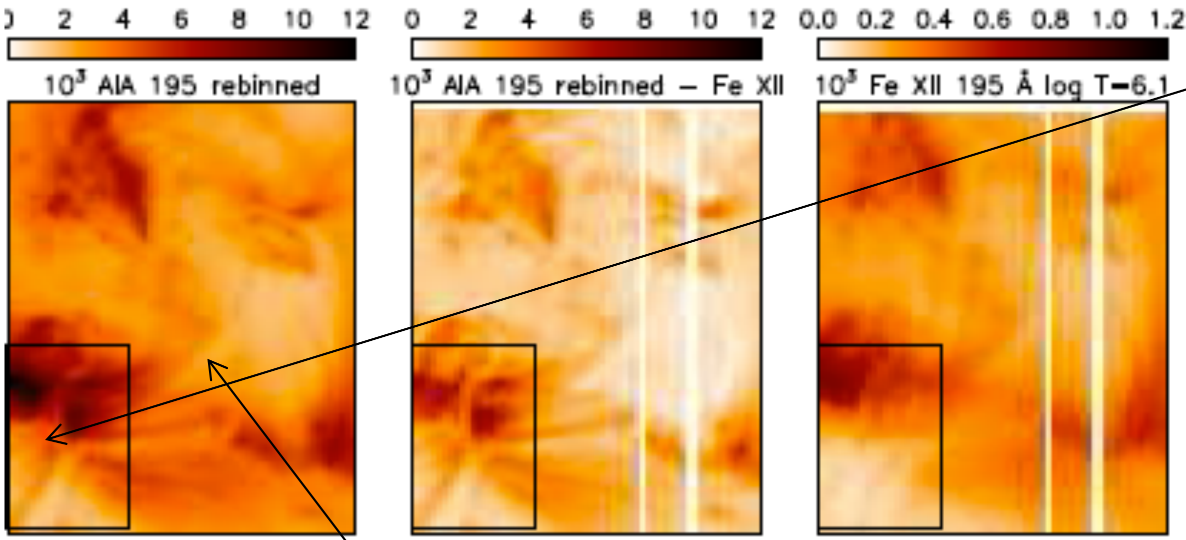

0 2 4 6 8 10 12
10³ AIA 195 rebinned
0 2 4 6 8 10 12
10³ AIA 195 rebinned – Fe XII
0.0 0.2 0.4 0.6 0.8 1.0 1.2
10³ Fe XII 195 Å log T=6.1


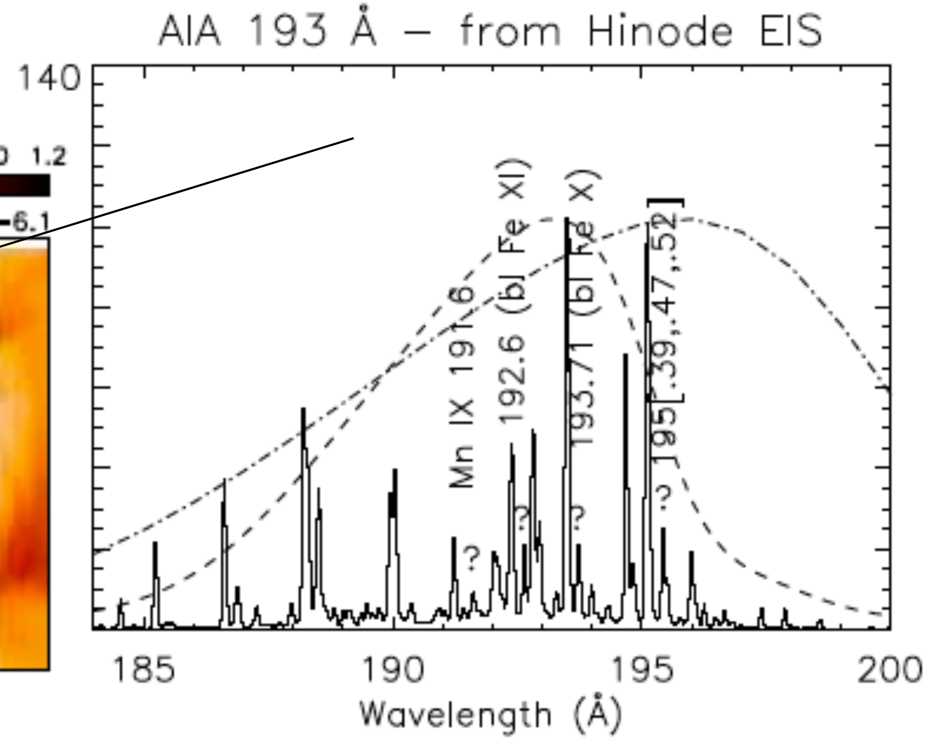

AIA 193 Å – from Hinode EIS
140
Mn IX 191.6
192.6 (bl Fe XI)
193.71 (bl Fe X)
195[.39,.47,.52]
?
185
190
195
200
Wavelength (Å)


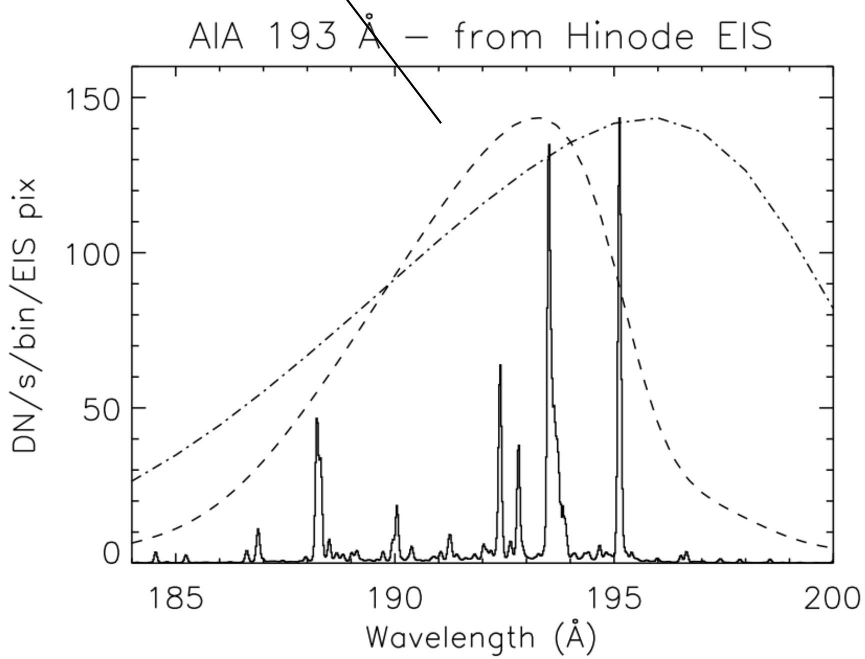

AIA 193 Å – from Hinode EIS
DN/s/bin/EIS pix
150
100
50
0
185
190
195
200
Wavelength (Å)


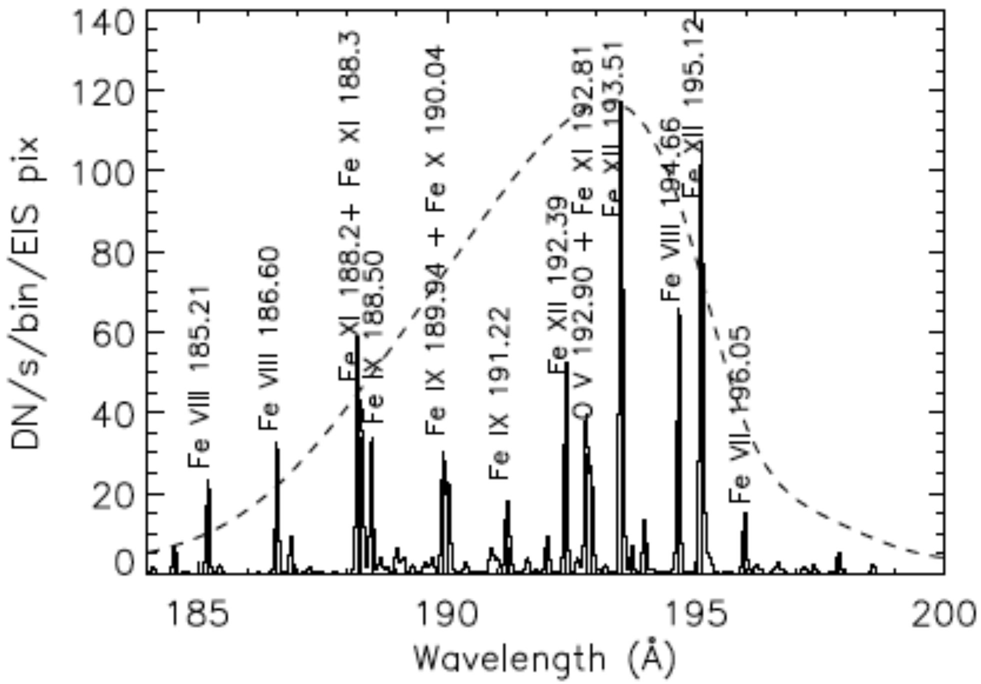

AIA 193 Å – from DEM
DN/s/bin/EIS pix
140
120
100
80
60
40
20
0
Fe VIII 185.21
Fe VIII 186.60
Fe XI 188.2+ Fe XI 188.3
Fe IX 188.50
Fe IX 189.94 + Fe X 190.04
Fe IX 191.22
Fe XII 192.39
O V 192.90 + Fe XI 192.81
Fe XII 193.51
Fe VIII 194.66
Fe XII 195.12
Fe VII 196.05
185
190
195
200
Wavelength (Å)

# AIA EUV 211 band

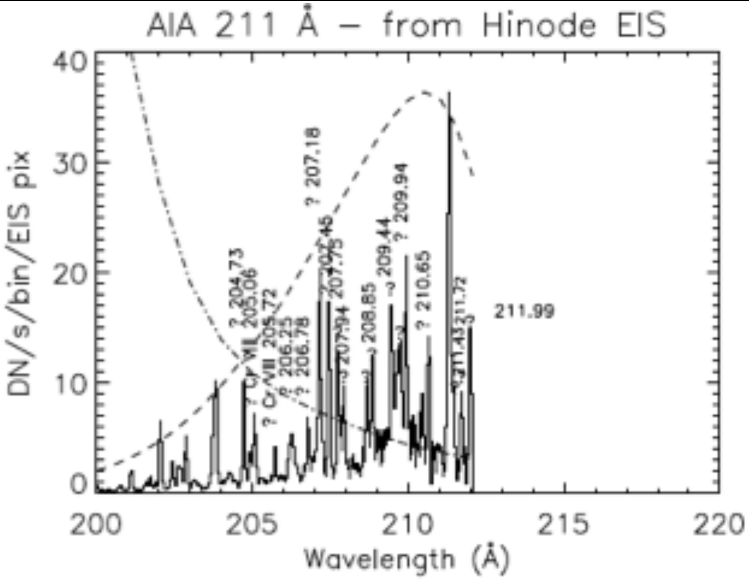


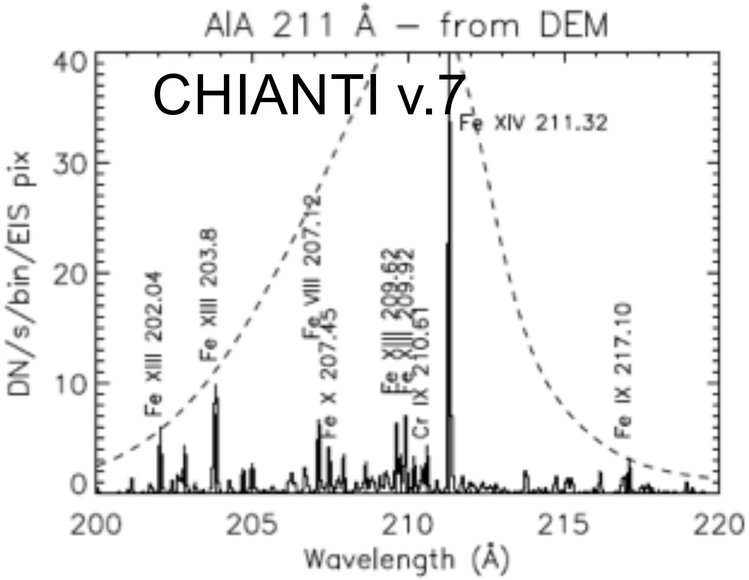


A lot of cool/unidentified lines in AIA bands (Del Zanna+2011).

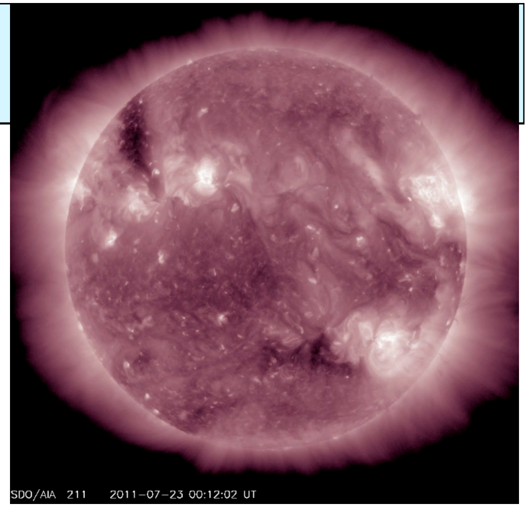


EBIT laboratory spectra showed many unidentified lines

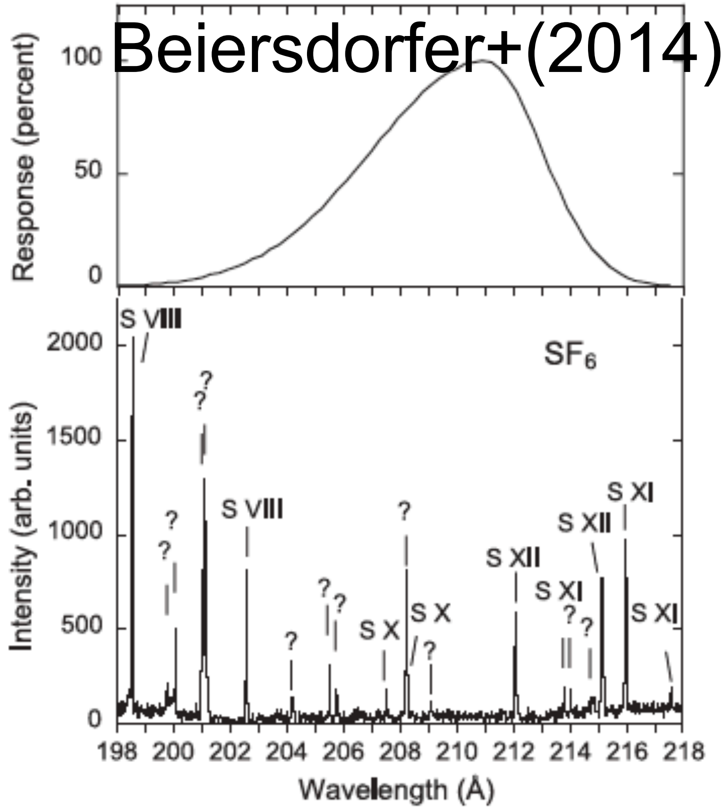


**Figure 3.** EUV spectrum of fluorine and sulfur produced by injecting $SF_6$ into the EBIT-I electron beam ion trap covering the spectral range λ198–λ218. The electron beam energy was 1000 eV, but the spectrum differs very little from observations at 600 eV. Identified spectral features are labeled by the corresponding spectrum. Unidentified features are labeled by a question mark. The response of the *SDO*/AIA λ211 channel is indicated on top.

# SDO AIA 94

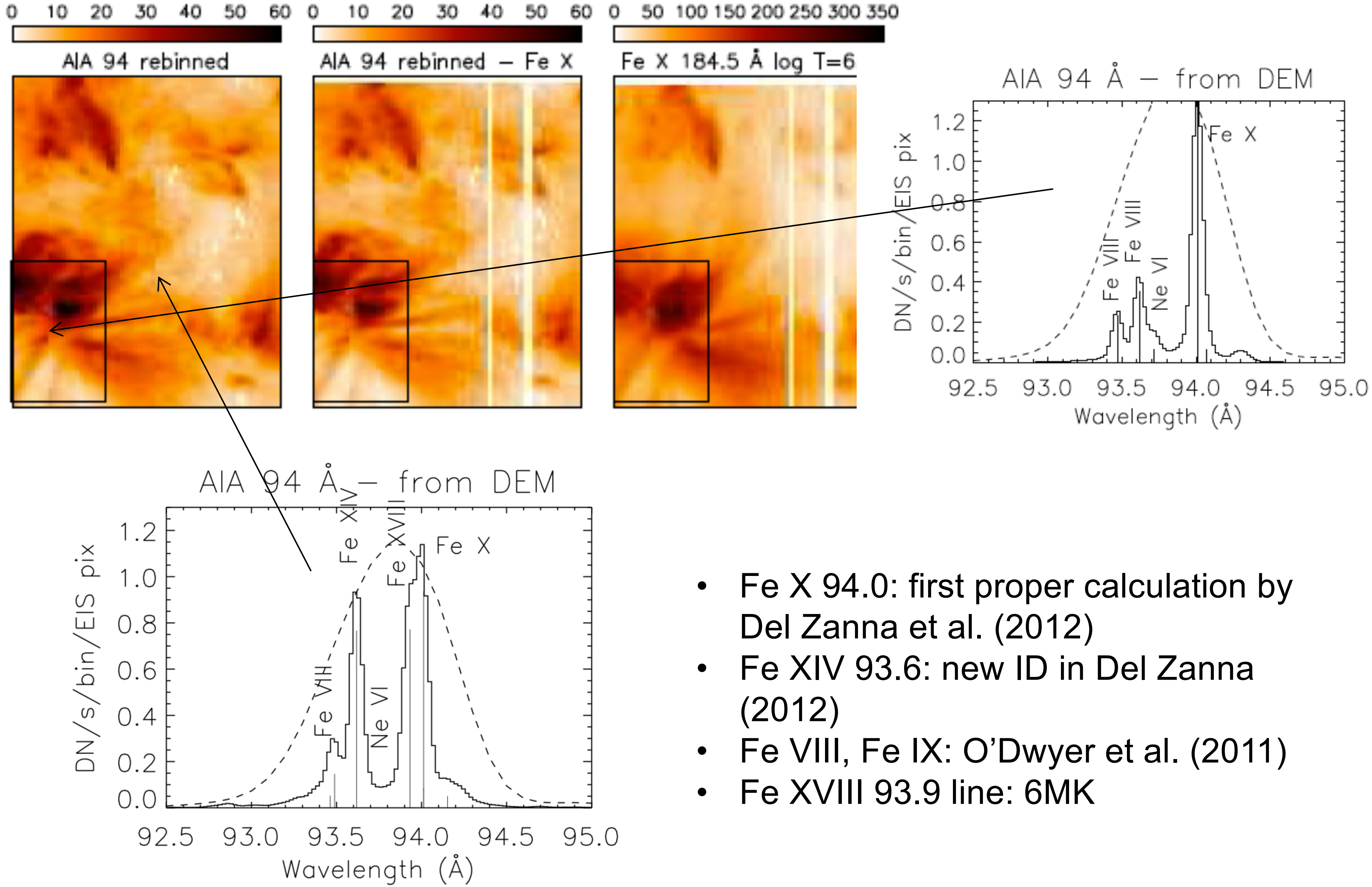


- Fe X 94.0: first proper calculation by Del Zanna et al. (2012)
- Fe XIV 93.6: new ID in Del Zanna (2012)
- Fe VIII, Fe IX: O'Dwyer et al. (2011)
- Fe XVIII 93.9 line: 6MK

# CHIANTI AIA responses (v.9)

```
AIA_RESP= ch_aia_resp( '20100522', pressure=1e15, $
abund_name=!xuvtop+'/abundance/sun_coronal_1992_feldman_ext.abund',$
ioneq_name= !xuvtop+'/ioneq/chianti.ioneq',/verbose )
```

- Bands are multi-thermal.
- Off-band contribution
- Degradation of the bands difficult to assess.
- Responses depend on chemical abundances

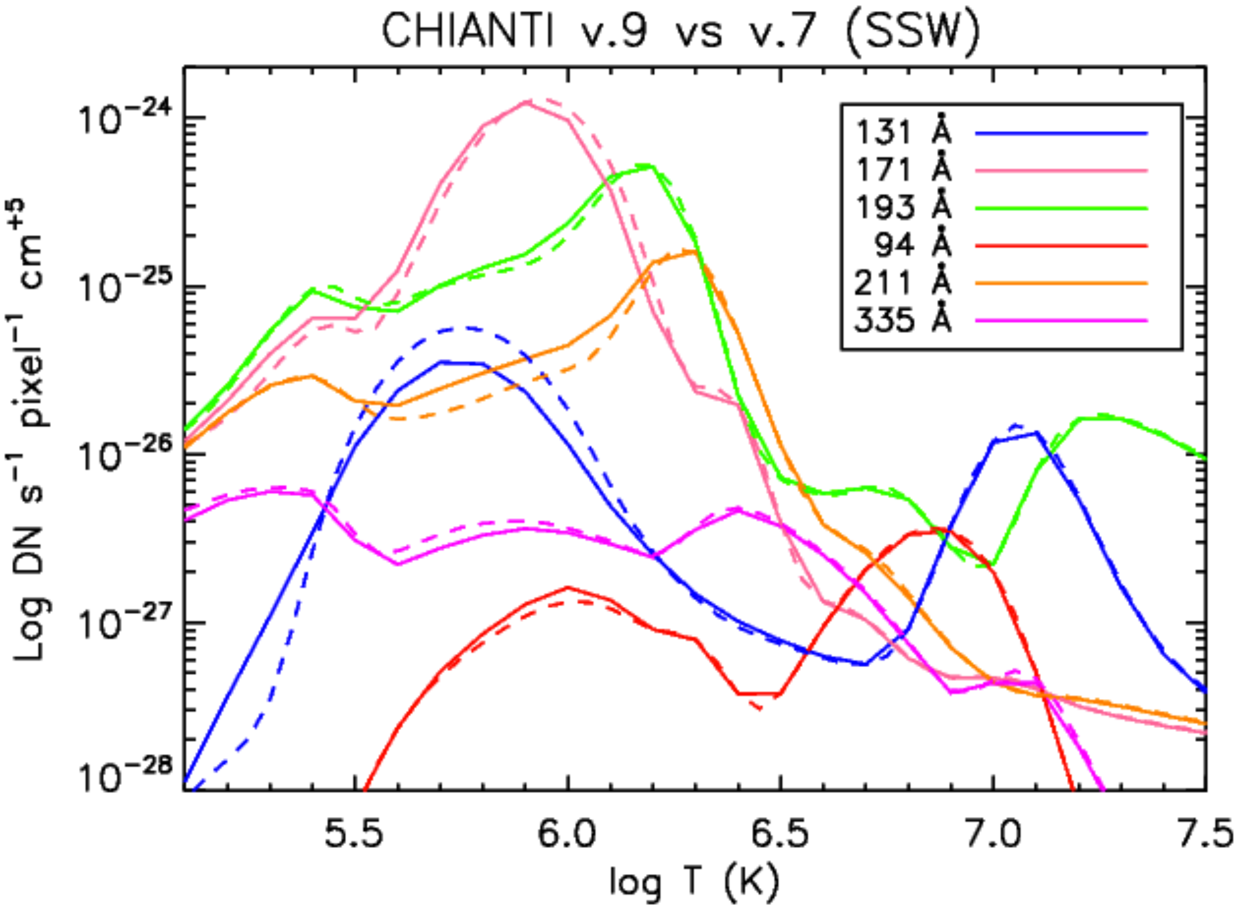

- High-resolution line spectroscopy is featuring in many future missions and proposals.
- Main instrument is EUVST.

# DKIST

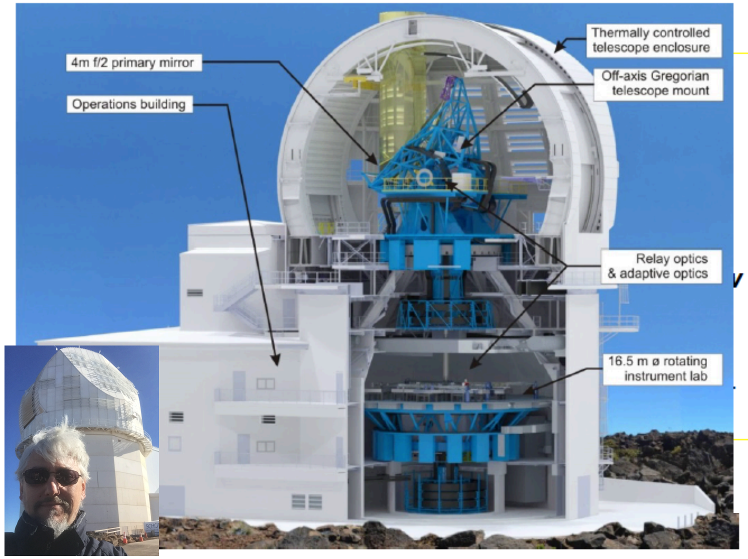


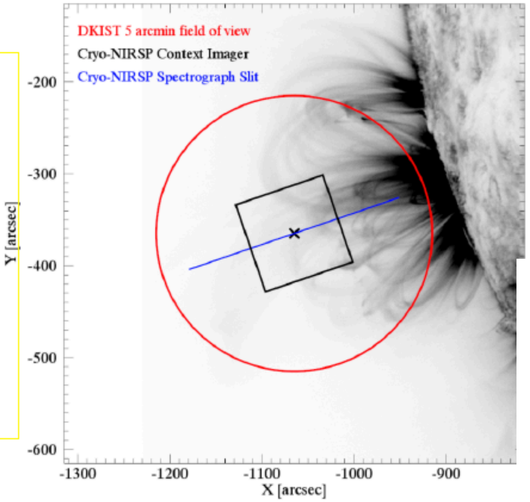


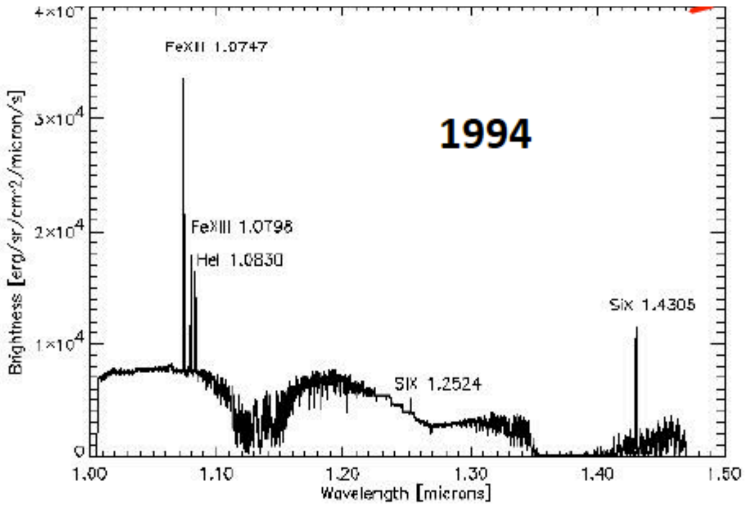


***Cryo-NIRSP Spectropolar.***

Fe XIII λ10747 ; Log(T) ~ 6.22
Fe XIII λ10797 ; Log(T) ~ 6.22
He I λ10830 ; Log(T) ~ 4*
Si X λ14300 ; Log(T) ~ 6.13
Si IX λ39350 ; Log(T) ~ 6.04

***Cryo-NIRSP Context Imager***

Fe XIII λ10747 ; Log(T) ~ 6.22
He I λ10830 ; Log(T) ~ 4*
Si IX λ39340 ; Log(T) ~ 6.04

DKIST Cryo-NIRSP will measure up to 1.5 Rsun:

1. coronal Ne (Fe XIII ratio and others),
2. non-thermal widths
3. Te (approx)
4. coronal B
5. in the future chemical abundances in coronal 1-3 MK plasma (Del Zanna & DeLuca 2018).



Images from Tom Schad

# Aditya VELC

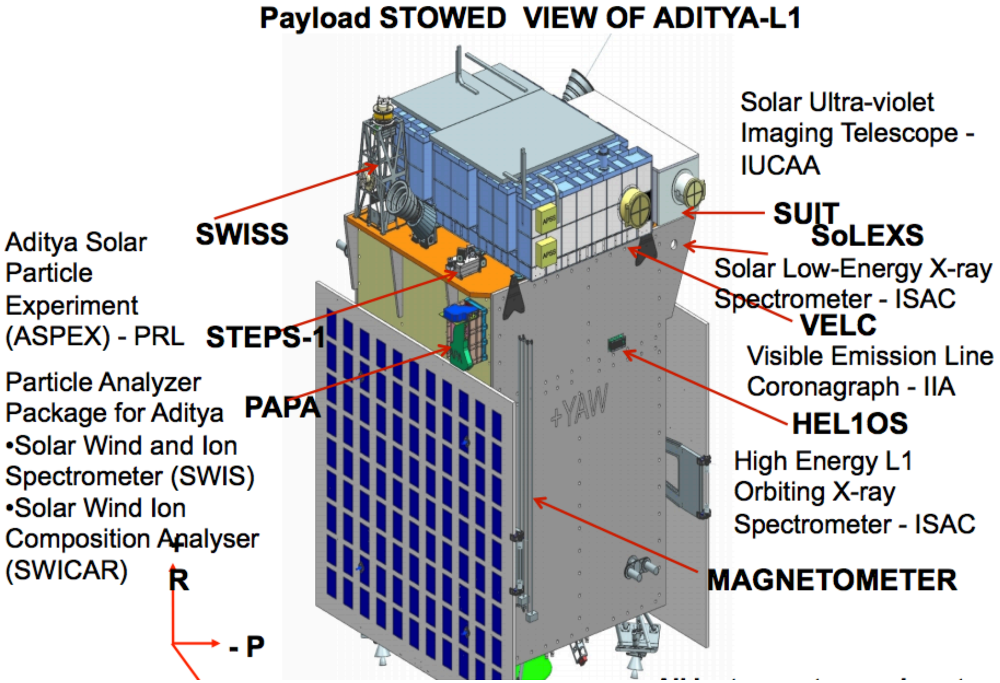


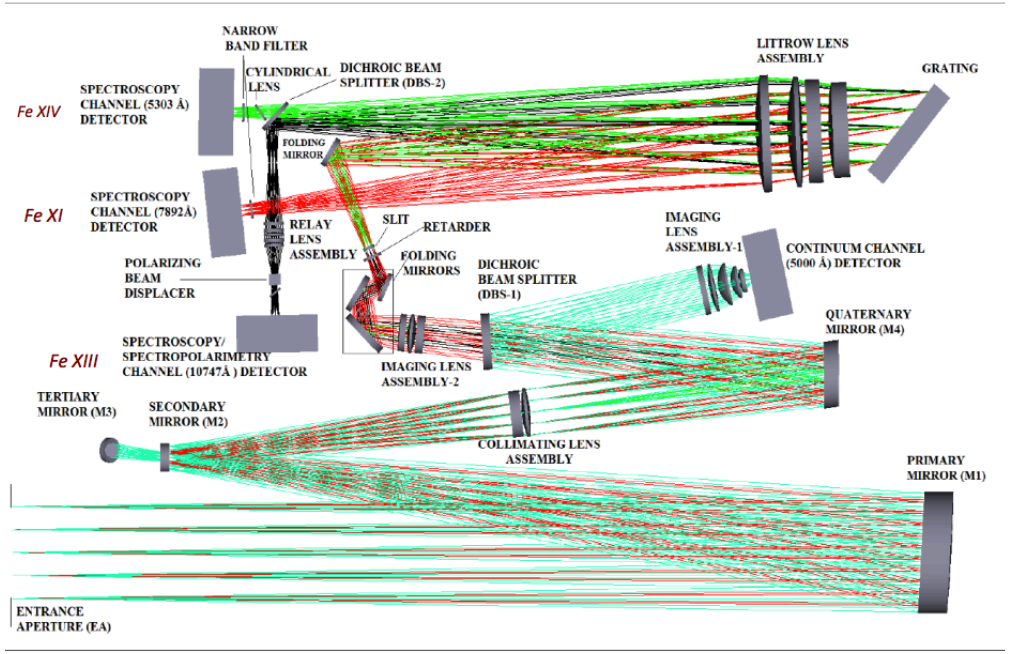


Spectroscopic mode !
FOV: 1.05 – 1.5 Ro (3 Ro imaging)
Spatial resolution: 5”
Cadence:1-5s
Fe XIV (green), Fe XI (7892 A),
Fe XIII (NIR), WL continuum
Spectropolarimetry in Fe XIII
→ **magnetic field**

Images: D.Banerjee

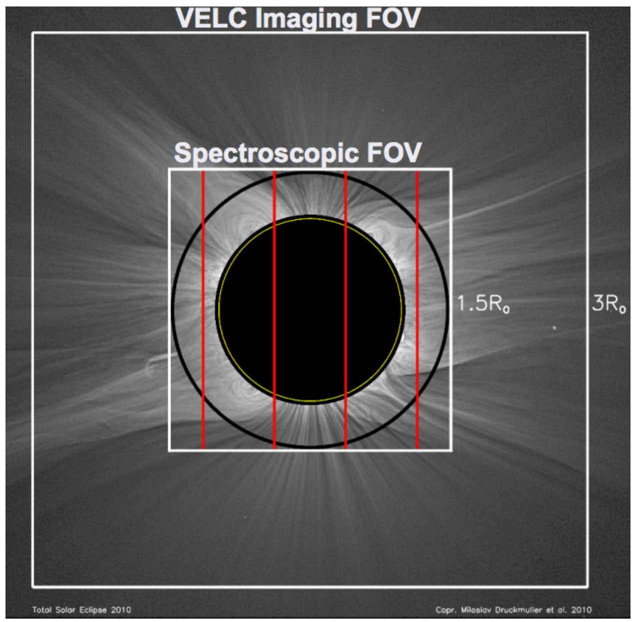

# Level designation

- Electrons occupy *nl* orbitals
- L = orbital angular momentum, represented by a letter: S=0, P=1, D=2, F=3 …
- S = spin angular momentum
- J = total angular momentum
- S and J take values 0, 1/2, 1, 3/2, 2, …
- Notation is $^{2S+1}L_J$
- E.g., for Fe XII, the ground configuration is

$[1s^2\ 2s^2\ 2p^6\ ]\ 3s^2\ 3p^3$

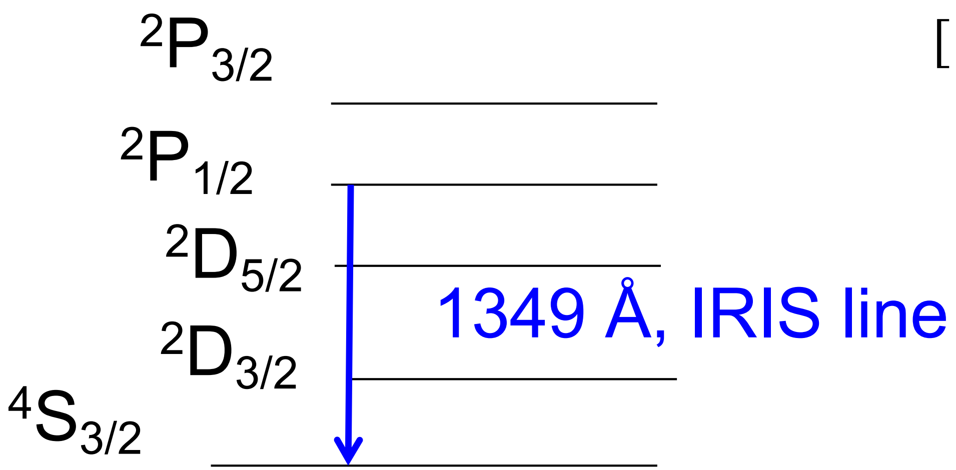

# Line emission

- Number of photons = $N_j\, A_{ji}$
- $A_{ji}$ is Einstein's probability for spontaneous decay
- $N_j$ fraction of ions in the state $j$
- Two main types
  - *forbidden* ($A_{ji} < 10^3$ s$^{-1}$)
  - *allowed* ($A_{ji} > 10^5$ s$^{-1}$)
- $\Delta$J=0, ±1 and $\Delta$ L=0, ±1
- $\Delta$S=1 intercombination have smaller $A_{ji}$
- All transitions *within* a configuration are forbidden
- If a level has no allowed transitions then it is *metastable*

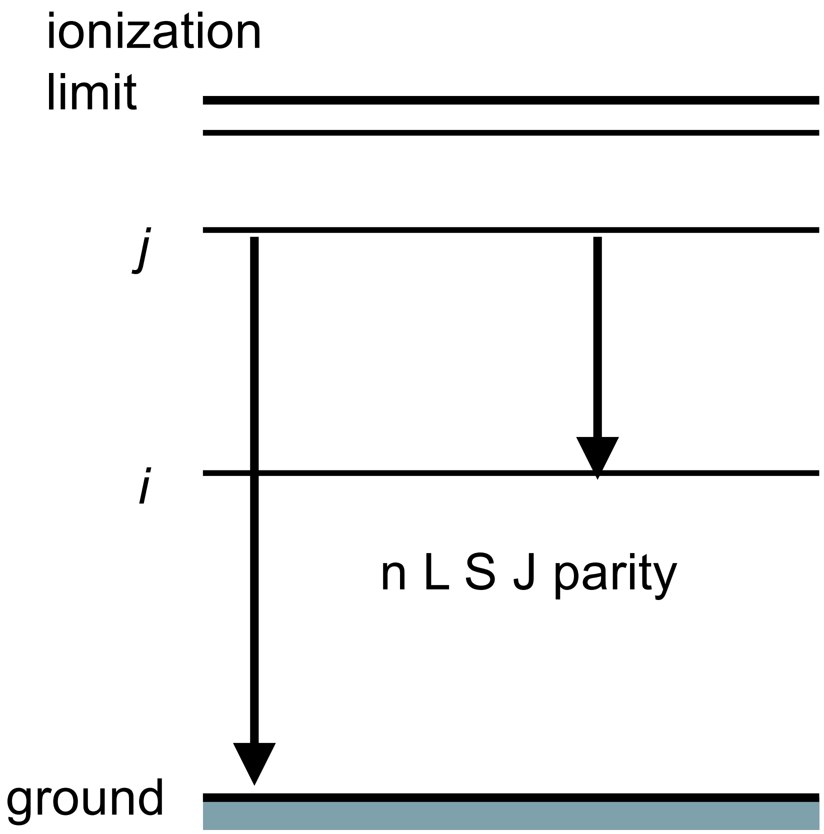

# Ionization vs. excitation

Ionizations/recombinations occur on timescales of 1-100s
Dipole-allowed lines decay in ~$10^{-10}$ s. Forbidden ones in $10^{-4}$ s or longer

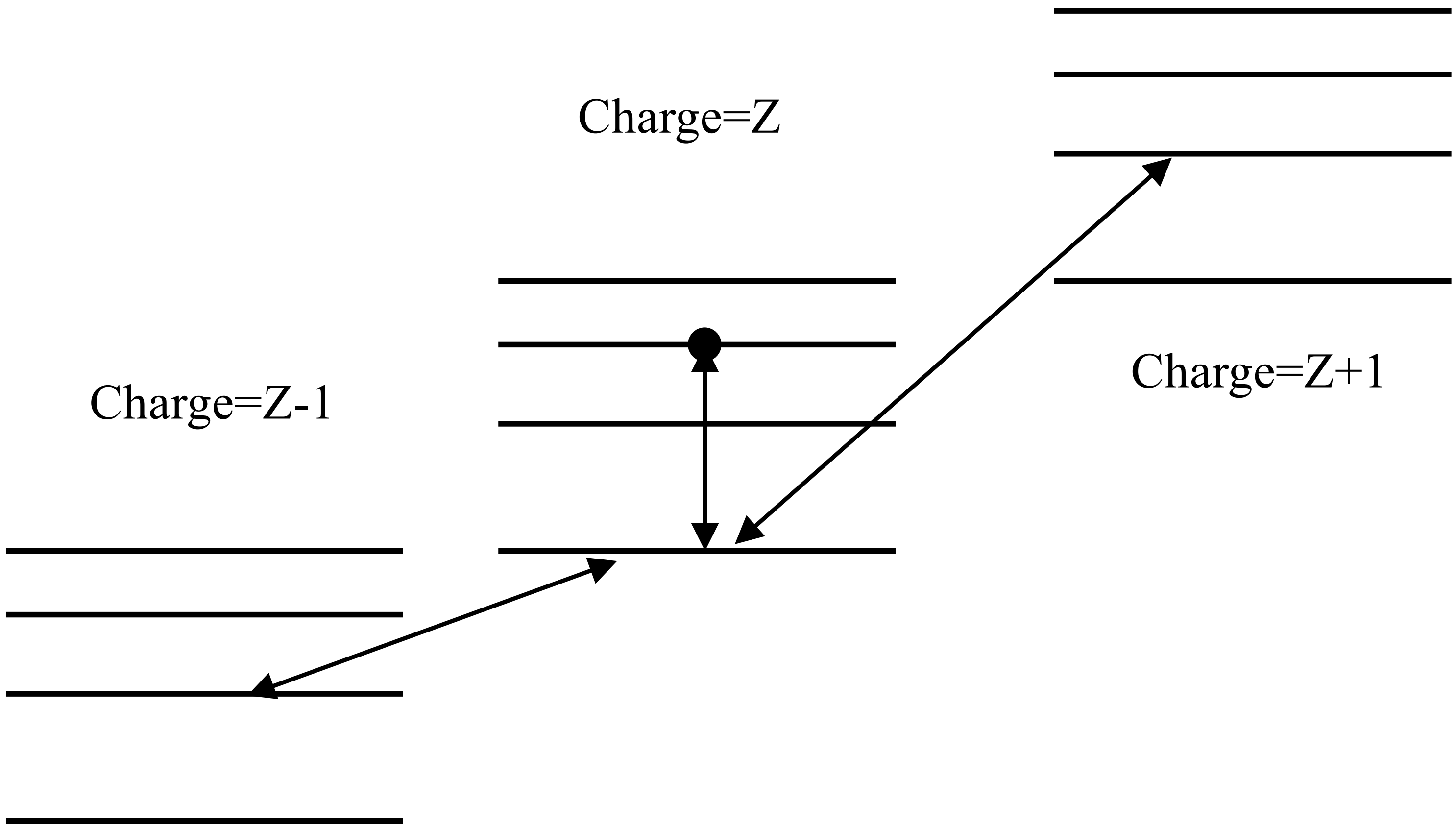


Usual to treat separately excitation / ionization, but collisional-radiative models (CRM) are actually necessary in many cases.

Most codes calculate ion balance assuming population is all in ground states.

# Line intensities

In optically-thin plasmas line intensities are proportional to:

$$I \sim n_j \, A_{ji} = \frac{N_j(X^{+m})}{N(X^{+m})} \, A_{ji} \, \frac{N(X^{+m})}{N(X)} \, \frac{N(X)}{N(H)} \frac{N(H)}{N_e} \, N_e$$

A-value

Level population

(Ne,Te)

Ion abundance (Te, Ne)

El. abundance

The Hydrogen/electron density depends on the elemental abundances relative to H. For the solar corona, H, He are fully ionised and the ratio is about 0.8--0.9.

# CHIANTI population modelling before v.9

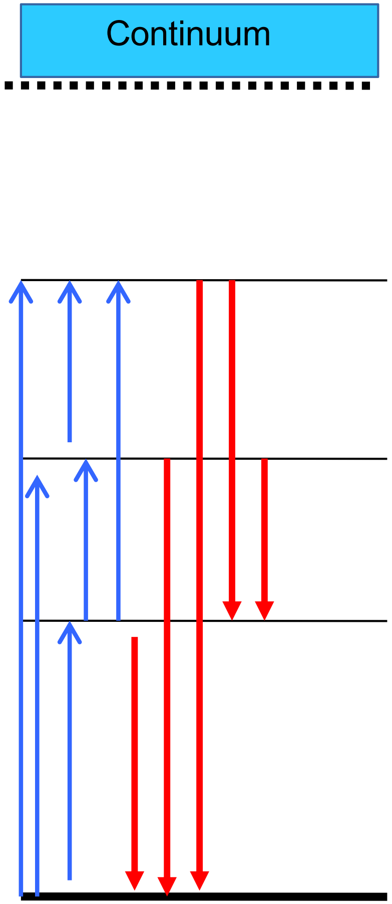


Collisional excitation (and de-excitation) by electron and proton impact

Radiative decay (spontaneous)

Photo-excitation (and de-excitation) by any radiation field can be added.

A single matrix is populated with all the rates and solved to get level population

# Contribution function

Spectral line intensity:

$$I(\lambda_{ij}) = \frac{h\nu_{ij}}{4\pi} \int N_j \; A_{ji} \; dh \; = \int Ab(X) C(T, \lambda_{ij}, N_e) N_e N_H dh \quad [\text{ergs cm}^{-2} \; \text{s}^{-1} \; \text{sr}^{-1}]$$

$$C(T, \lambda_{ij}, N_e) = \frac{h\nu_{ij}}{4\pi} \; \frac{A_{ji}}{N_e} \; \frac{N_j(X^{+m})}{N(X^{+m})} \; \frac{N(X^{+m})}{N(X)} \quad [\text{ergs cm}^{+3} \; \text{s}^{-1}]$$

Note that in the literature there are various definitions of contribution functions. Aside from having values in either photons or ergs, sometime the factor $\pi$ is not included. Sometimes a value of 0.83 for N(H)/N(e) is assumed and included. Sometimes the element abundance factor is also included.

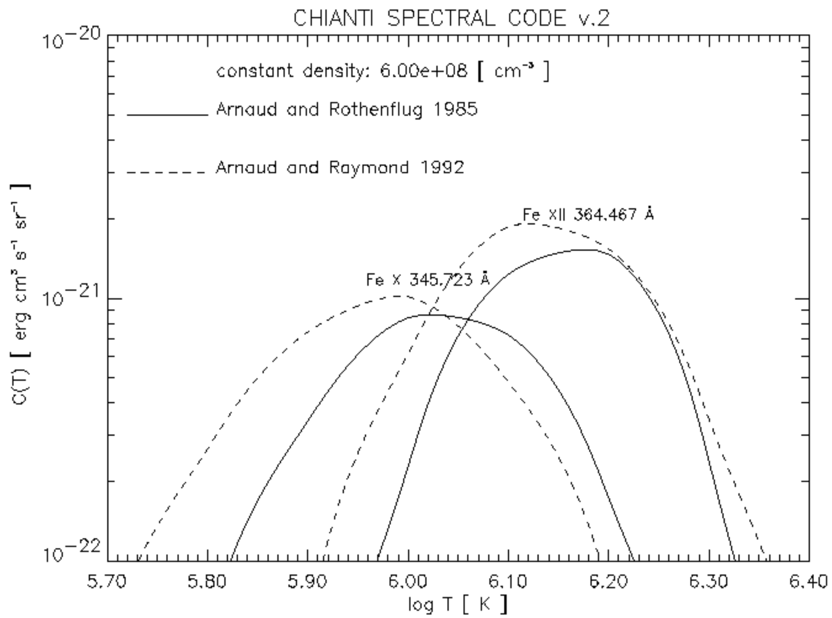

# Atomic data for astrophysics

**CALCULATION:**

UK **APAP Network** http://www.apap-network.org/
(STFC funded): main ion atomic data provider
for fusion and astrophysics (PI: Badnell, Strathclyde)

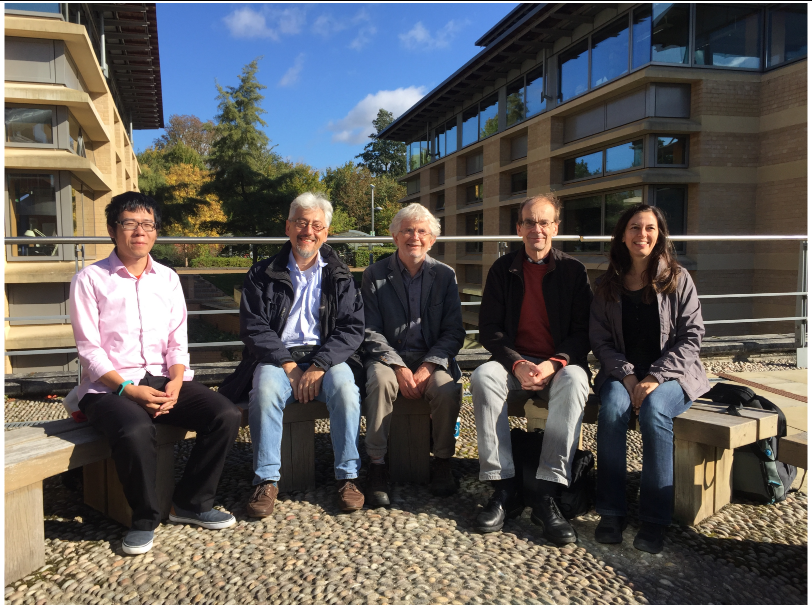

**BENCHMARK:**

EUV line identifications and benchmark

**DISTRIBUTION:**
**CHIANTI** (www.chiantidatabase.org)
**CHIANTI Google user group**

**IDL suite (stand-alone, SSW)**
**Chiantipy (Dere) in Python**
CHIANTI-VIP (Del Zanna) in Python

Latest version 10: Del Zanna+2021

# Atomic physics

Mike Seaton (UCL)
Alan Burgess (Cambridge)

Most theory and programs developed over a long period of time with significant contributions in the UK from UCL (Seaton's group),
QUB (e.g. Burke, Hibbert), Cambridge (Burgess),
and a few groups in Europe.

Atomic structure theory and codes received significant contributions from C. Froese Fisher and I. Grant (Oxford).

Atomic physics went out of fashion long ago and soon we will go back to the middle ages.

# Collisional excitation (CE) and de-excitation

The main processes affecting the level populations within one ion are scattering with particles.

Most abundant particles in the quiescent corona are thermal electrons, protons, alpha.

Electron collisions are the main excitation process in the low corona.

Proton collisions are also important when level separation is small.

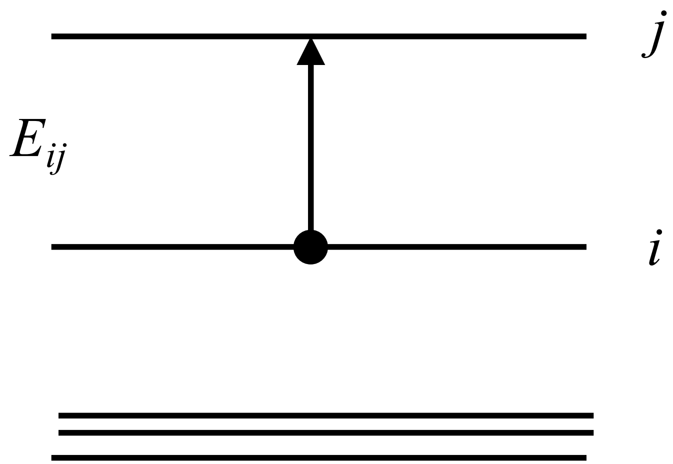


Within CHIANTI, a matrix with all the upward and downward rates (no bf) is solved to obtain the level populations (since v.9 I introduced a two-ion CRM)

# Collision strength

The number of transitions form level i to level j due to electron collisions per unit volume and time is given by Ni Ne *Cij* where *Cij* is the rate:

$$C_{ij}^{e} = \int_{v_o}^{\infty} v\sigma_{ij}(v) f(v) dv$$

with $v_o$ the velocity corresponding to the threshold energy for the transition and the cross section normally written as a function of a symmetric adimensional quantity, function of the kinetic energy of the colliding electron, called the ***collision strength***

$$\sigma_{ij} = \frac{\pi a_0^2}{g_i} \frac{E_H}{E} \Omega_{ij}(E)$$

$a_0$ the first Bohr orbit radius for the hydrogen, $g_i$ the statistical weight of the level i, $E_H$ the ionization energy for H I (13.6 eV). Assuming a Maxwellian distribution function *f*:

$$C_{ij}^{e} = 8.63\ 10^{-6} \frac{\Upsilon_{ij}}{T_e^{1/2} g_i}\ exp\left(-\frac{E_{ij}}{kT_e}\right)$$

# Collision strength

The Maxwellian-averaged collision strength:

$$\Upsilon_{ij} = \int_0^\infty \Omega_{ij}\ exp\left(-\frac{E_j}{kT_e}\right) d\left(\frac{E_j}{kT_e}\right)$$

*$E_j$* is the energy of the scattered electron relative to the energy of the final state of the ion.

The electron de-excitation rate is obtained with the principle of detailed balance:

$$C^e_{ji} = \frac{g_i}{g_j} C^e_{ij}\ exp\left(\frac{E_{ij}}{kT_e}\right)$$

# Collision strength- example: Mg IX

intercombination

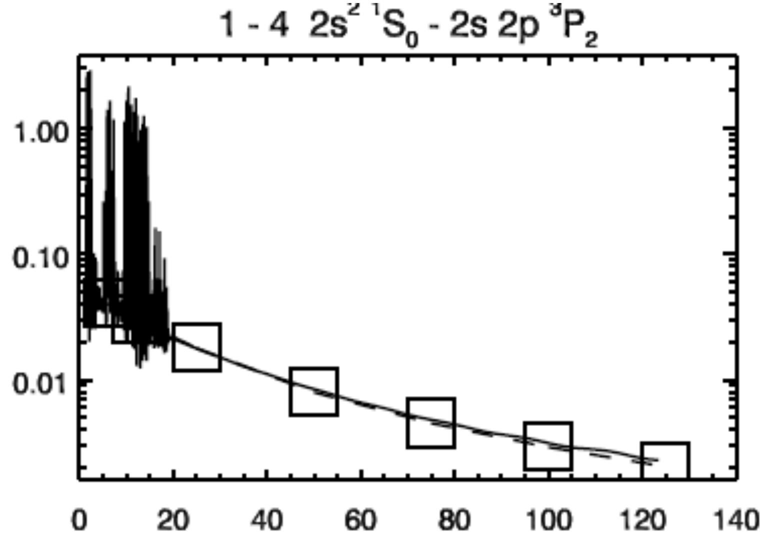


allowed

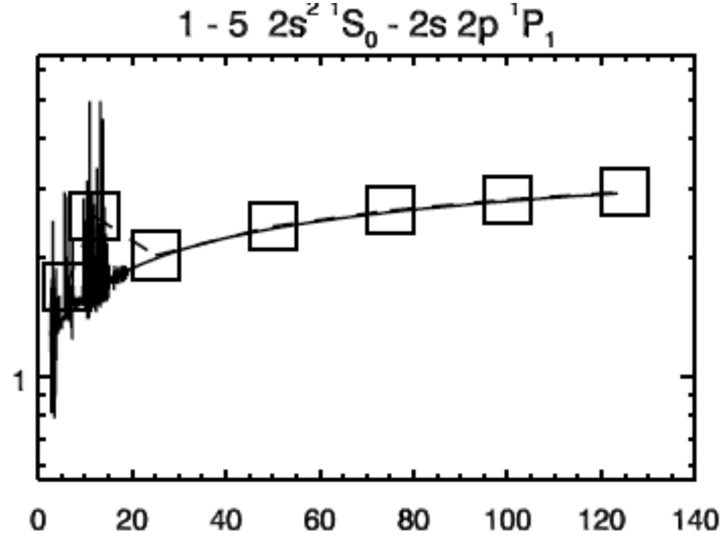


Coll.

strength

Energy (Ryd) incident electron

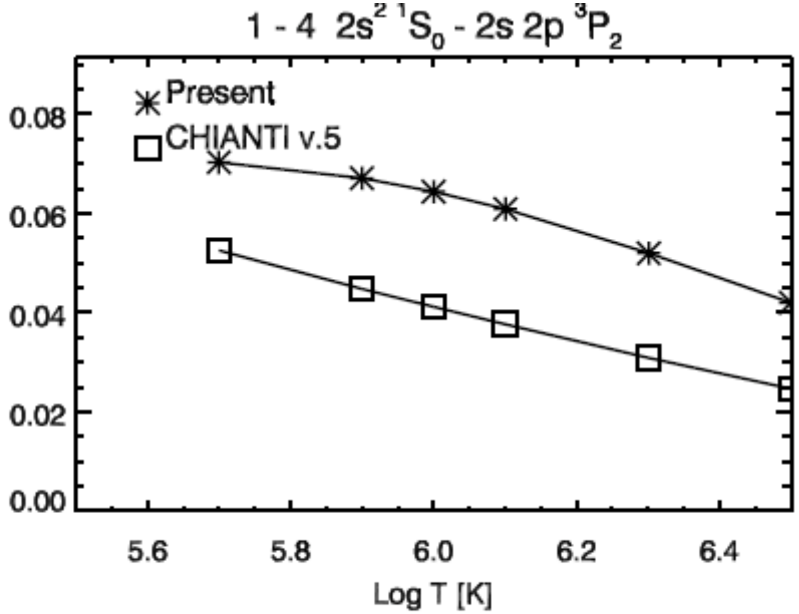


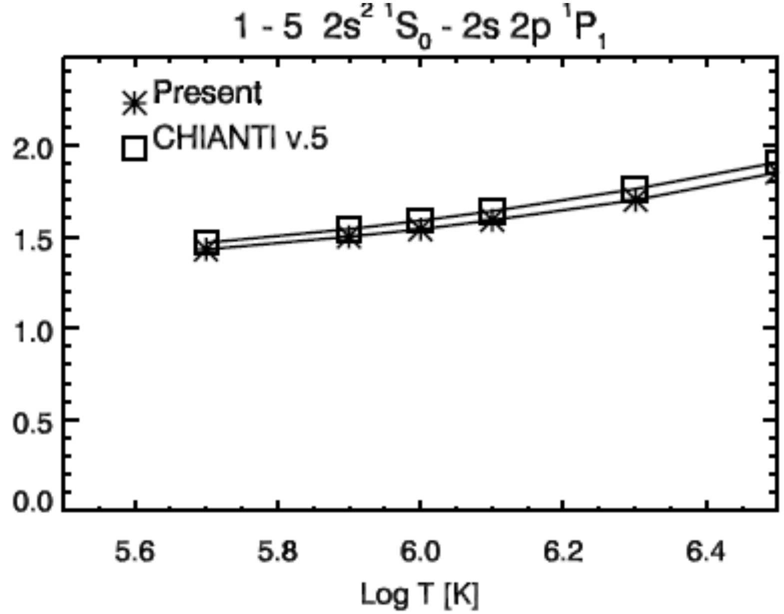


Maxwellian avg. Coll.

strength



Del Zanna Rozum Badnell 2008

# CHIANTI data

Currently, for each ion at least ascii files:

| | |
|---|---|
| fe_12.elvlc | Energy levels (theoretical, observed), level descriptions |
| fe_12.wgfa | Transition probabilities, gf values, theoretical, observed wavelengths |
| fe_12.scups | Maxwellian-averaged e- collision strengths on a scaled domain |

- + proton rates only for a few levels and ions.

# Non-Maxwellian e- (NMED)

Non-thermal particles are also present, especially during flares.

Most codes in astrophysics assume Maxwellian particles.

There is evidence that in solar active regions non-Maxwellian electron distributions (NMED) are present (Lorincik+2020).
Within CHIANTI, there is a way to treat NMED assuming sums of Maxwellians

$$f(E; a_i) = \sum_i a_i f_M(E, T_i)$$

$$\begin{aligned} C_{jk} &= \int_{E_{jk}}^{\infty} Q_{jk} v f(E; a_i) \mathrm{d}E \\ &= \sum_i a_i \int_{E_{jk}}^{\infty} Q_{jk} v f_{\mathrm{M}}(E, T_i) \mathrm{d}E \\ &= \sum_i a_i C_{jk}(T_i) \end{aligned}$$

The collisional excitation rate is the sum.
The coefficients $a_i$ are passed via a keyword

Alternatively, if you assume a k-distribution you can use the KAPPA package (being updated for CHIANTI v.8) or ask for cross-sections.

# Level population and coronal model

Without proton CE:

$$\frac{dN_j}{dt} = \sum_{k>j} N_k A_{k,j} + \sum_{k>j} N_k N_e C^{d}_{k,j} + \sum_{i<j} N_i N_e C^{e}_{i,j} + \sum_{i<j} N_i B_{i,j} J_{\nu_{i,j}} + \sum_{k>j} N_k B_{k,j} J_{\nu_{k,j}} - N_j \left( \sum_{i<j} A_{j,i} + N_e \sum_{i<j} C^{d}_{j,i} + N_e \sum_{k>j} C^{e}_{j,k} + \sum_{i<j} B_{j,i} J_{\nu_{j,i}} + \sum_{k>j} B_{j,k} J_{\nu_{k,j}} \right)$$

In a two-level ion model (e.g. a ground state $g$ and an excited state $j$) and neglecting photoexcitation:

Two-level ion

$$N_g N_e C^{e}_{gj} = N_j (N_e C^{e}_{jg} + A_{jg})$$

so the relative population of the level $j$ is

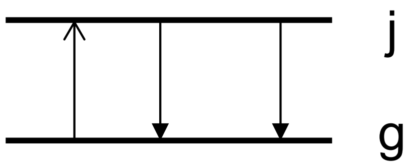


$$\frac{N_j}{N_g} = \frac{N_e C^{e}_{gj}}{N_e C^{e}_{jg} + A_{jg}} \qquad (15)$$

i.e. depends strongly on the relative values between the radiative rate $A_{jg}$ and the collisional de-excitation term $N_e C^{e}_{jg}$.

# Metastable levels- electron density diagnostics

Density diagnostics involve metastable levels. Best are ratios of allowed lines

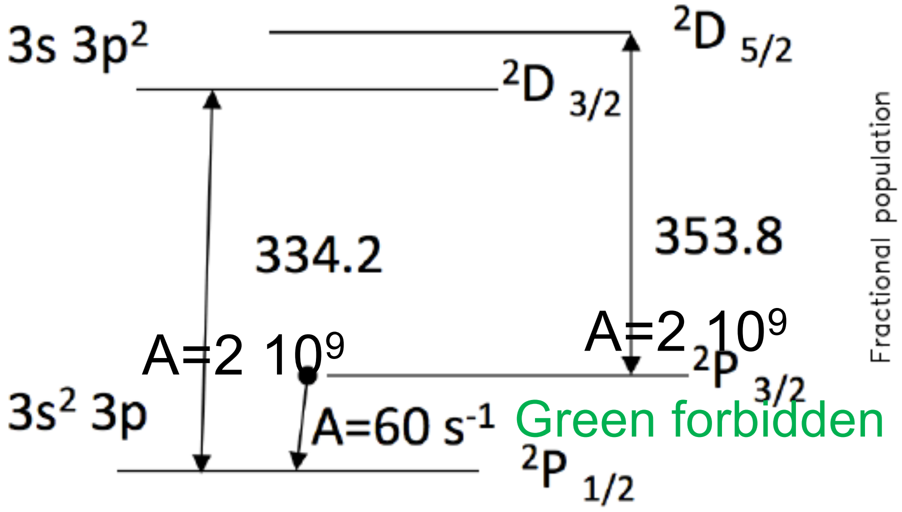


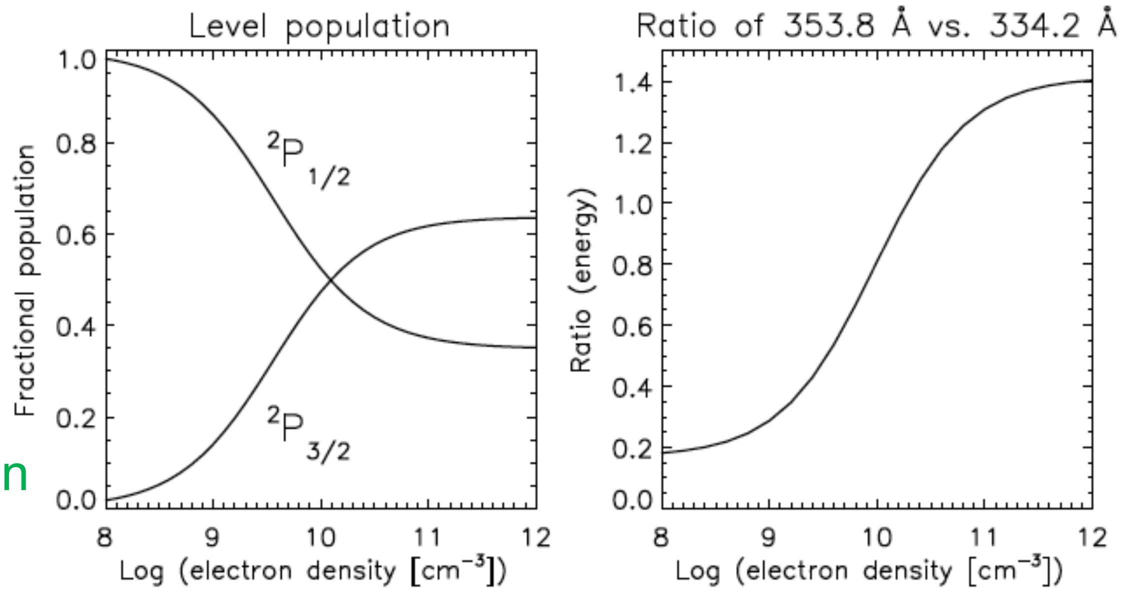


CHIANTI: IDL>plot_populations, 'fe_14',2e6

The number of photons emitted by the transition per second and per ion is:

$$A_{jg}\frac{N_j}{N_g} = A_{jg}\frac{C^e_{gj}}{C^e_{jg}}\left(1+\frac{A_{jg}}{N_e C^e_{jg}}\right)^{-1} = \frac{g_j}{g_g}\exp\left(\frac{-\Delta E_{gj}}{kT_e}\right)A_{jg}\left(1+\frac{A_{jg}}{N_e C^e_{jg}}\right)^{-1}$$

At low densities the intensity is then proportional to the density but independent of the $A$ value: $N_e C^e_{gj}$. The emission is directly related to the collision.

At high densities the intensity is

$$A_{jg}\frac{g_j}{g_g}\exp\left(\frac{-\Delta E_{gj}}{kT_e}\right),$$

# Fe XII

The 186/195 is a good density diagnostic for Hinode EIS. The populations of the metastable levels are hard to calculate.

Del Zanna (2012): the population of the $3s^2\,3p^3\,{}^2D_{5/2}$ is 50 % higher than previous models (Storey et al. 2005; Del Zanna & Mason 2005).

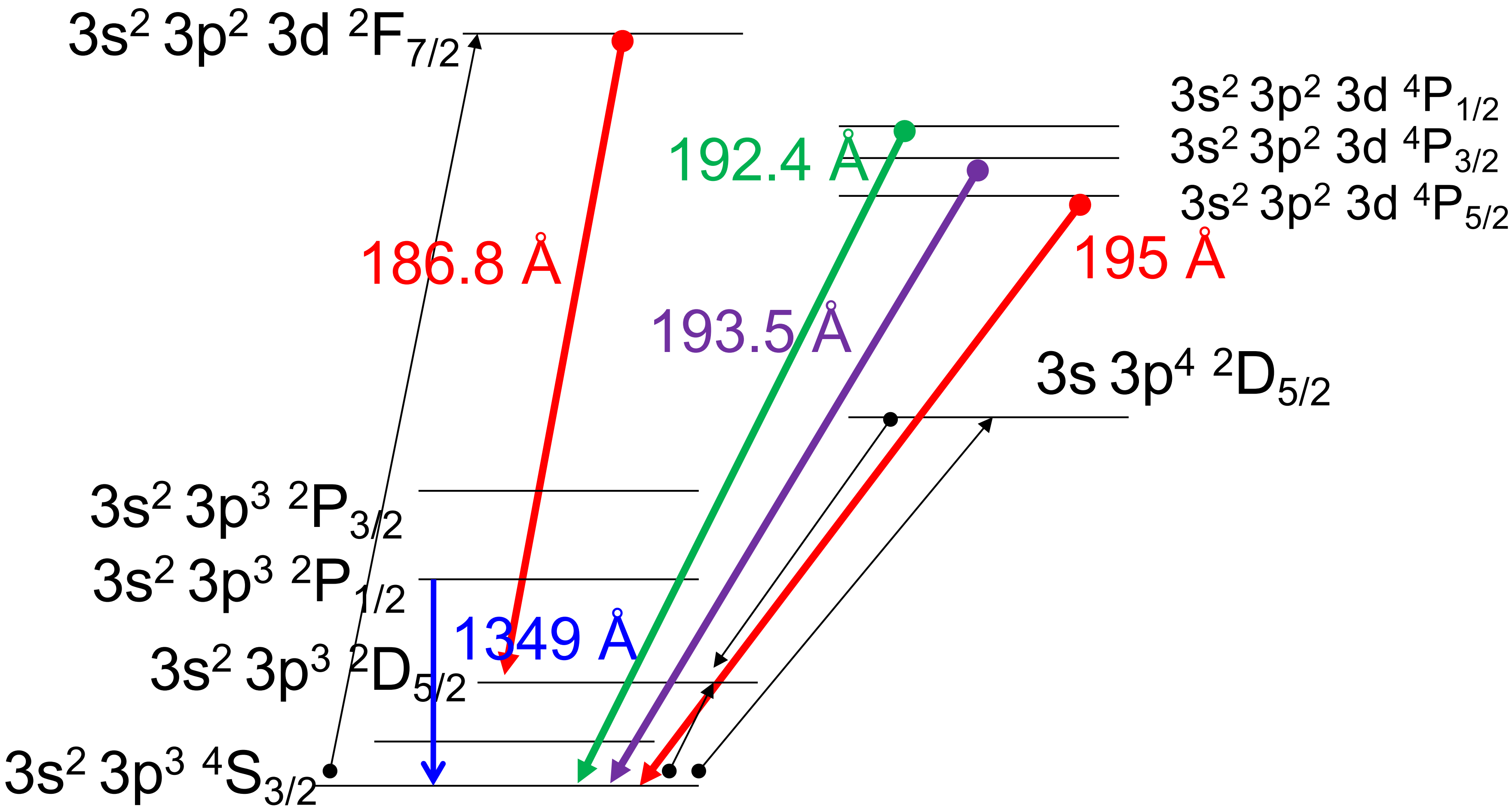

# Fe XIII – log Ne=8

Complex cascading effects (Yu, Del Zanna+2018; Del Zanna & Mason 2018).

Large differences in collisional data !!!!!

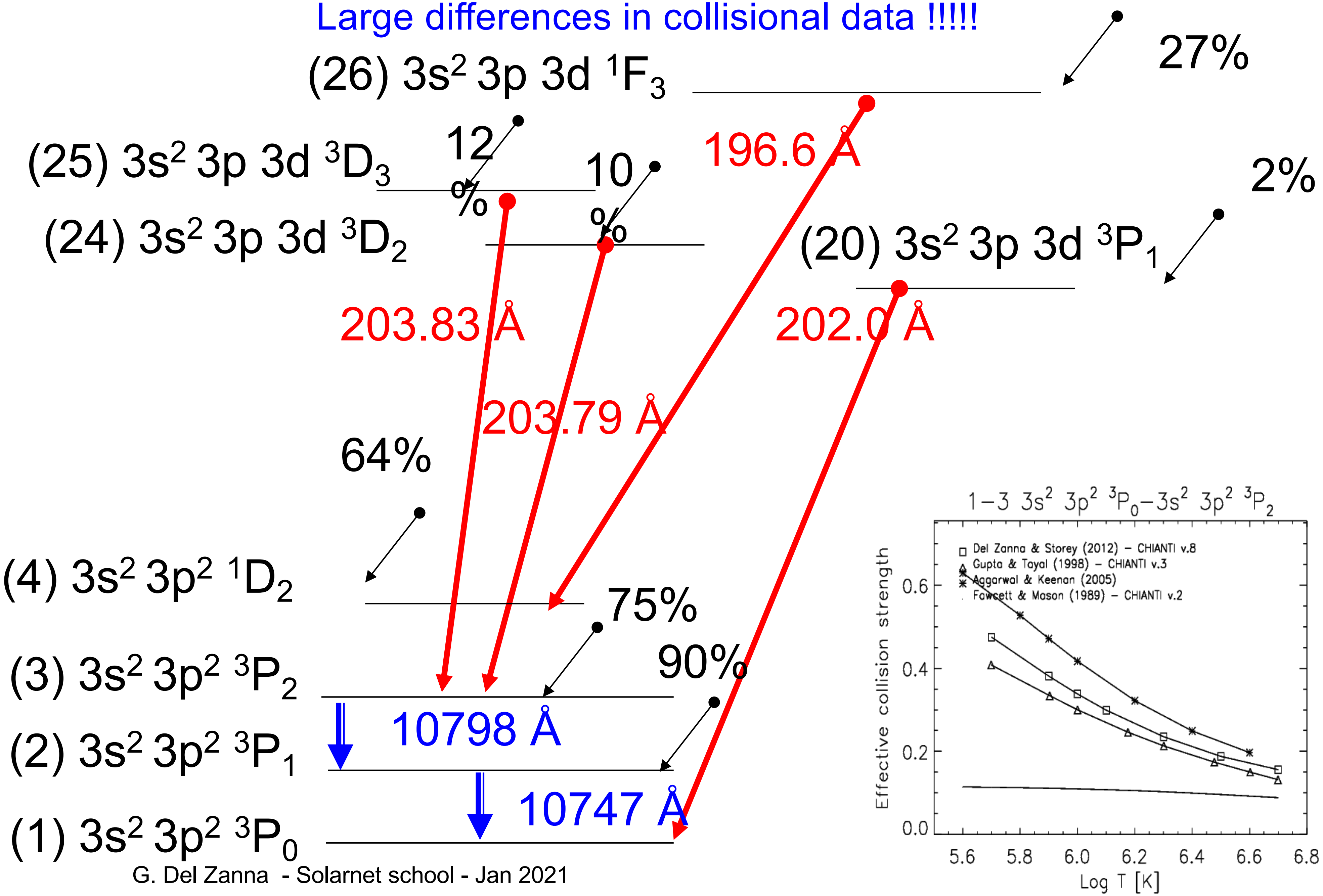

# Measuring densities

When more than one line ratio is available, a convenient way is the emissivity ratio method (Del Zanna et al. 2004)

$$F_{ji}(N_e, T_e) = C \frac{I_{ob} N_e}{N_j(N_e, T_e)\, A_{ji}}$$

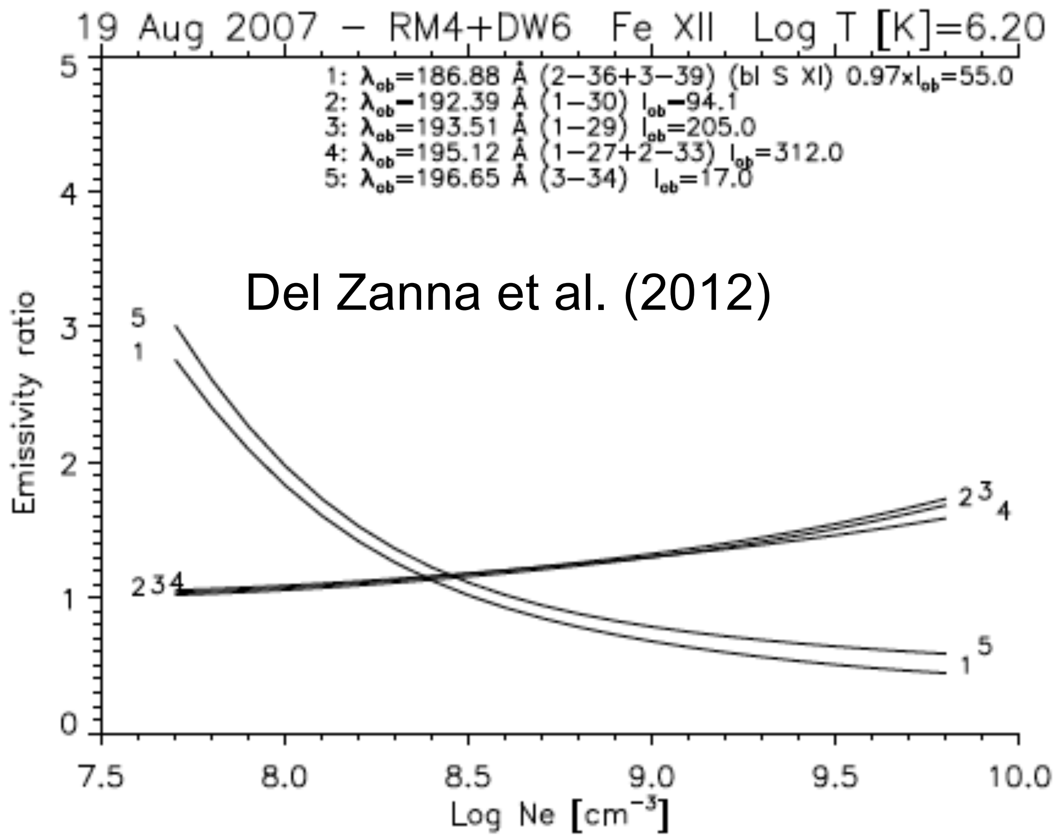

# IRIS densities

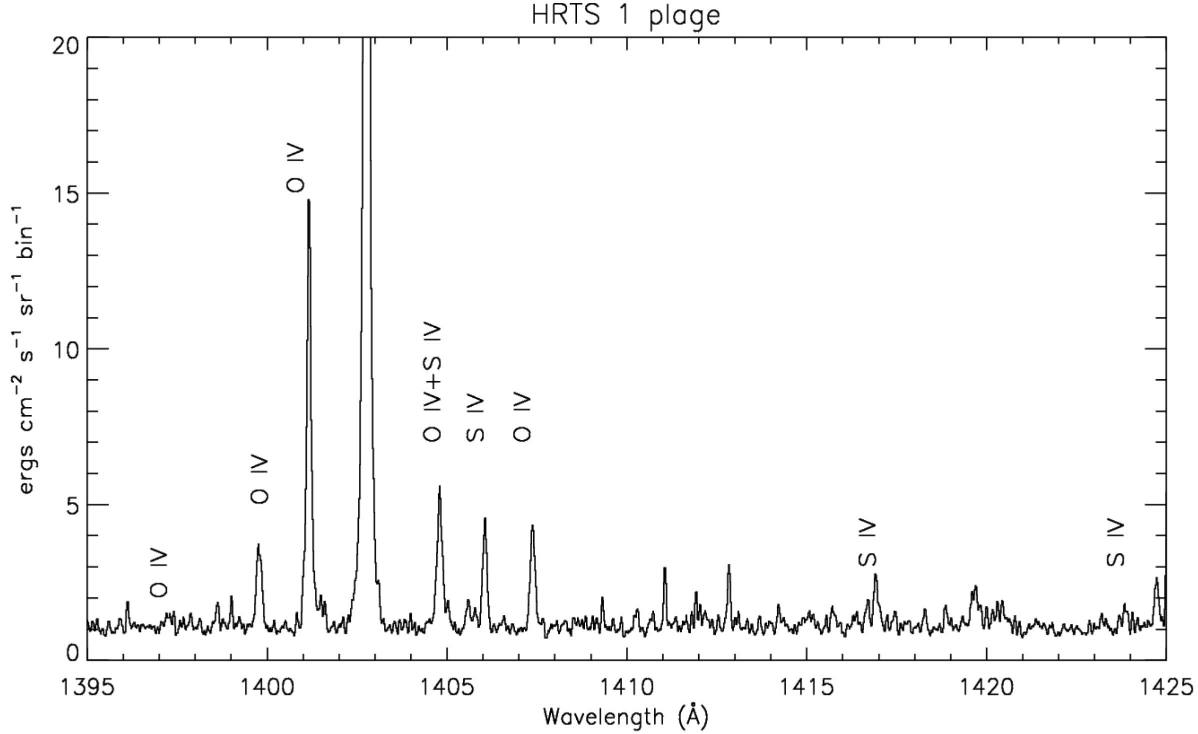


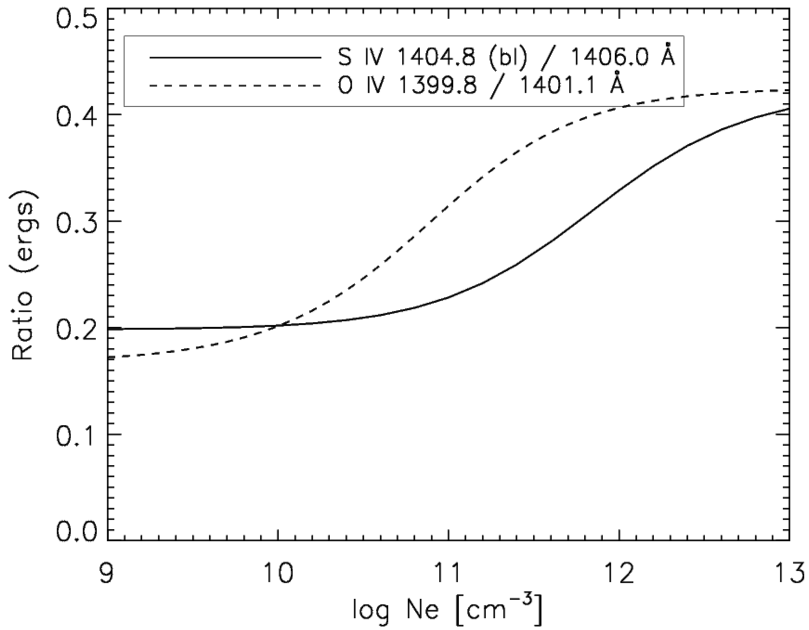


Table 3: O IV transitions commonly used to measure densities.

| Transitions | λ (Å) | Instrument | log $N_e$ |
|---|---|---|---|
| $^2P_{3/2}$ - $^4P_{5/2}$ | 1401.16 | | |
| $2s^2\ 2p\ ^2P_{3/2}$ - $2s\ 2p^2\ ^4P_{3/2}$ | 1404.78 (bl S IV) | Skylab, HRTS, SMM/UVSP | |
| | | SUMER, IRIS | 9–12 |
| $2s^2\ 2p\ ^2P_{1/2}$ - $2s\ 2p^2\ ^4P_{1/2}$ | 1399.78 | | |

# B-like

## Oxygen

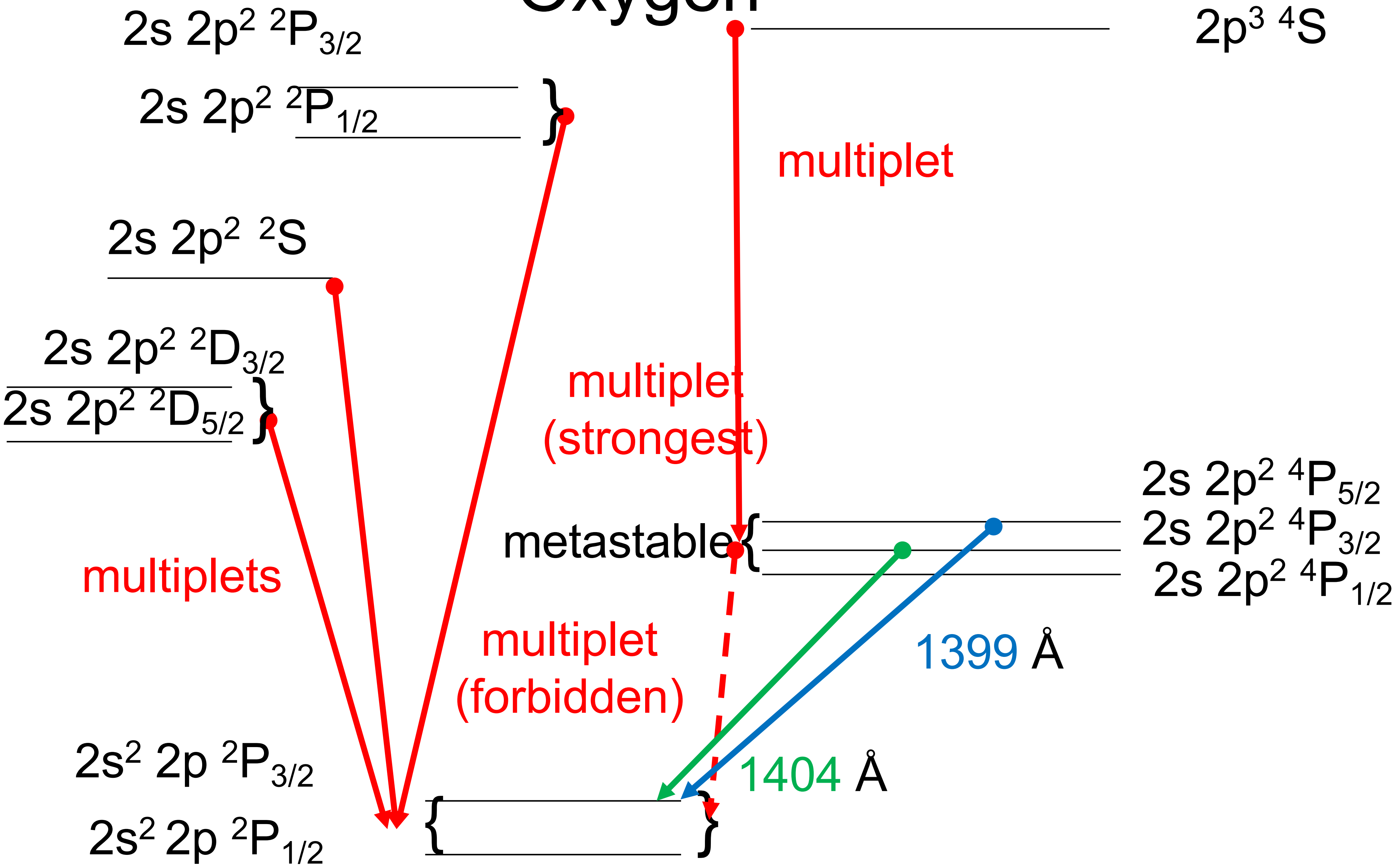

# CHIANTI GUI applications


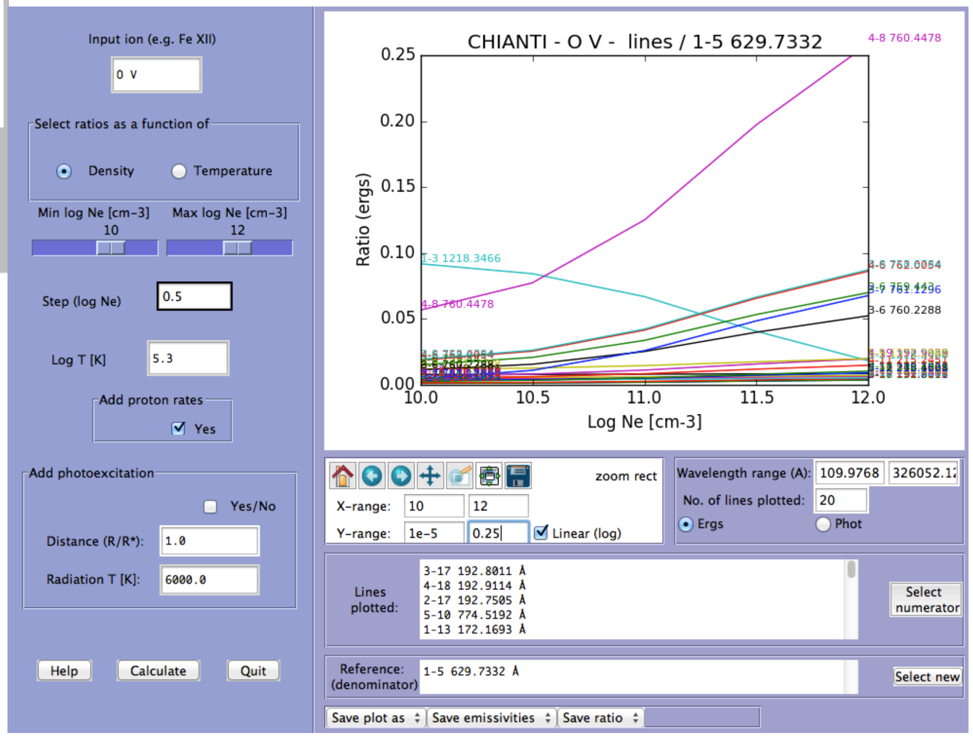

# ‘Direct’ temperature diagnostics

For allowed lines, intensities are proportional to the excitation rate.

$$I_{jg} \sim h\nu_{gj} N_\mathrm{e} N_g C^e_{gj} \sim h\nu_{gj} N_\mathrm{e} N_g \frac{\Upsilon_{gj}}{T_\mathrm{e}^{1/2} g_g} \; exp\left(-\frac{E_{gj}}{kT_e}\right)$$

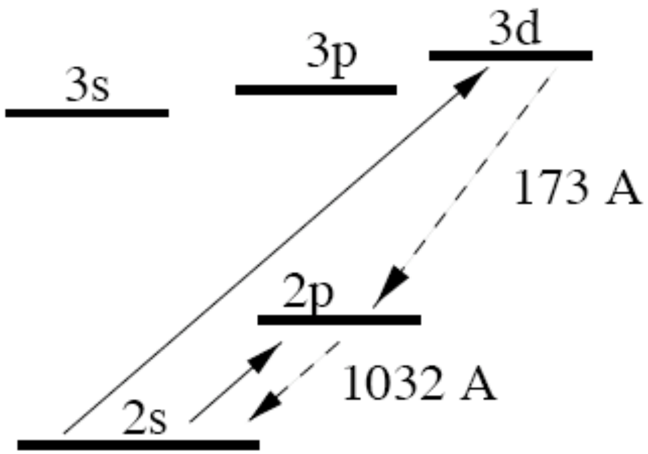


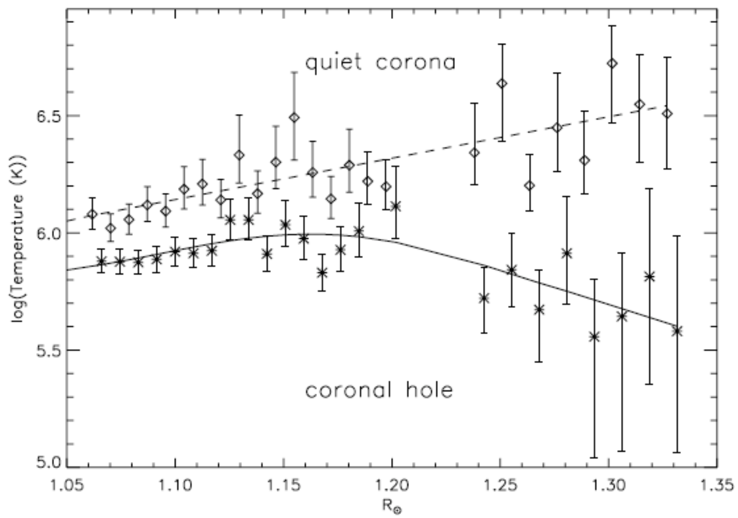


Ratios of lines with very different excitation energies are T-sensitive.

O VI SOHO GIS + SUMER David et al. (1998)

At flare temperatures very good measurements can be obtained from the satellite lines in the X-rays, with different diagnostics.

# Measuring Te with Mg IX

One of the best Te diagnostic for 1 MK plasma (Del Zanna et al. 2008).

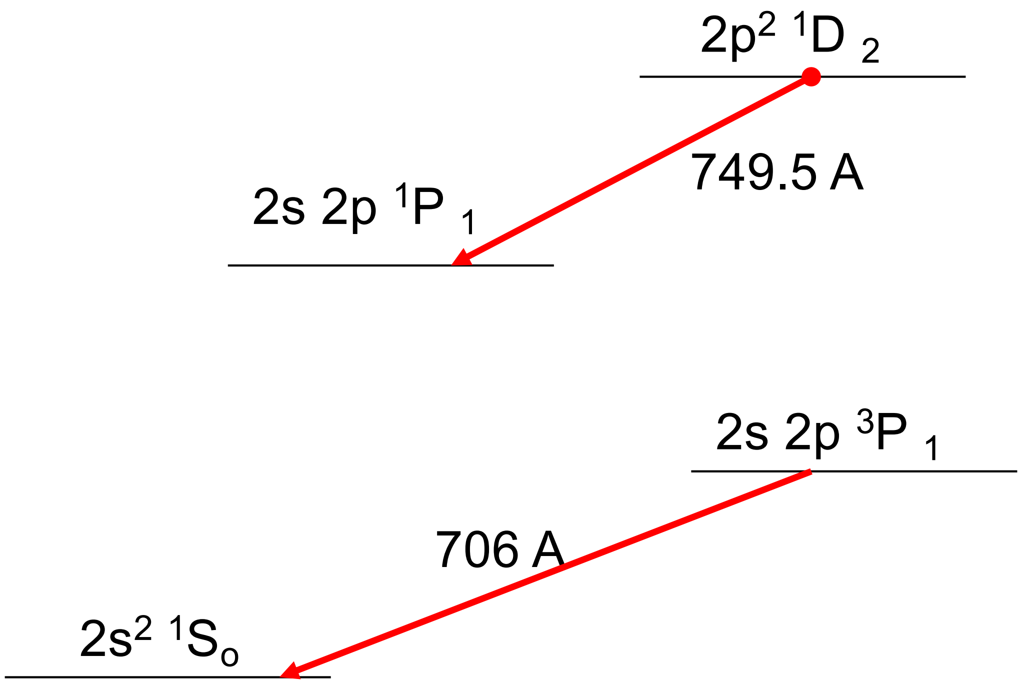


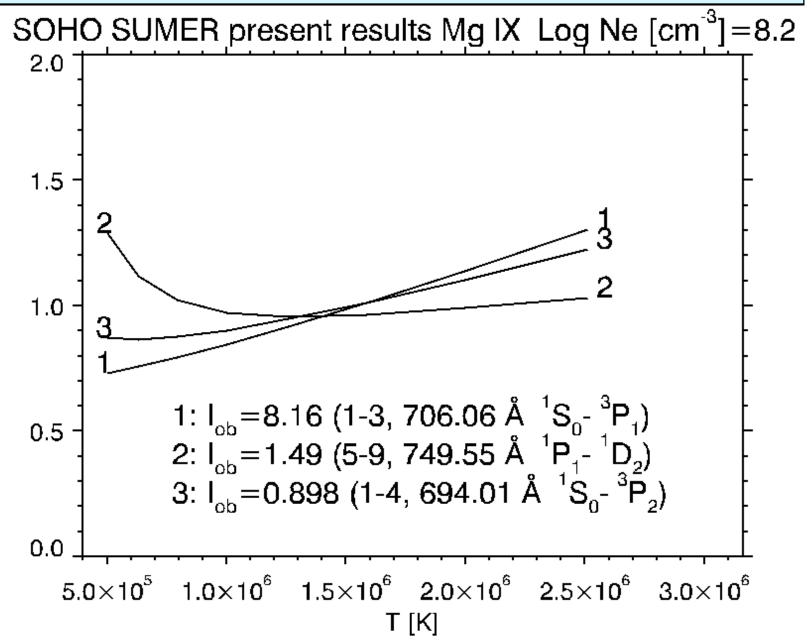


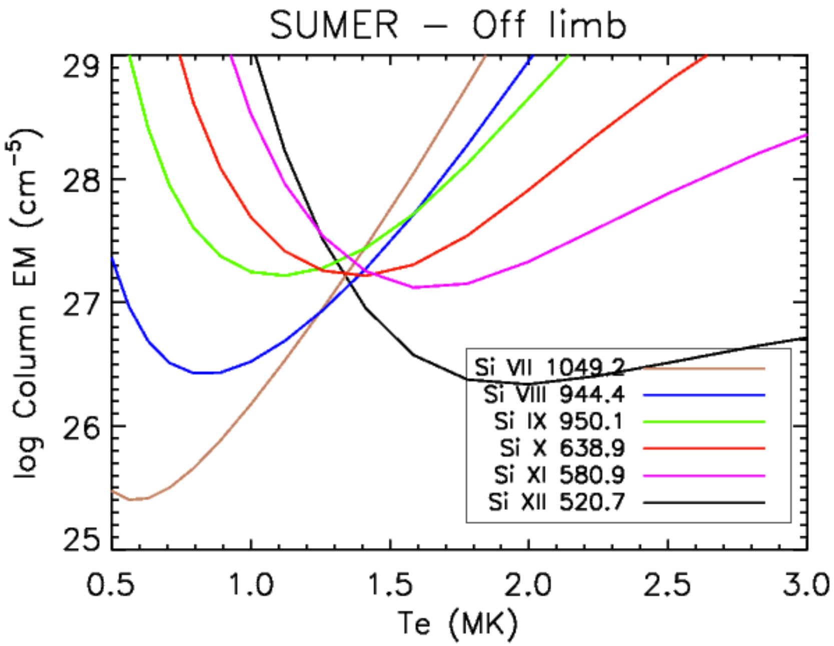

Break out hands-on session?

# Line widths

$$I_\lambda = \frac{I}{\sqrt{2\pi}\sigma} exp[-(\lambda - \lambda_0)^2/2\sigma^2]$$

For a Maxwellian distribution

$$\sigma^2 = \frac{\lambda^2}{2c^2}\left(\frac{2kT}{M_{\rm i}} + \xi^2\right) + \sigma_I^2$$

Ion mass $M_{\rm i}$

gaussian instrumental width $\sigma_I$

most probable non-thermal velocity $\xi$

$$< v^2 >^{1/2} = (3/2)^{1/2}\xi$$

A key issue is the ion temperature – not easy to know. Te has hardly been measured. The ionization temperature is normally used.

# Opacity in coronal lines

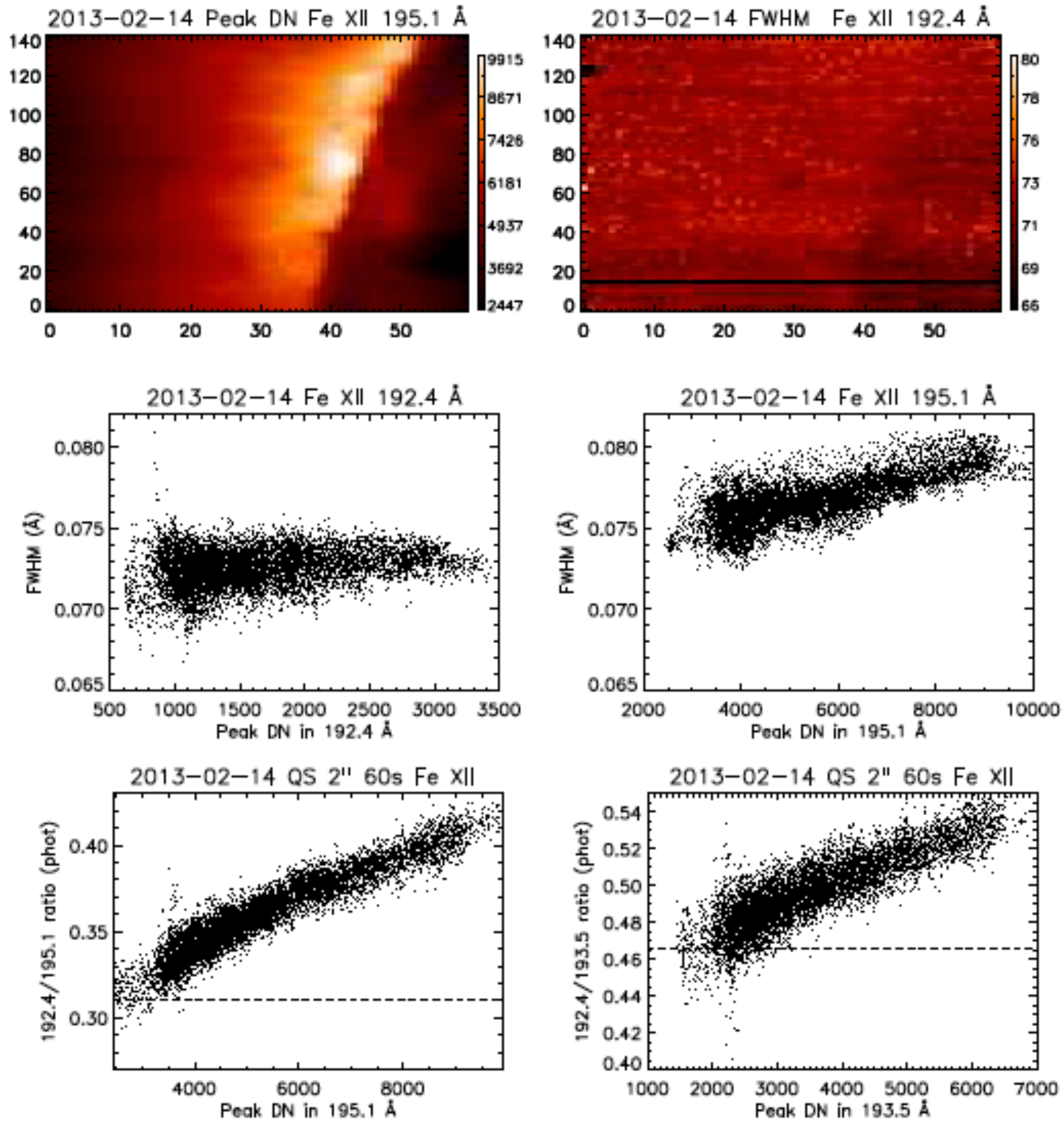


The EIS Fe XII 192,193.5,195 Å Lines should have the same width and constant ratios. They do not in AR and some off-limb observations.

Del Zanna+2019

$$\tau_0 = 8.3\,10^{-21}\, f_{lu} \frac{\lambda^2}{\Delta\lambda_{FWHM}}\, N_l\, \Delta S \quad (4)$$

with $\lambda$ and $\Delta\lambda_{FWHM}$ expressed in Å. For the 195 Å line, $f_{lu}$ = 2.97/4, neglecting the weaker line blending the main line.

The population of the lower level can be written as

$$N_l = \frac{N_l}{N(\mathrm{Fe\,XII})} \frac{N(\mathrm{Fe\,XII})}{N(\mathrm{Fe})} Ab(\mathrm{Fe}) \frac{N_\mathrm{H}}{N_\mathrm{e}} N_\mathrm{e}\ , \quad (5)$$

where $N_l/N(\mathrm{Fe\,XII}) = 0.9$ is the relative population of the ground state at quiet Sun densities, $N(\mathrm{Fe\,XII})/N(\mathrm{Fe}) = 0.25$ is the peak relative population of the ion, $Ab(\mathrm{Fe}) = 3.16\,10^{-5}$ is the Fe photospheric abundance, $N_\mathrm{H}/N_\mathrm{e} = 0.83$, and $N_\mathrm{e}$ is the averaged electron number density. We therefore have $\tau_0 = 6.9\,10^{-20}\, N_\mathrm{e}\ \Delta S$ [$\mathrm{cm}^{-2}$] assuming $\Delta\lambda_{FWHM}$ =0.02 Å.

```
plot_populations, 'fe_12',1.5e6,20, densities=1e8*[1,3,5]
plot_ioneq, 'fe', ion=[12]
```

for Ne=7 $10^8$ and a path = 1.8 $10^{10}$ cm (from the EM) we get τ = 0.9 for the 195 Å line.

Del Zanna+2019

Assuming that the source function does not vary alos:

$$I_\nu = S_\nu \left(1 - e^{-\tau_0}\right) \ ,$$

**while the the line source function $S_\nu$ is:**

$$S_\nu = \frac{2h\nu^3}{c^2} \left(\frac{g_u N_l}{g_l N_u} - 1\right)^{-1} \ ,$$

for τ (195 Å ) = 0.9 , τ (192 Å ) = 0.3,
the ratio of the source functions is close to 1,
and the 195/192 Å ratio decreases by ~30%,
close to what observed.

Break out hands-on session?

# Photo-excitation (PE)

Photoexcitation and stimulated emission depend on the local radiation field. It is not so important in the low corona and EUV/UV lines.

It is very important for the forbidden lines in the corona, when densities are low and little CE is present.

Also, for all cool lines in the corona (esp. H,He), and low charge states in the TR/chromosphere.

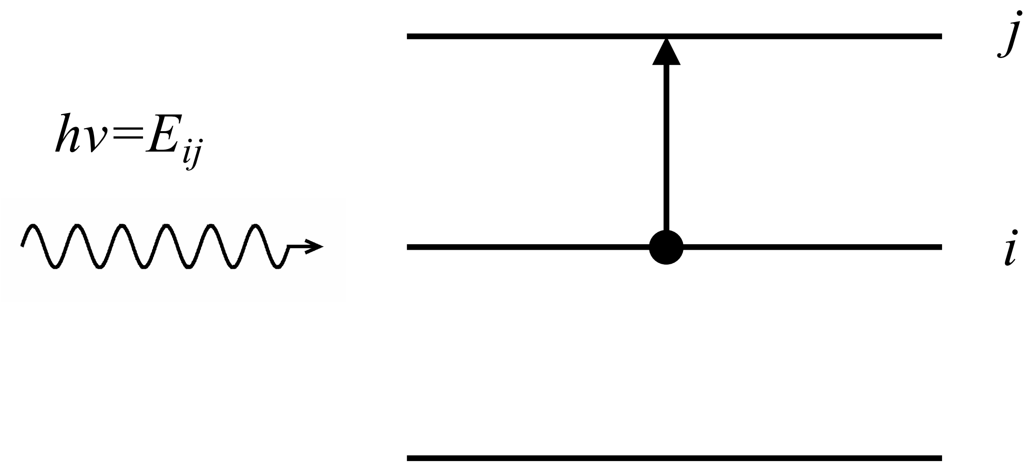

# PE for H, He in the corona

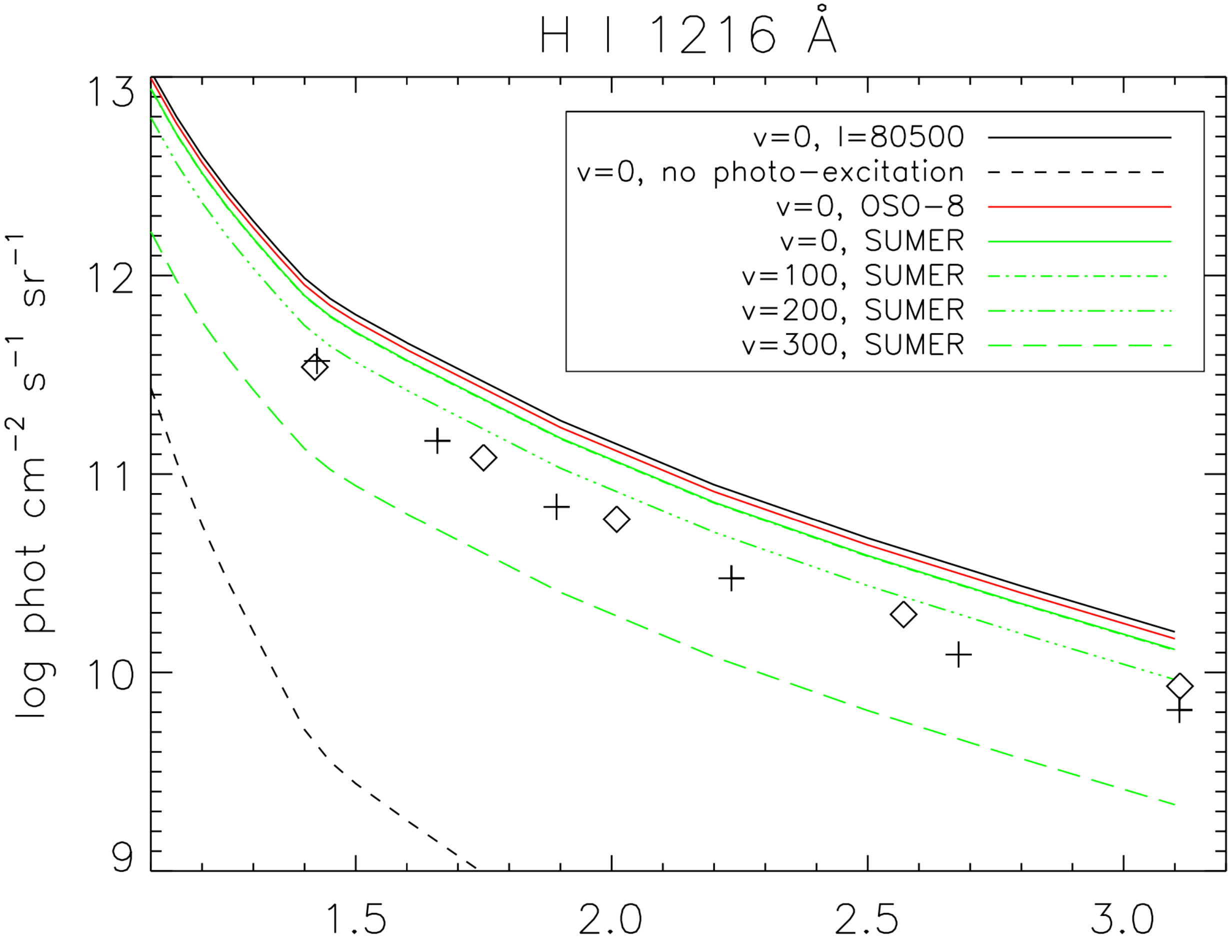


The abundance of H in the corona is $10^{-7}$, still the Ly $\alpha$ is the strongest coronal line!

Related to modelling the outer corona (Del Zanna+2018)

Neutral He is also strongly affected by PE (Del Zanna+2020)

# PE

Assuming a uniform disk intensity:

$$J_\nu = \frac{\Delta\Omega}{4\pi}\,\overline{I_\nu} = W(r)\,\overline{I_\nu} \tag{25}$$

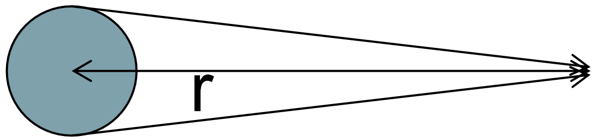


where $W(r)$ is the *dilution factor* of the radiation, i.e., the geometrical factor which accounts for the weakening of the radiation field at a distance $r$ from the Sun, and $\overline{I_\nu}$ is the averaged disk radiance at the frequency $\nu$.

Assuming spherical symmetry (i.e., the solar photosphere a perfect sphere), and indicating with $r$ the distance from Sun centre $R_\odot$ the solar radius, we have:

$$W(r) = \frac{1}{4\pi}\int_0^{2\pi}\int_0^{\theta_0} sin\,\theta\,d\theta\,d\phi = \frac{1}{2}(1 - cos\,\theta_0) = \frac{1}{2}\left(1 - \left[1 - \left(\frac{R_\odot}{r}\right)^2\right]^{1/2}\right) \tag{26}$$

where $\theta_0$ is the angle sub-tending $R_\odot$ at the distance $r$, i.e., $sin\theta_0 = R_\odot/r$.

In terms of the energy density per unit wavelength, $U_\lambda$, the photoexcitation rate for a transition $i \rightarrow j$ is:

$$P_{ij} = A_{ji}\,W(r)\,\frac{g_j}{g_i}\,\frac{\lambda^5}{8\pi hc}U_\lambda \tag{27}$$

where $A_{ji}$ is the Einstein coefficient for spontaneous emission from $j$ to $i$, $g_j$ and $g_i$ are the statistical weights of levels $j$ and $i$, and $W(r)$ is the radiation dilution factor.

# Photo-excitation (PE)

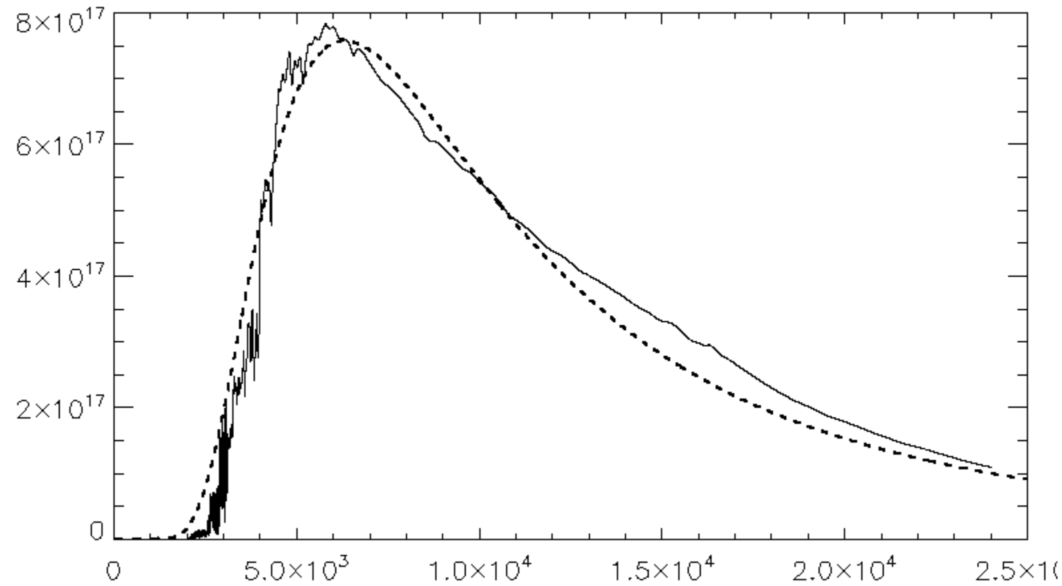


For lines in the vis/IR, I=B (black-body) and the correction to the A-value depends on $T_*$
which is about 6000 K

In CHIANTI, PE is included as a correction to the A-value:

$$\mathcal{A}_{ij} = \begin{cases} W(r) A_{ji} \frac{g_j}{g_i} \frac{1}{\exp(\Delta E / kT_*) - 1} & i < j \\ A_{ji} \left[ 1 + W(r) \frac{1}{\exp(\Delta E / kT_*) - 1} \right] & i > j \end{cases}$$

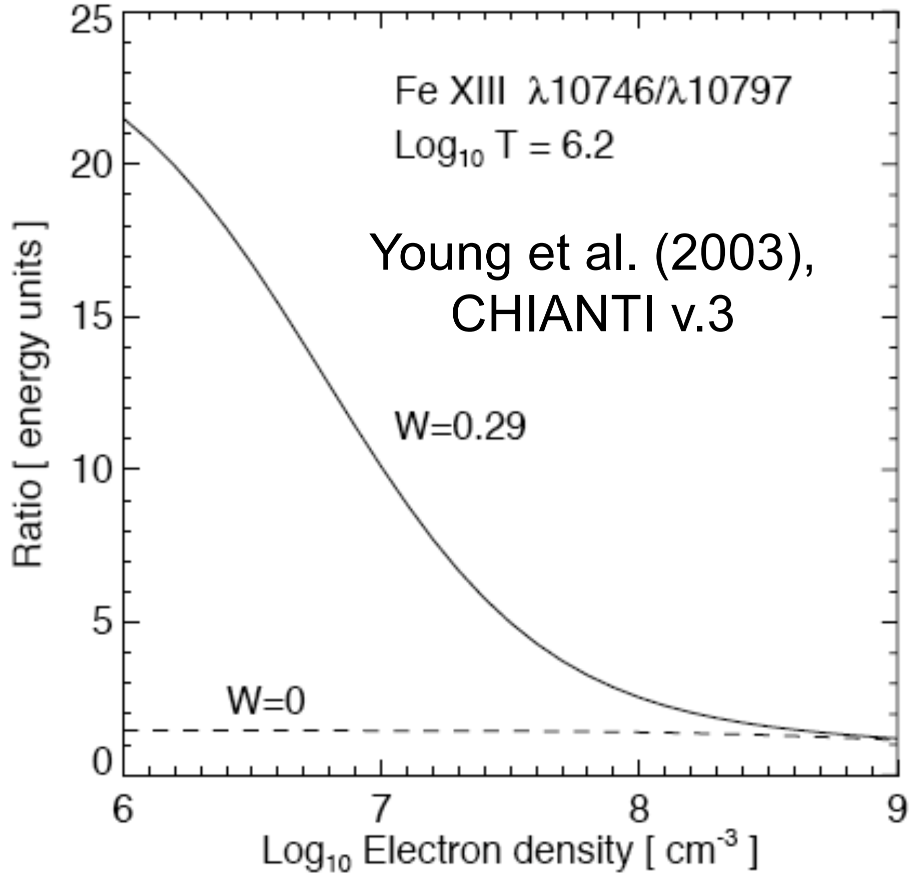


FIG. 3.—Fe XIII λ10746/λ10797 ratio plotted as a function of density for two different dilution factors. $W = 0$ corresponds to no radiation field, while $W = 0.29$ corresponds to 0.1 source radii above the source surface ($r_* = 1.1$).

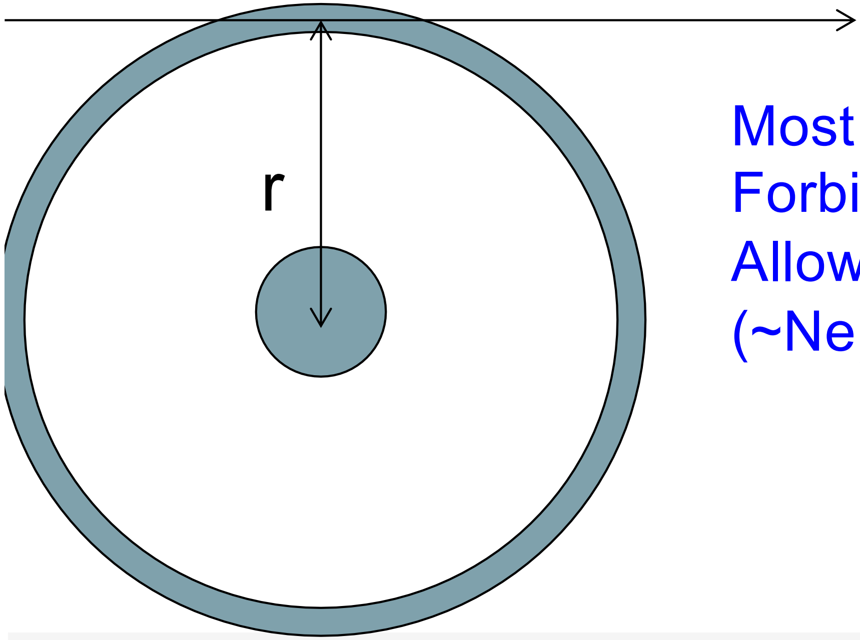


Most allowed (EUV) transitions: C(T); I~ $Ne^2$
Forbidden: C(T, Ne, r, $I_{disk}$)
Allowed, forbidden and scattered $I_{disk}$ emission (~Ne) is not necessarily co-spatial

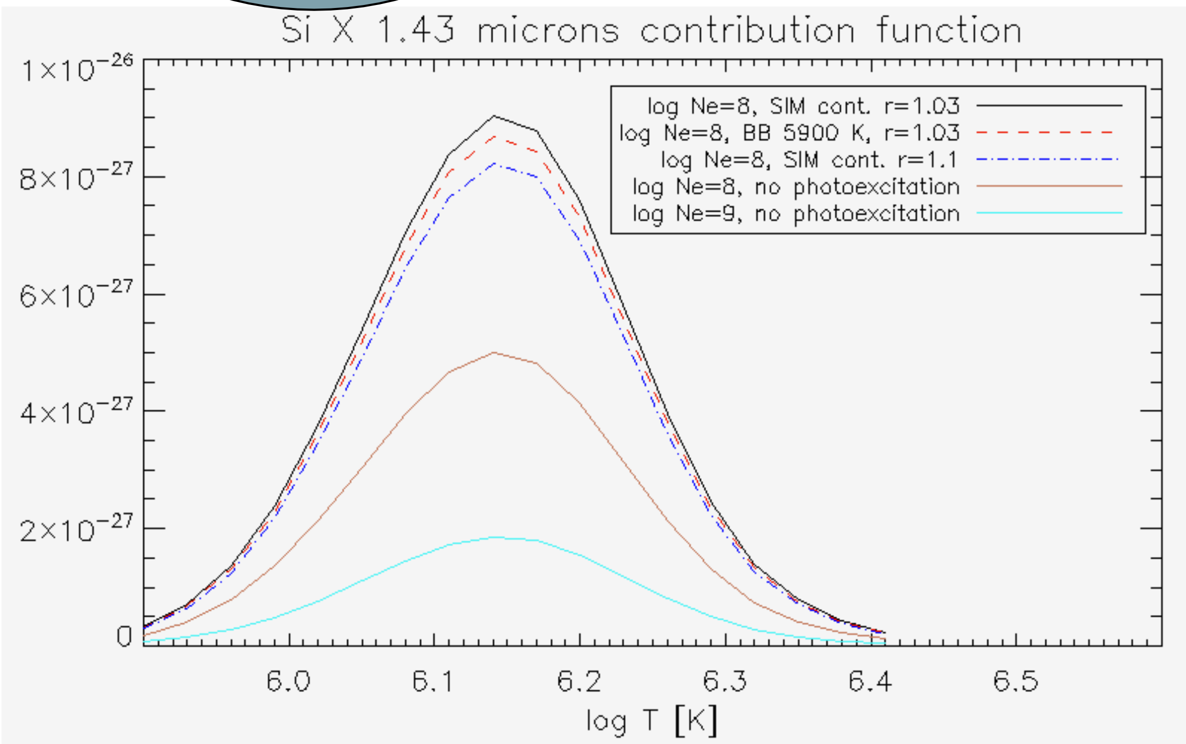


Photo-excitation from disk can be modelled using CHIANTI, with user-defined disk radiances.

**Unlike allowed transitions, a good model of Ne alos is fundamental**

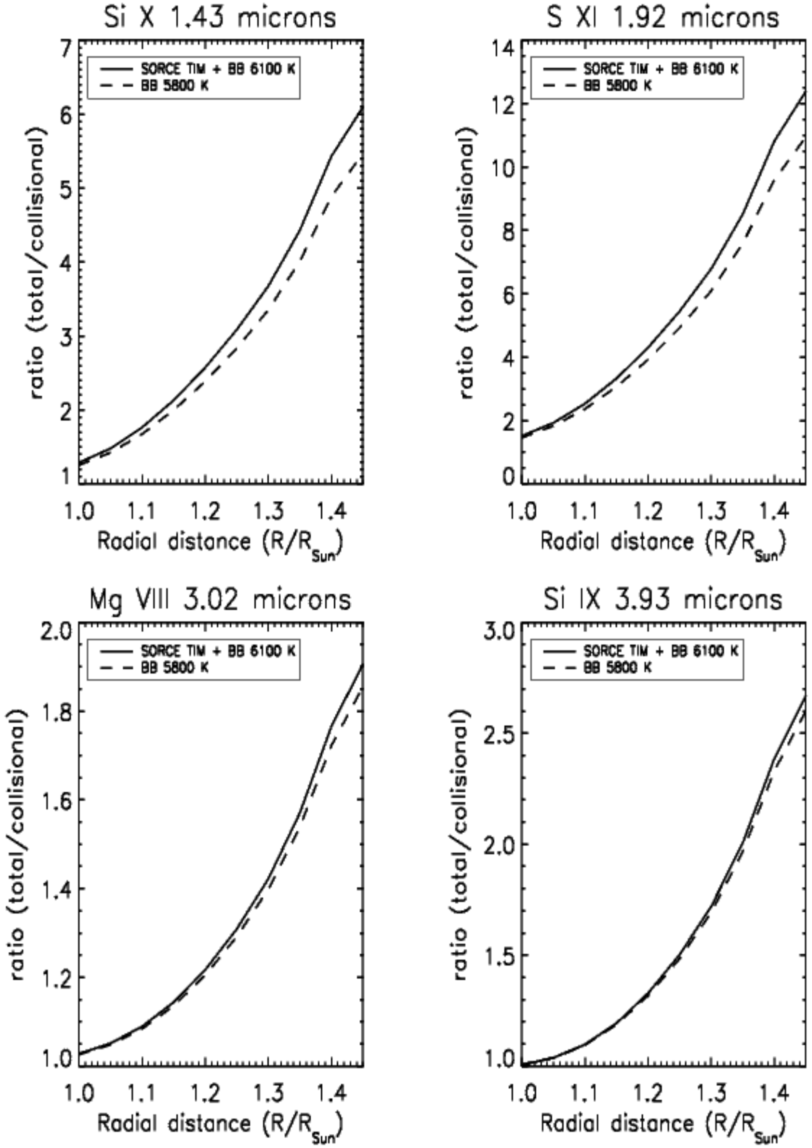


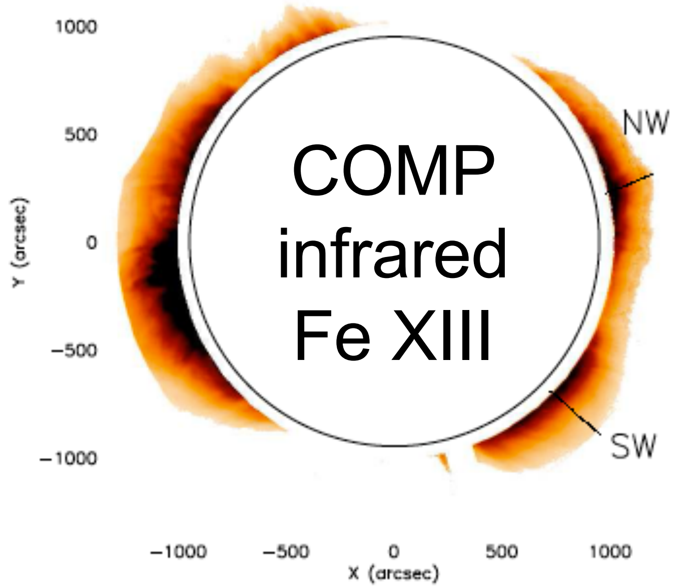


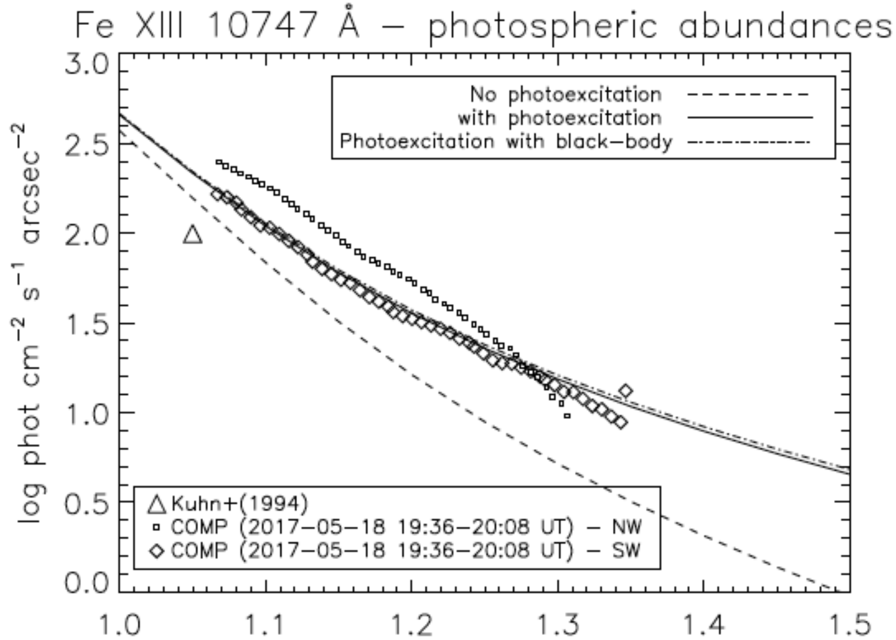


Photo-excitation is pumping the forbidden lines. Each spectral line is sensitive to Ne and disk radiation in a different way.

Del Zanna+2018

# PE and coronal lines

Forbidden lines in the visible/IR are great to measure

- Ne via line ratios or actual radiances
- T (ionisation T, but also Te in combination with EUV)
- Chemical abundances
- Non-Thermal effects (line widths, non-thermal electrons)
- Magnetic field (see CoMP Science paper by Yang, Zihao+2020)

However:

- Atomic data not simple to calculate. Latest calculations (Del Zanna+ 2012, several A&A papers), made available to CHIANTI v.8 Del Zanna+(2015) showed increases of ~2 in the intensities. (cf. Del Zanna & Mason, 2018, Liv. Rev. Sol. Phys.)
- Visible/IR nearly unexplored ! (see Del Zanna & DeLuca (2017)
- Modelling the signal is not trivial (see e.g. Del Zanna+2018, Dudik+2020)
- Significant atmospheric absorption in the IR (DKIST)

# PE in CHIANTI

Is included as a correction to the A-value (resonant process) with a dilution W. A black-body is one option. Alternatively an user-defined energy density U file can be passed as a keyword, with RADFUNC= 'my_function,lambda, a, b'. The function must return an array of energy density with the same dimensions of the wavelength array lambda, which is internally defined.

Note: the relation between radiance and energy density is:

$$I_\lambda = \frac{c}{4\pi} U_\lambda.$$

The optional two parameters can e.g. be the velocity for the Doppler dimming and a temperature.

Doppler dimming is a powerful diagnostic to measure the plane-of-sky solar wind outflow velocity.

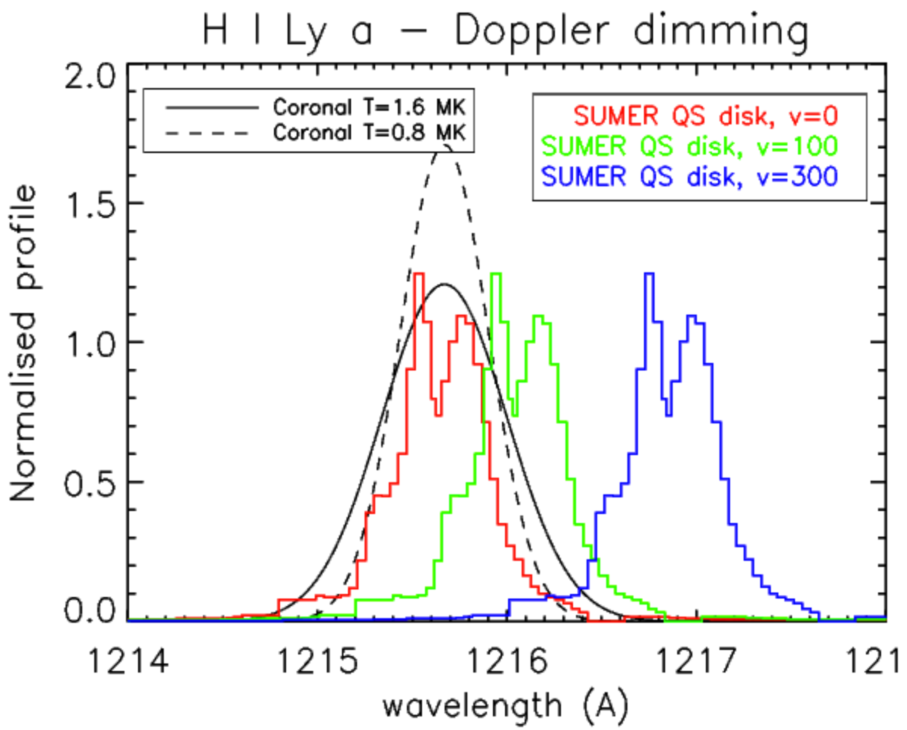

Break out hands-on session?

# Ionization/Recombination

Processes that depopulate the upper ionization state:
(1): radiative recombination, induced ~ $N_{r+1}$ $N_e$ $R^i_{r+1}$
(2): radiative recombination, spontaneous ~ $N_{r+1}$ $N_e$ $R^r_{r+1}$
is the inverse process of photoionization (cf Badnell 2006)
(3): dielectronic recombination ~ $N_{r+1}$ $N_e$ $R^d_{r+1}$ (Burgess 1964,1965)

Processes that populate the upper ionization state:
(4): collisional ionization (+auto) by direct impact by electrons (inverse of three-body recombination) ~ $N_r$ $N_e$ $S^e_r$
(5): photoionization ~ $N_r$ $R^i_r$

$$R^i_r \sim \int I_\nu d\Omega$$

LTE: detailed balance of (1), (2), (5) --> Saha equation

$$\frac{N_{r+1}}{N_r} = \frac{u_{r+1}}{u_r} e^{-\chi_{r+1}/kT} \frac{2\ (2\pi mkT)^{3/2}}{N_e h^3} \qquad u_r = \sum_n\ g_{r,n}\ exp(E_{r,n}/kT)$$

Partition function

At low densities plasmas become optically thin and most of radiation escape, therefore processes (1) and (5) are attenuated. The Saha equation does not apply.

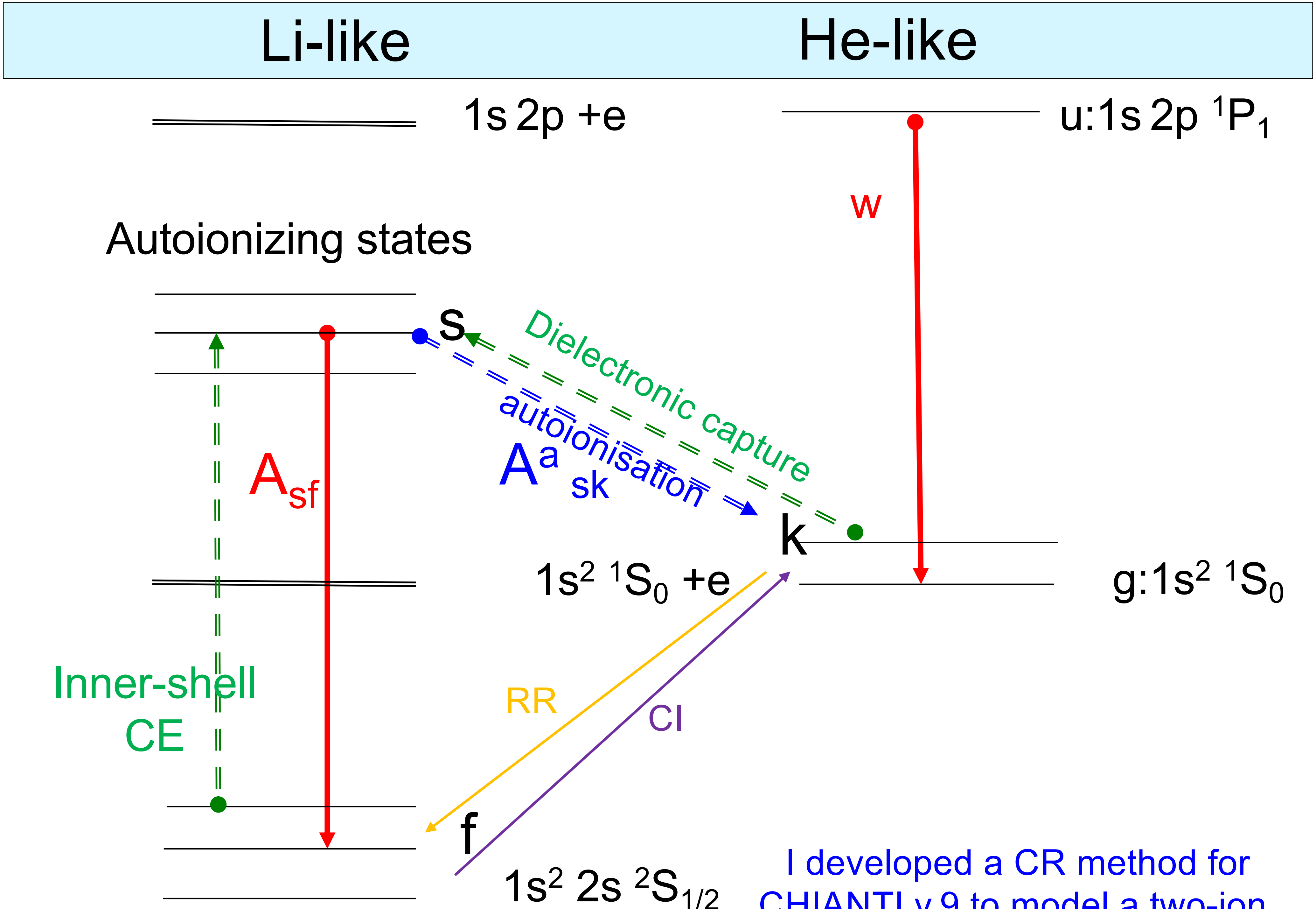


I developed a CR method for CHIANTI v.9 to model a two-ion, including autoionizing states

# Direct Ionization (DI) by electron impact

$$S^e = \int_{v_0}^{\infty} v\sigma(v) f(v) dv \quad (\mathrm{cm}^{-3} s^{-1})$$

direct impact coefficients for ionization by collision with electrons (much more efficient than the protons).

Dere (2007) calculated ab-initio direct-ionization (DI) cross-sections between ground states and compared them with available experimental data. They are available in CHIANTI.

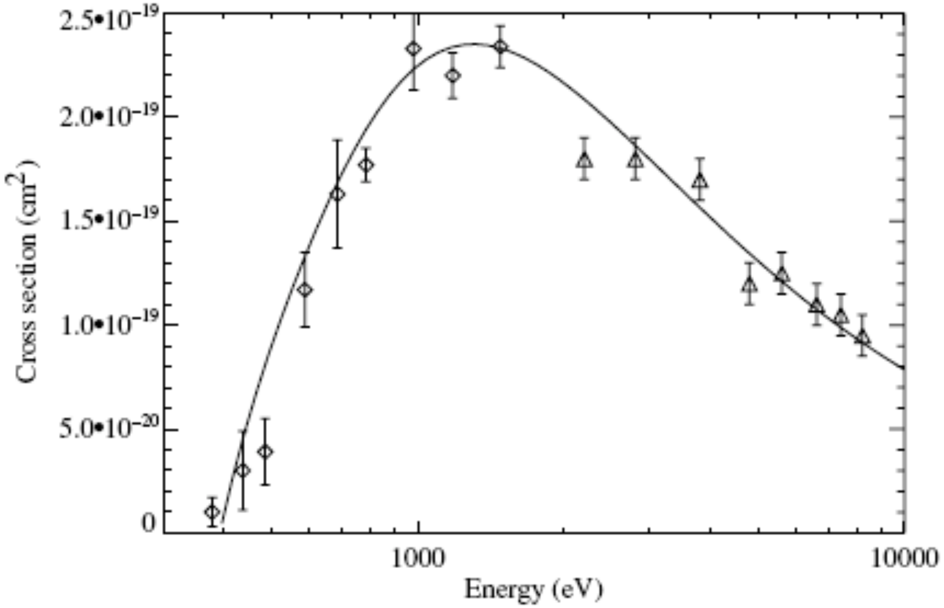


**Fig. 3.** FAC DI cross sections for C V and the measurements of Crandall et al. (1979a) (diamonds) and Donets & Ovsyannikov (1981) (triangles, plotted with an arbitrary 10% experimental error).

There are discrepancies among calculations and (sparse) experiments (see also Dufresne & Del Zanna 2019,2020)

CHIANTI:

```
IDL>e= 350+ 10.*indgen(1000)
plot_oi, e,ioniz_cross('c_5',e),chars=2,/xst
```

# EA collisional ionisation

- Ionisation via excitation-autoionization (EA) is an additional process important for some ions at higher temperatures.
- Available calculations are sparse. See Dufresne & Del Zanna for examples and references.

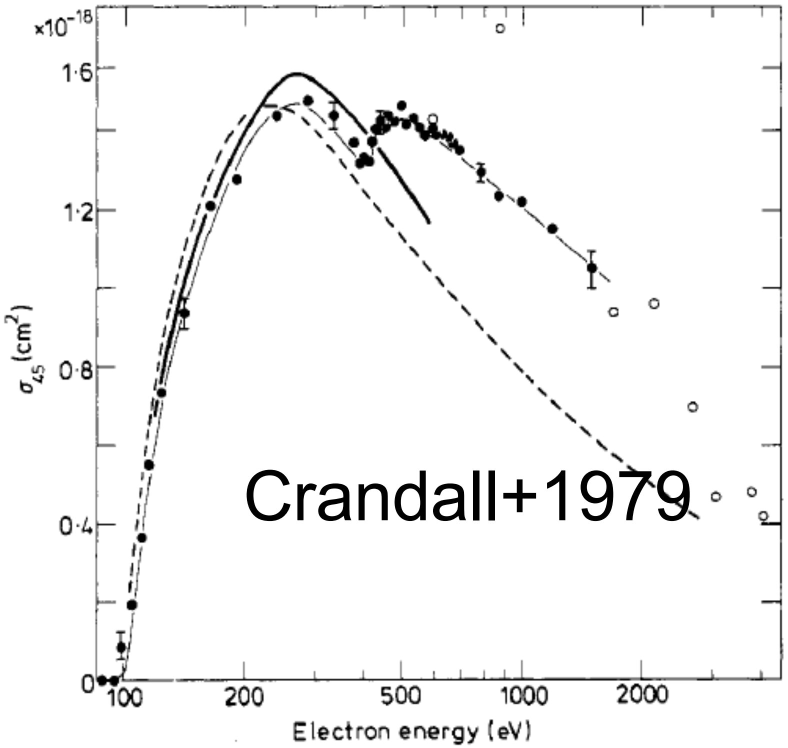


**Figure 2.** Cross section for electron impact ionisation of $N^{4+}$. The connected full circles are present data; open circles are data of Donets and Ovsyannikov (1977); broken curve is scaled Coulomb–Born of Golden and Sampson (1977); full bold curve is Coulomb–Born by Moores (1978).

CHIANTI:

```
IDL>e= 100+ 10.*indgen(1000)
plot_oi, e,ioniz_cross(‘n_5',e),chars=2,/xst
```

# 3-Body recombination

Three body recombination is the inverse process of collisional ionization. The rate coefficient for the three body recombination $C_{ji}^{3\mathrm{B}}$ can be obtained by applying the principle of detailed balance:

$$N_\mathrm{e}\, N_i(Z^{+r})\, C_{ij}^{\mathrm{I}} = N_\mathrm{e}\, N_j(Z^{+r+1})\, C_{ji}^{3\mathrm{B}} \quad ,$$

which leads to

$$C_{ji}^{3\mathrm{B}} = C_{ij}^{\mathrm{I}} = \frac{g_i}{g_j}\frac{N_\mathrm{e}}{2}\left(\frac{h^2}{2\,\pi\, m\, kT_\mathrm{e}}\right)^{3/2}\,\mathrm{e}^{-(E_i - E_f)/kT_\mathrm{e}}$$

for Maxwellian electrons

# Radiative recombination (RR)

- It is a recombination by a free electron. The photon-induced is not usually relevant. Rates are normally obtained from the PI cross-sections via detailed balance. Level-resolved (initial and final) cross-sections are needed. Very accurate values are available for H, He and several ions.
- Level-resolved rates for all ions obtained from simplified PI (background distorted-wave) are available at the UK APAP network.
- CHIANTI has the total of these rates, between ground states. Since v.9 CHIANTI introduced some level-resolved rates in two-ion models (Del Zanna, see Appendix of Dere+2019).

# Dielectronic recombination (DR)

When a free electron is captured into an autoionization state of the recombining ion while a bound electron is excited. The ion is in a doubly-excited unstable state. It can then autoionize (releasing a free electron) or produce a radiative transition into a bound state (a satellite line) producing a recombined ion.

Shown by Burgess (1964,1965) to be a very important effect for the solar corona at high temperatures, typically 10 times more effective than RR

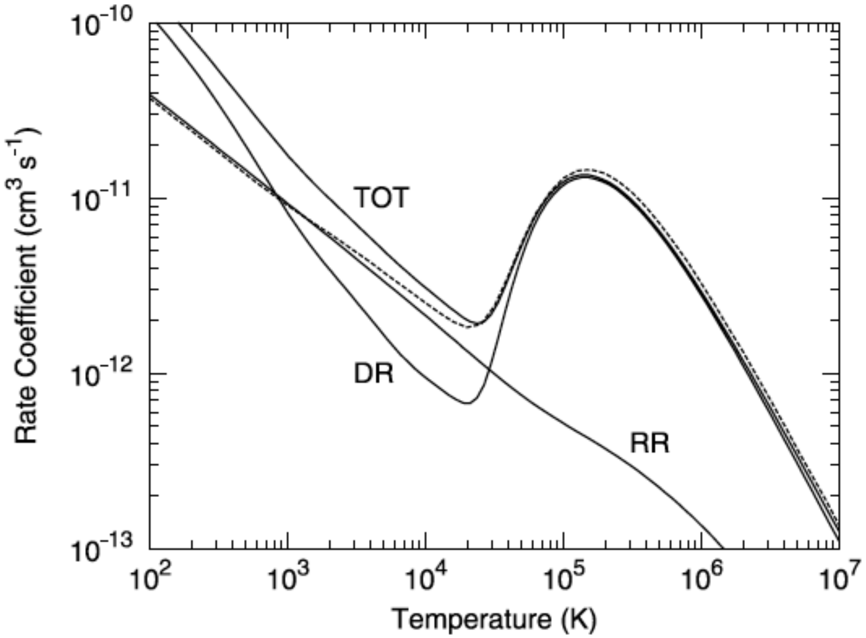


FIG. 9.—Total ground state rate coefficients for $O^{2+}$. *Solid curves*, RR (present), DR (Zatsarinny et al. 2004), and total (DR + RR) from AUTOSTRUCTURE; *dashed curve*, total (unified DR + RR) from ***R***-matrix (Nahar 1999).

Badnell (2006)

CHIANTI:

```
IDL> t= 100+ 10.*lindgen(1e6)
plot_oo, t, recomb_rate('o_3’,t,$
/radiative),chars=2,/xst

oplot, t, recomb_rate('o_3',t, /diel),line=2
```

# DR

Level-resolved (final states) DR rates from ground and metastable states are available for many ions at the UK APAP network, calculated as part of the DR project (Badnell+1998)

CHIANTI mostly has these DR rates , but totals and from ground states only

There is a series of papers with experimental results

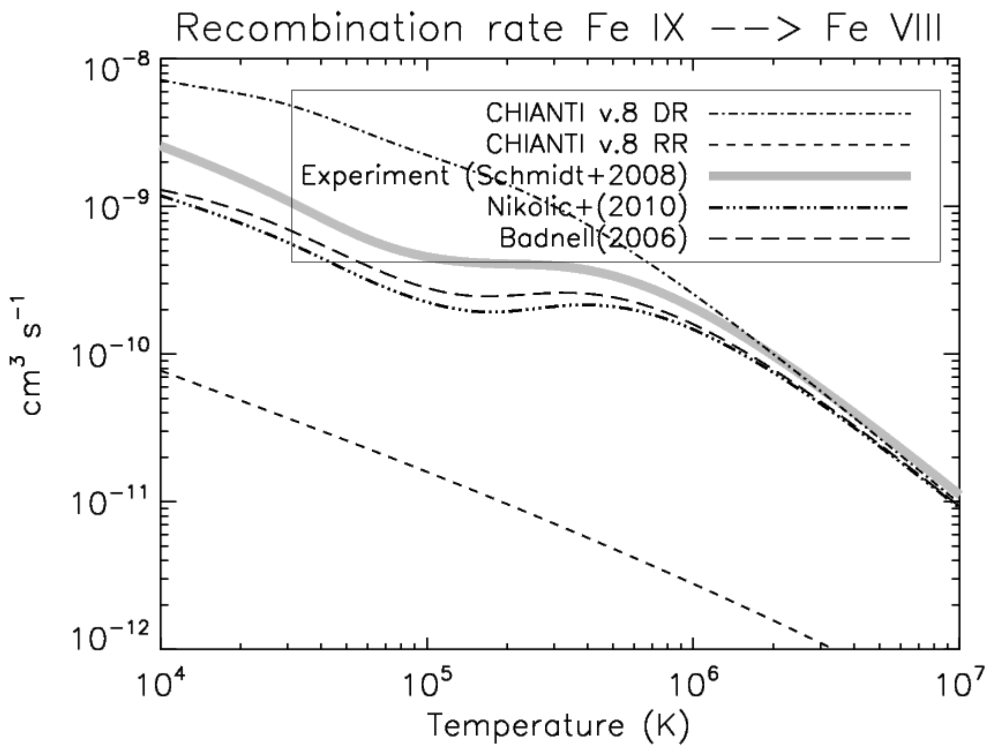

# Density dependence on DR

High electron densities affect the DR rate coefficients in a complex way.

Discussed by
Burgess & Summers (1969)
(see also Summers 1972,1974).

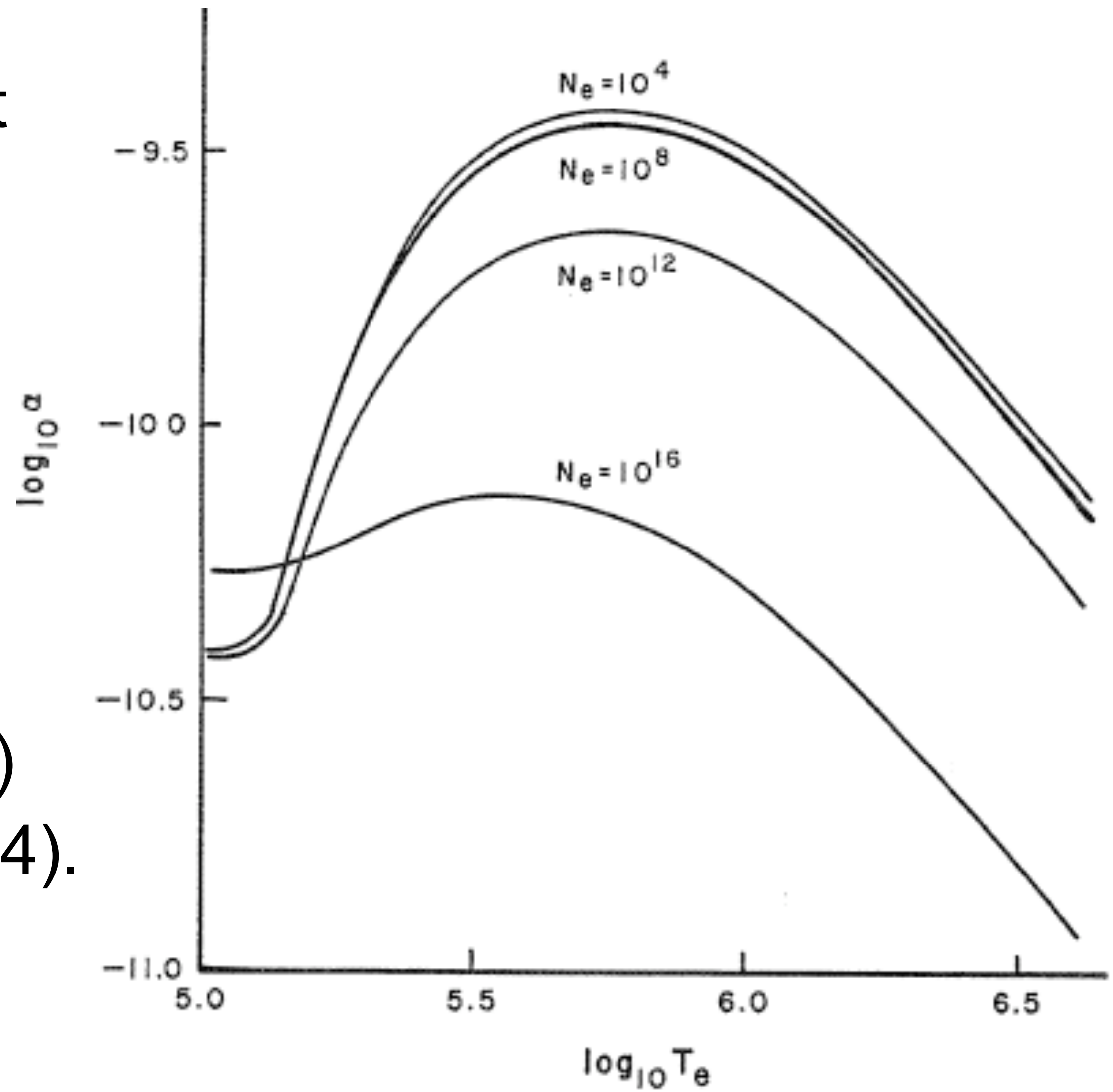


FIG. 7.—Fe $^{+8}$ + $e$ recombination coefficient

# Ionisation equilibrium at zero density

$$\frac{1}{N_e}\frac{dN_r}{dt} = N_{r-1}S_{r-1} - N_r(S_r + \alpha_r) + N_{r+1}\alpha_{r+1}$$

Each ion is considered to be in the ground state and rates only depend on Te
Usually called coronal approximation, but in reality it is a **zero density**
(lower than densities of planetary nebulae)

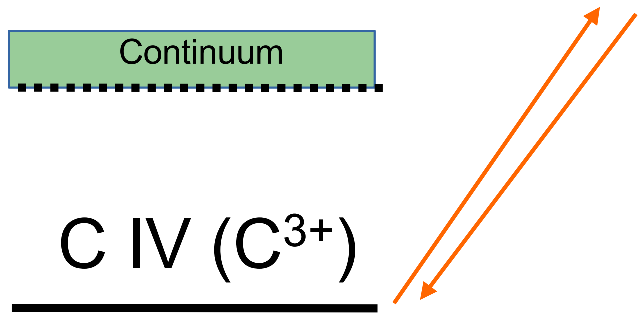


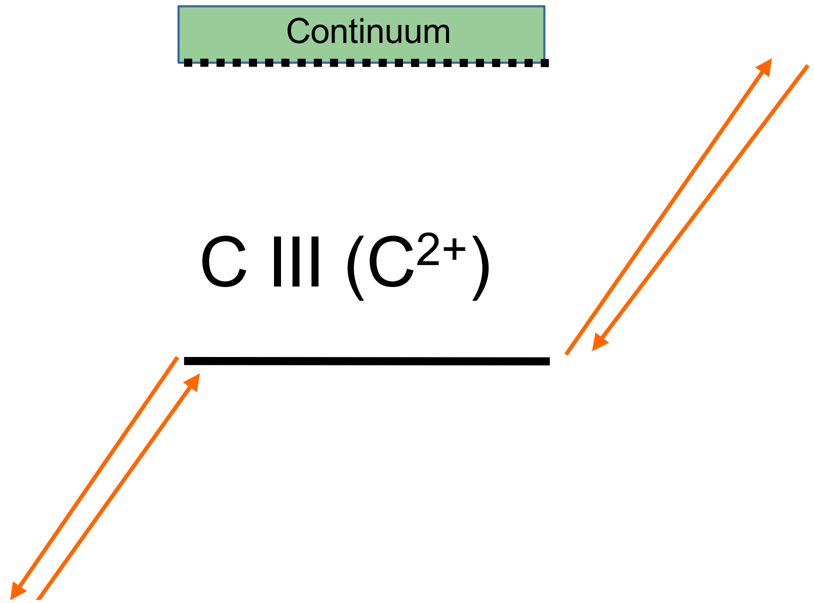


In equilibrium, the relative two-ion abundance is obtained from the ratio of the rates:

$$\frac{N_{r+1}}{N_r} = \frac{S_r(T)}{\alpha_{r+1}(T)}$$

the timescales for $N_r$ to ionise are $1/(N_e S_r^e)$, while to recombine $1/(N_e \alpha_r)$

# CI - DR

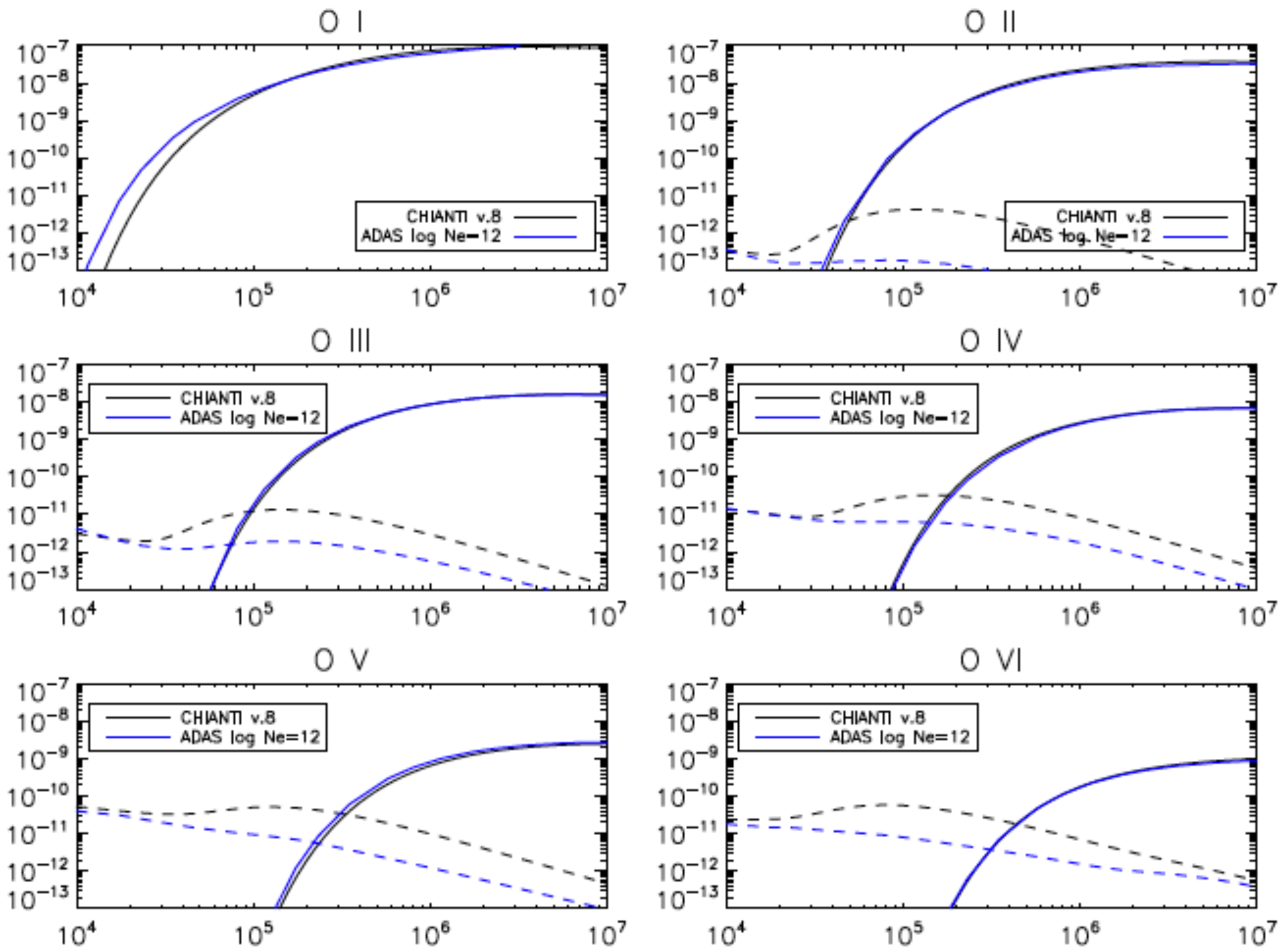


There are CHIANTI routines to plot these rates.
Note the Ne-dependence of the DR rates (ADAS)

t=10^[5.+0.2*indgen(10)]
plot_io, chars=2 ,alog10(t), ioniz_rate('o_4',t)

# Zero density

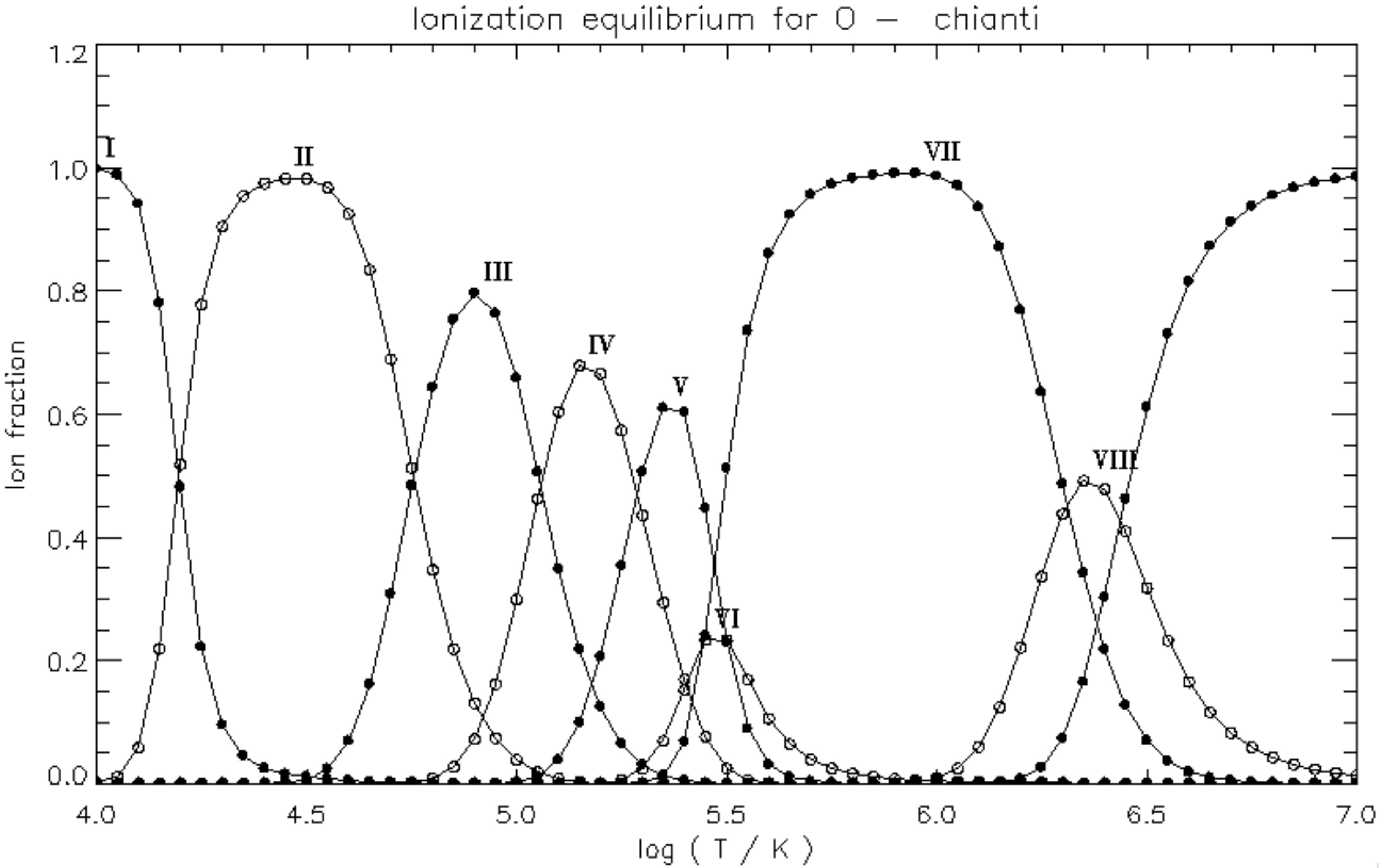


CHIANTI: IDL> plot_ioneq,’o’

# ionisation T - DKIST

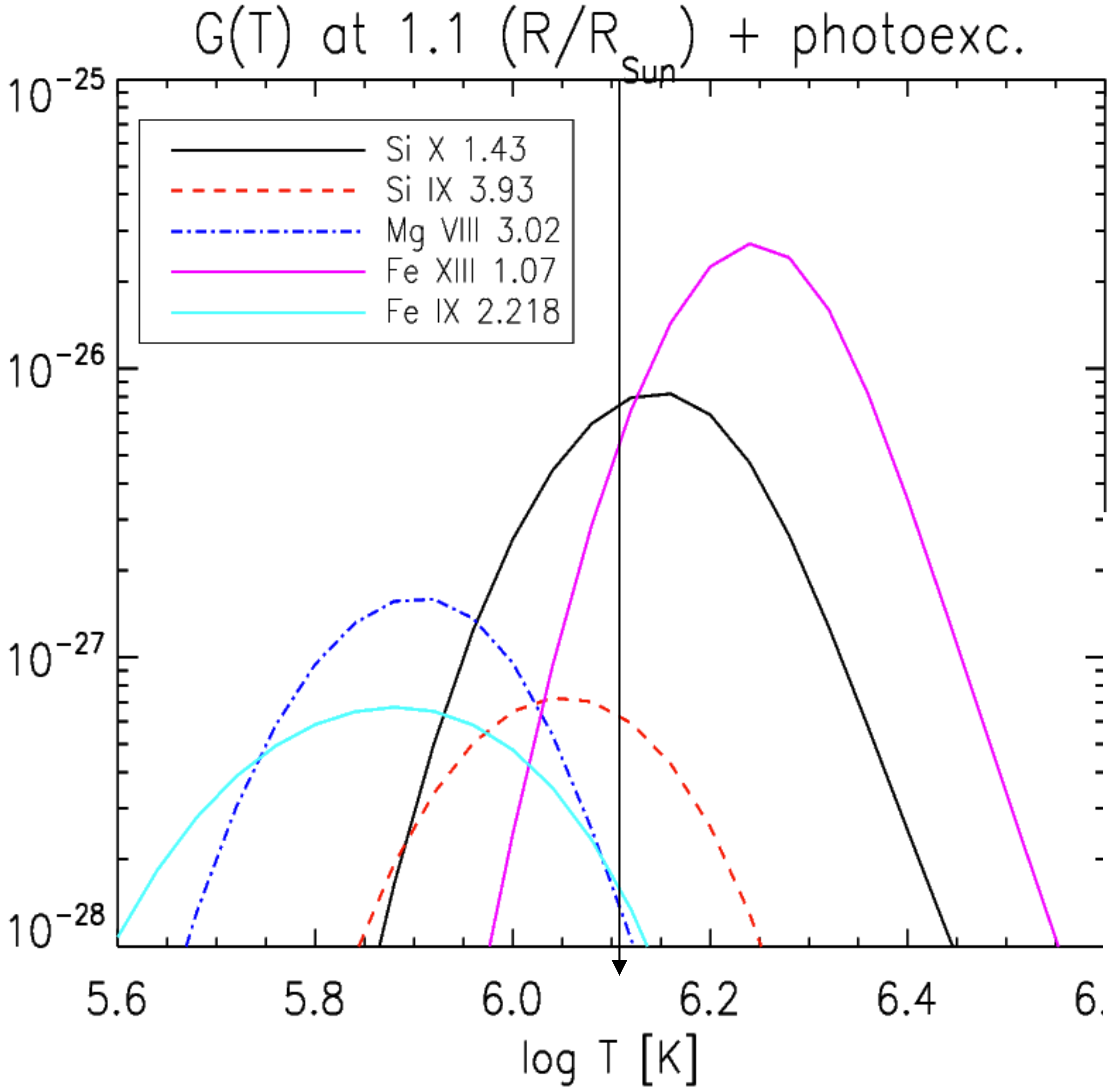


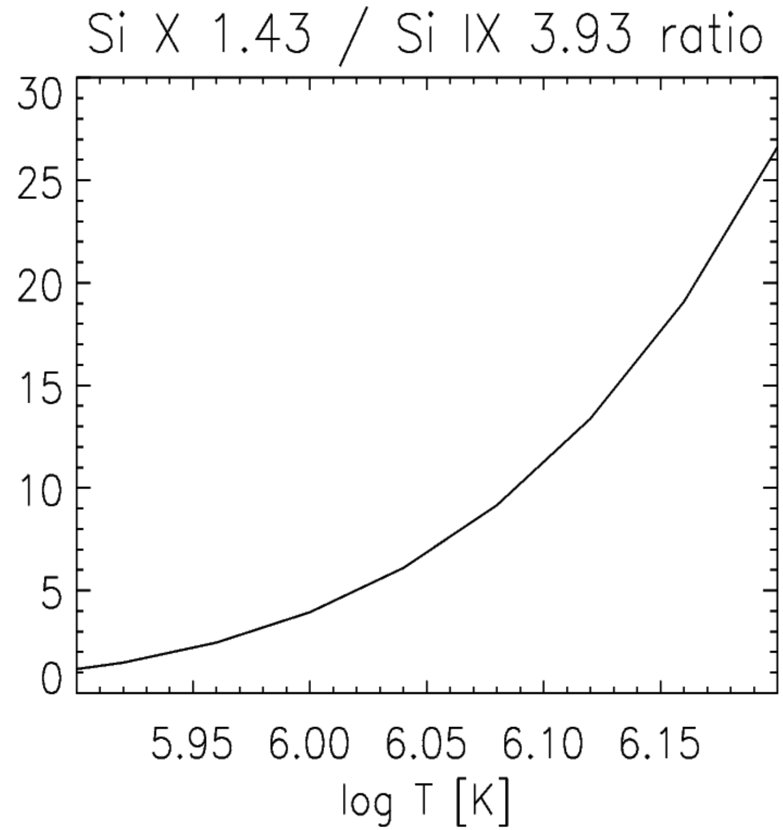

# Photo-Ionisation (PI)

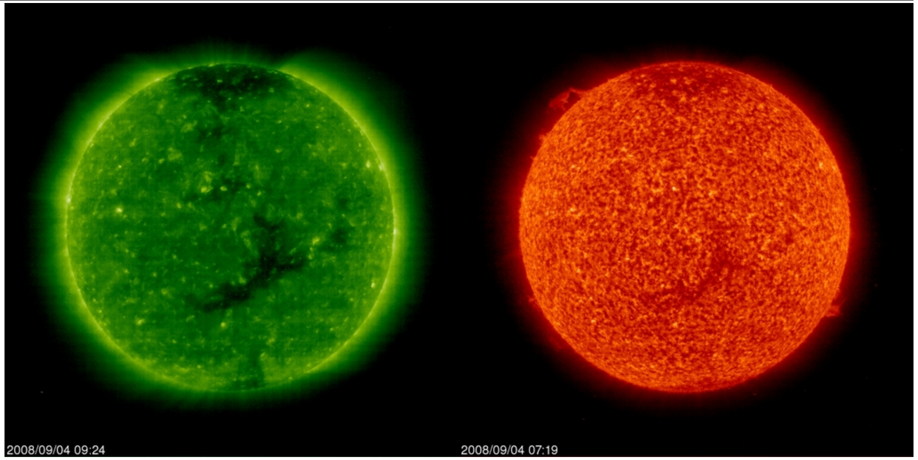


Photoionization is normally negligible in the lower solar corona. But it is important for example for prominences, the low transition region and the outer corona.

Important for H, He which recombine after being ionized by the coronal radiation.

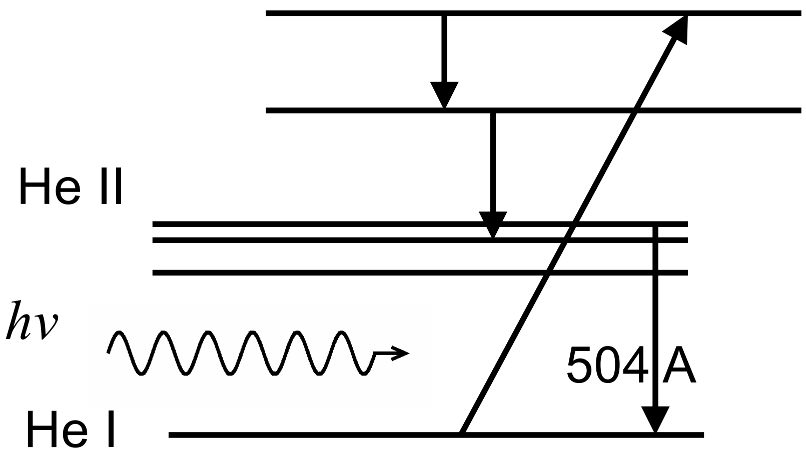


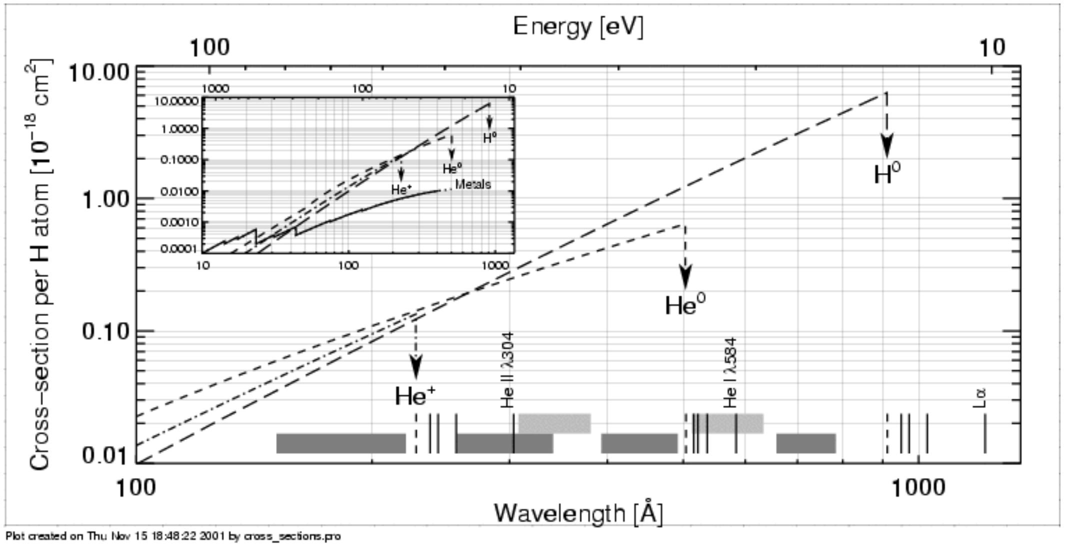


Andretta, Del Zanna, Jordan (2003)

# PI

$$\alpha_{ic}^{\mathrm{PI}} = 4\pi \int\limits_{\nu_0}^{\infty} \frac{\sigma_{ic}^{(\mathrm{bf})}(\nu)}{h\nu} J_\nu \, \mathrm{d}\nu$$

$$J_\nu = \frac{\Delta\,\Omega}{4\pi}\,\overline{I_\nu} = W(r)\,\overline{I_\nu}\,,$$

$$W = \frac{1}{2}\left[1 - \left(1 - \frac{1}{r^2}\right)^{1/2}\right]$$

$$r = \frac{R}{R_*}$$

Data are available from the Opacity Project (Seaton+), the UK APAP Network and the literature.

Only cross-sections from ground states are available in CHIANTI.

PI from populated excited states can be very important, see e.g. Dufresne, Del Zanna+ (2019,2020,2021) and for He Del Zanna+2020

# C III PI for QS

```
lam=1.+lindgen(300)
plot, lam, verner_xs(6,3, lam), chars=2, ytit='10!U-18!N cm!U-2!N',$
xtit='Wavelength (Angstroms)
```

The spectrum close to the PI edge is important.

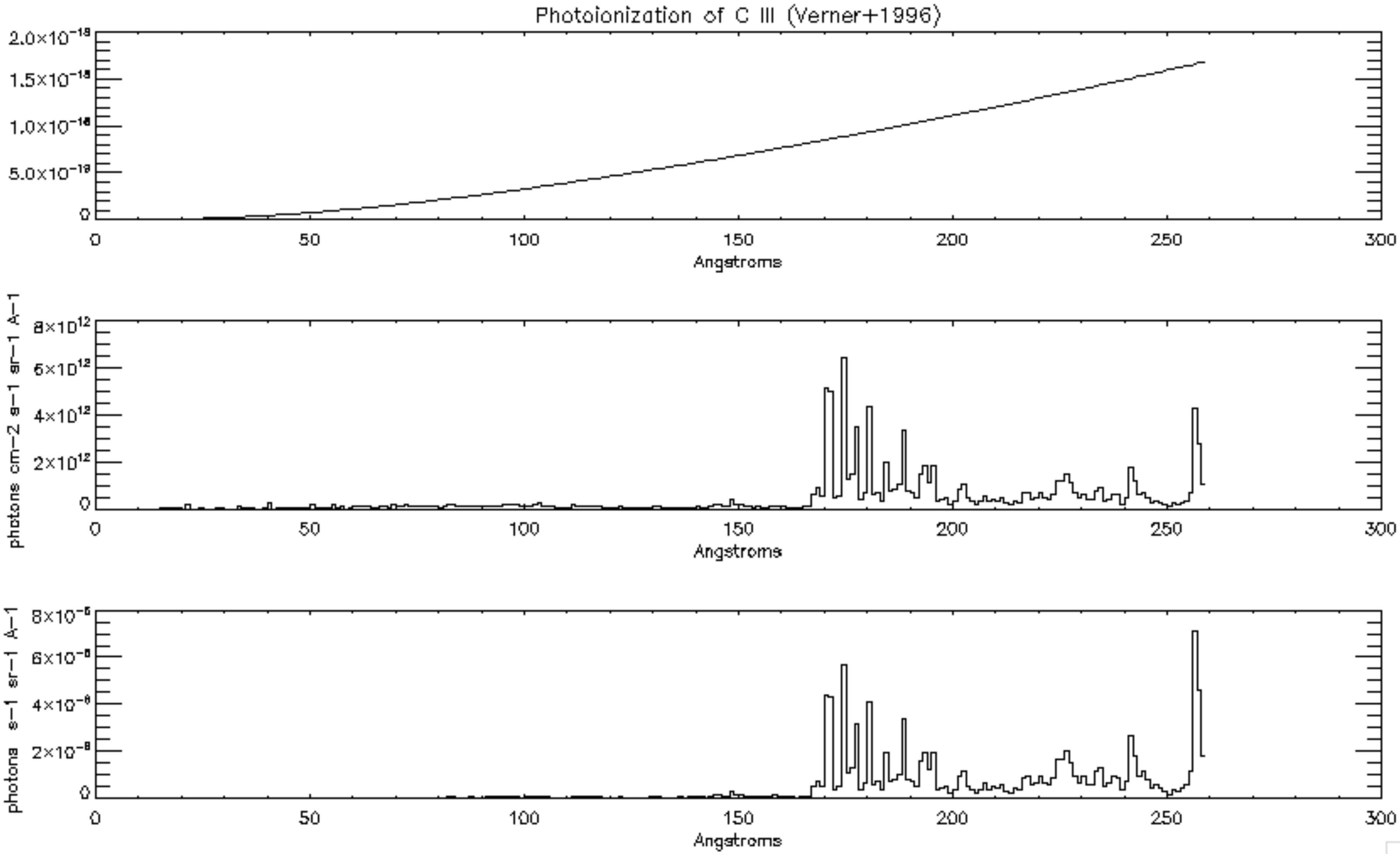

# PI

PI is also important when H,He absorbs background emission as in filaments, spicules, etc.

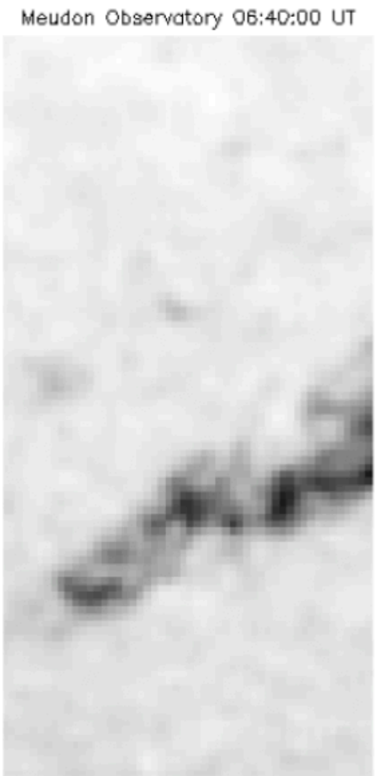


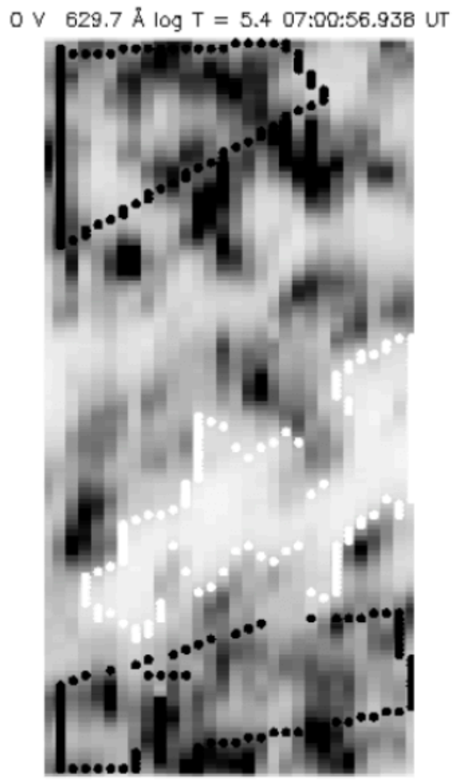


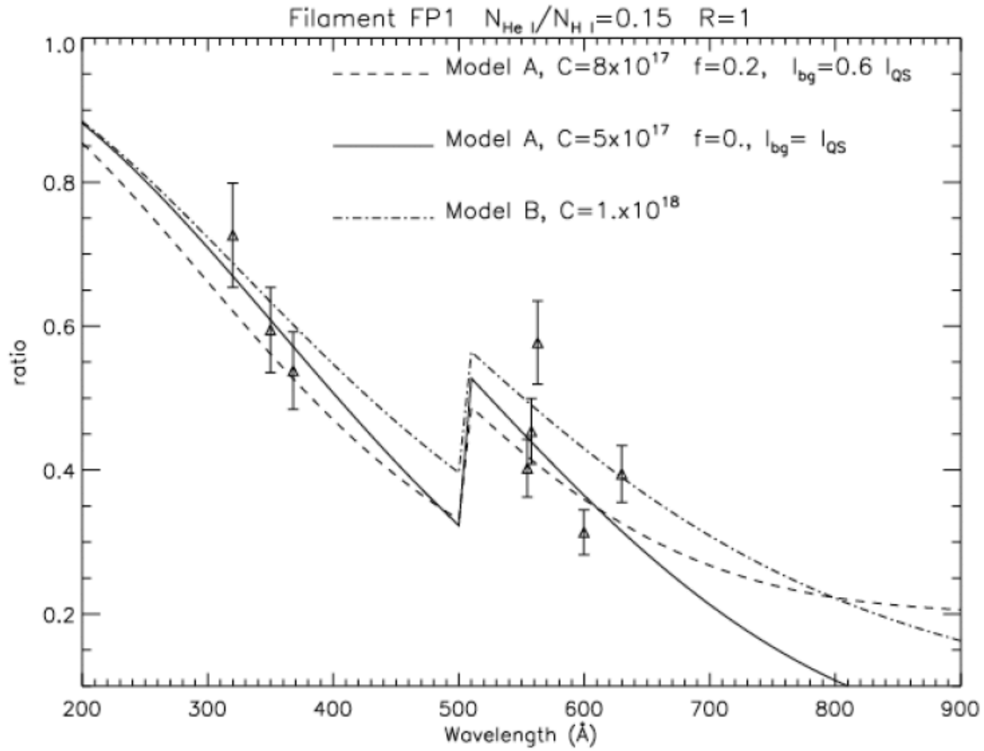


Del Zanna+2004

# PI for O

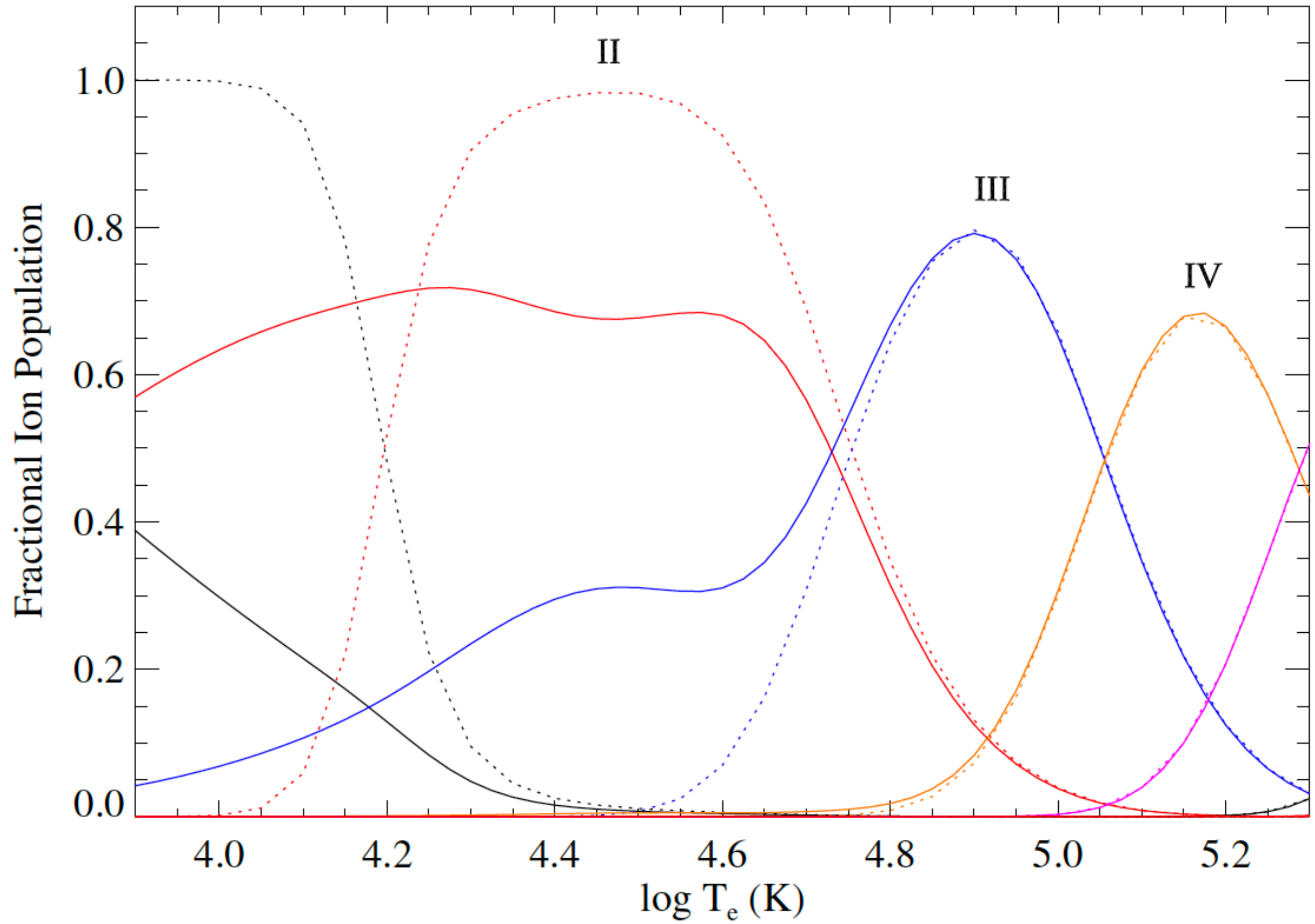


Dufresne Del Zanna
Badnell (2020)

**Figure 3.** Coronal approximation for oxygen: solid line - this work including photo-ionisation only, dotted - CHIANTI v.9. Ions are highlighted by Roman numerals and different colours.

# CR Modelling: Level-Resolved

Two main effects: 1) suppression of DR and 2) CI from metastable levels.
A new approach – building a level-resolved matrix with all the main levels for all the ions, see Dufresne & Del Zanna (2019,2020) with some approximations. Full CRMs are being built.

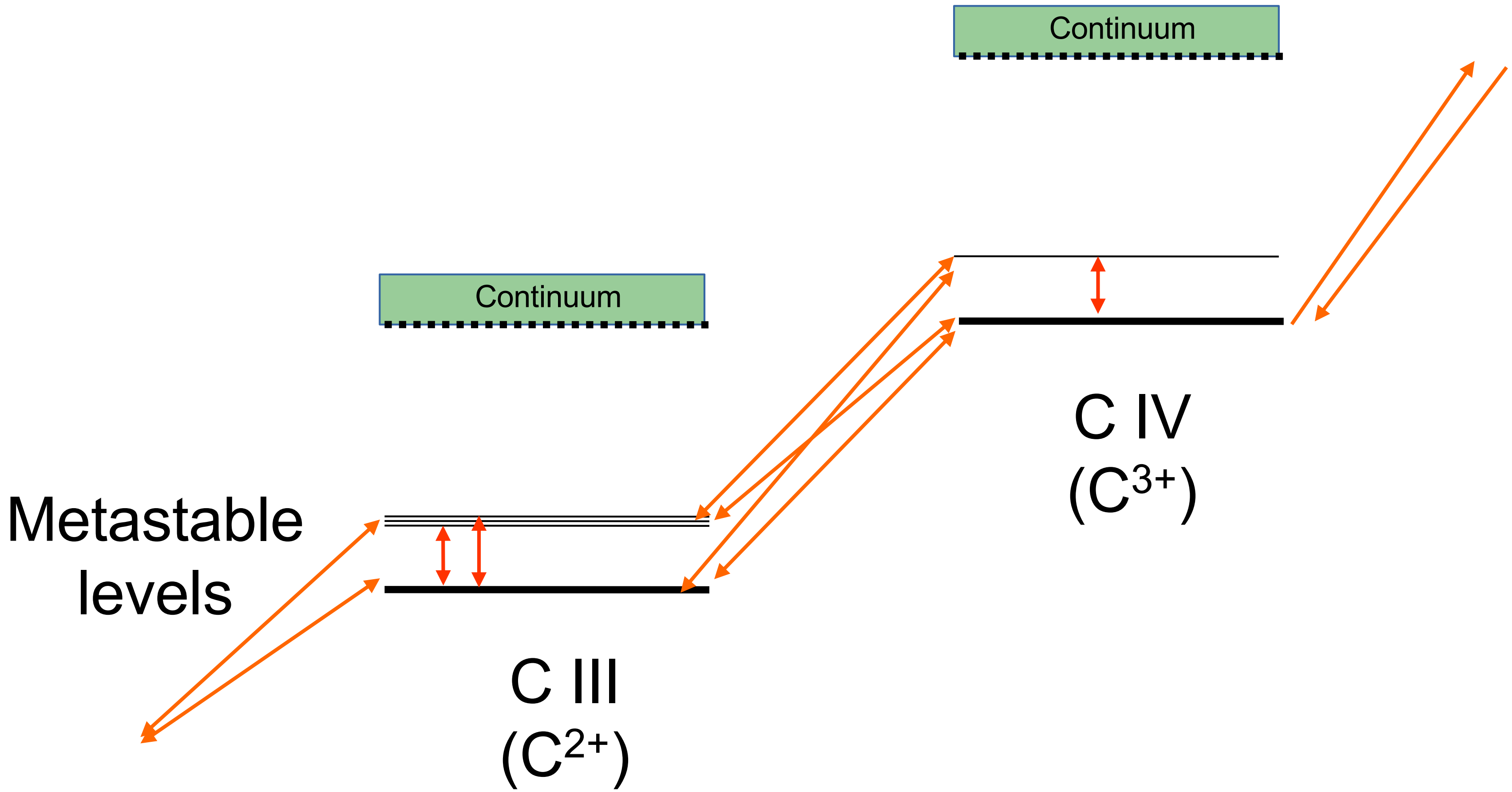

# Combined CI and DR effects - C

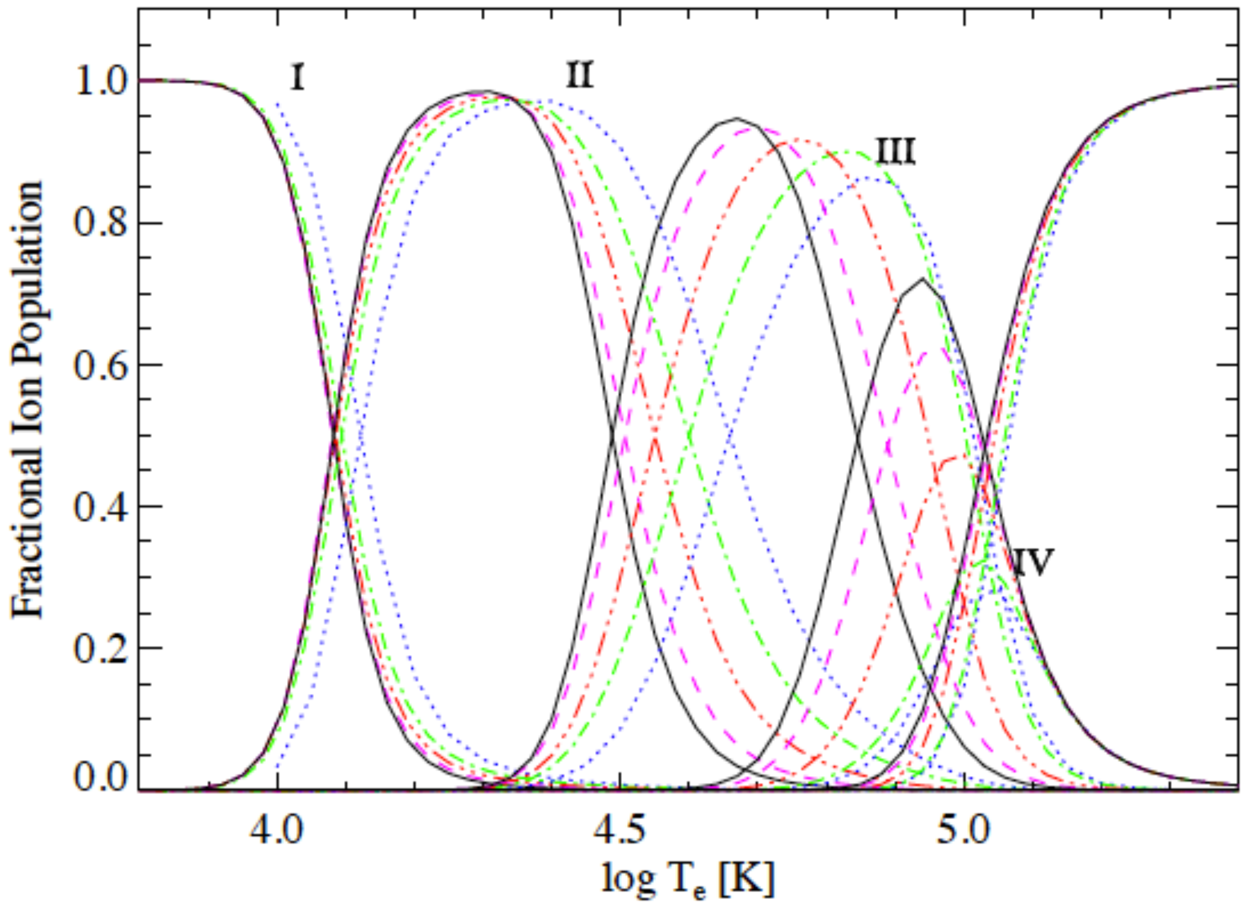


**Fig. 12.** Combined effect of density on level-resolved, electron impact ionisation and DR suppression in the CR model; blue dotted line - CHIANTI v.8, green dash-dotted - this work at $10^4$ cm$^{-3}$ density, red dash-dot-dotted - $10^8$ cm$^{-3}$, purple dashed - $10^{10}$ cm$^{-3}$, black solid - $10^{12}$ cm$^{-3}$.

Dufresne & Del Zanna

# Combined CI and DR effects - O

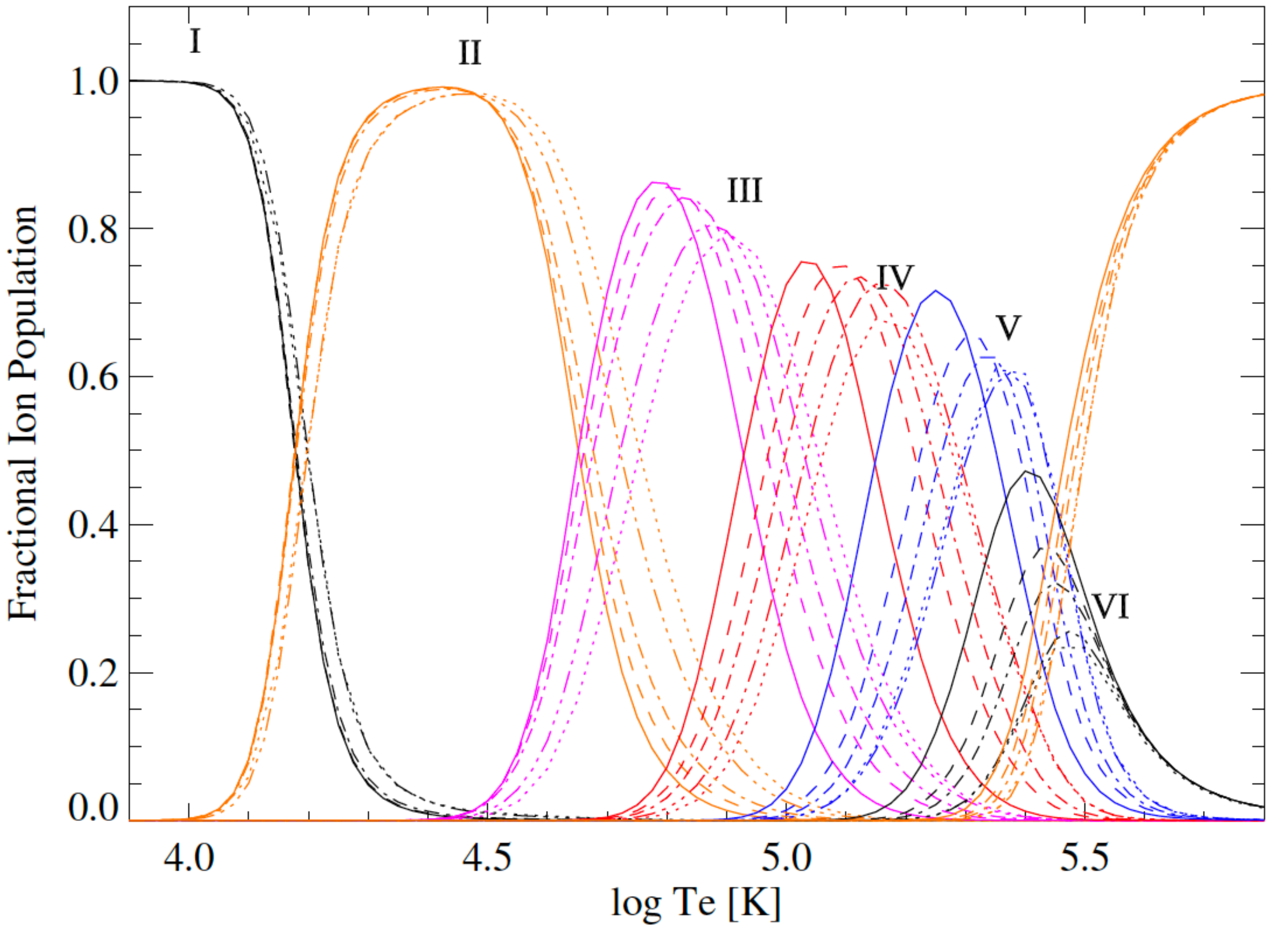


**Figure 9.** Final ionisation equilibrium of oxygen at various densities; dotted line - CHIANTI, dash-dot-dotted - this work at $10^4$ $cm^{-3}$ density, dash-dotted - $10^8$ $cm^{-3}$, dashed - $10^{10}$ $cm^{-3}$, solid - $10^{12}$ $cm^{-3}$. Individual charge states are highlighted by Roman numerals and different colours.

Dufresne
Del Zanna,
Badnell

# Charge tranfer (CT)

Very important for low charge states of some elements. Mostly due to interaction (both ways) with neutral H,He, which themselves are difficult to model (see issues with He in the corona in Del Zanna+2020). Availability of CT rates is sparse.

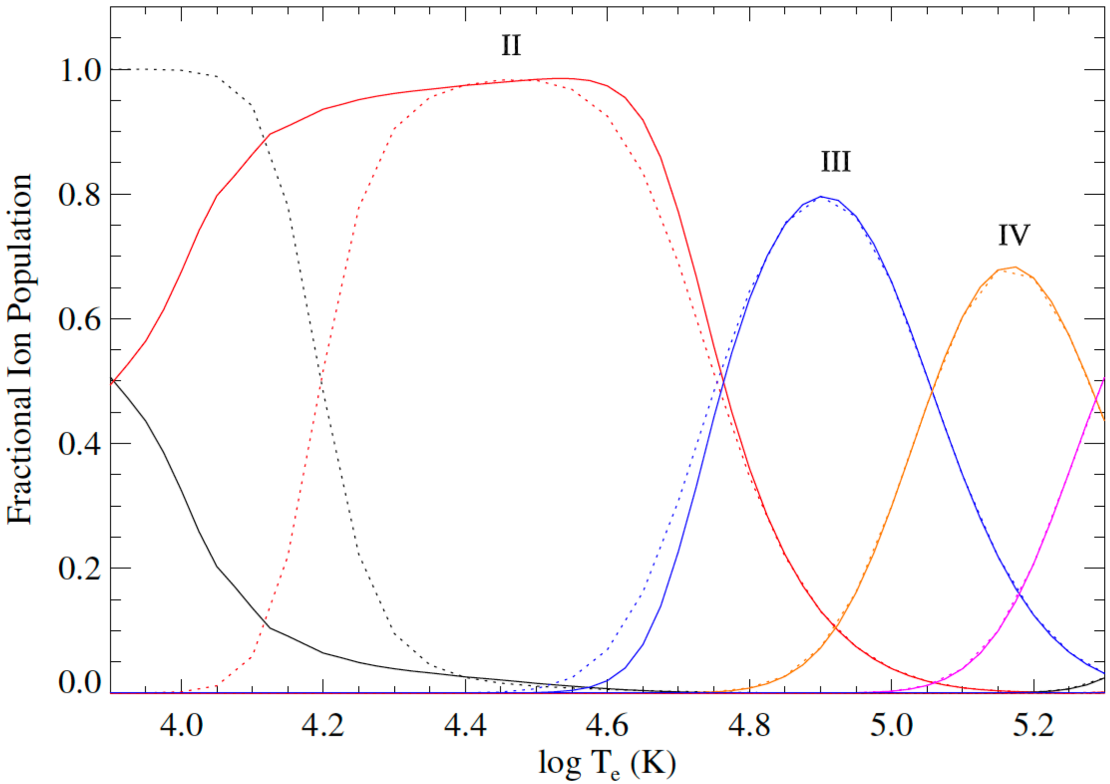


**Figure 4.** Coronal approximation of oxygen: solid line - this work including charge transfer only, dotted - CHIANTI v.9. Ions are highlighted by Roman numerals and different colours.

O results for quiet Sun

Dufresne, Del Zanna
Badnell 2021

# Ne-dependent CI, DR, + PI, CT

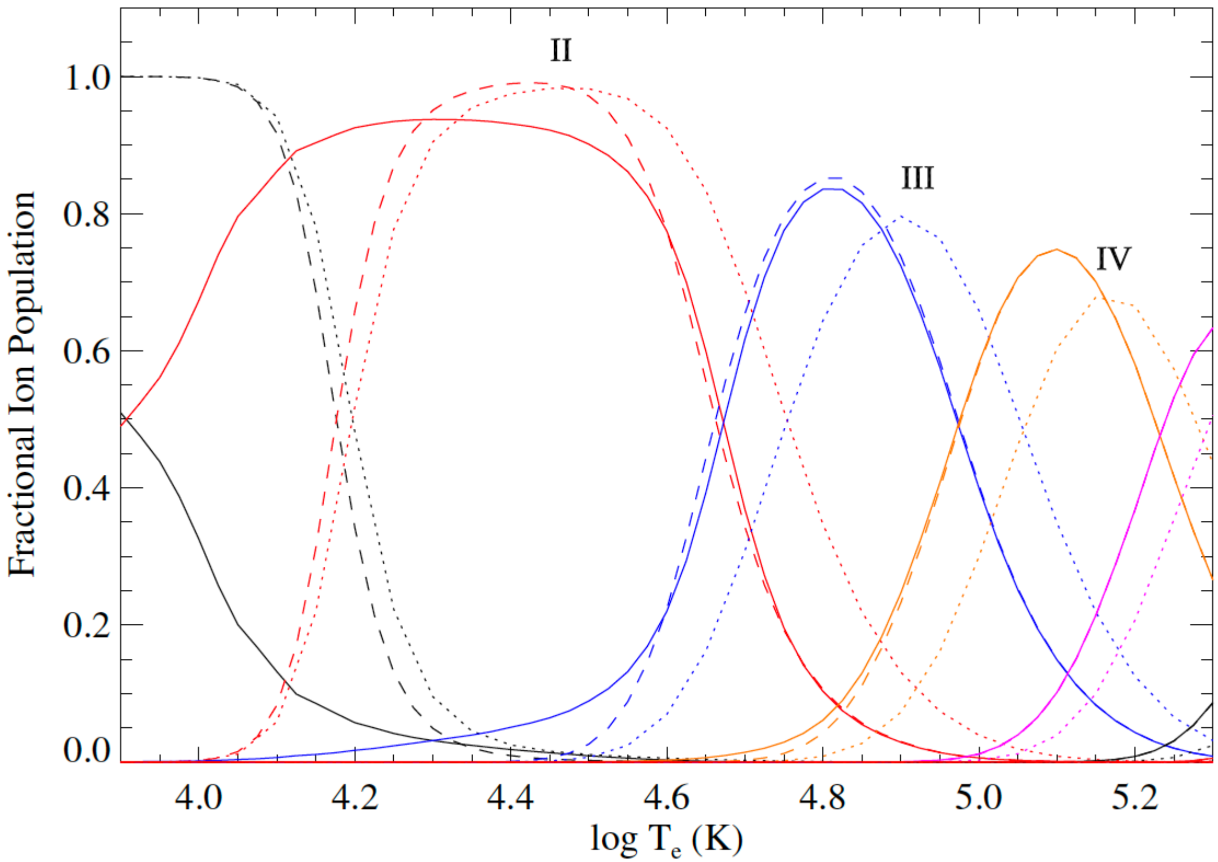


**Figure 5.** Ionisation equilibrium of oxygen: solid line - full model, dashed - Dufresne et al. electron collisional model, dotted - CHIANTI v.9. Ions are highlighted by Roman numerals and different colours.

O results for quiet Sun

Dufresne, Del Zanna
Badnell 2021

# Ionisation (time dependent)

Time-dependent ionization can substantially affect ion populations. Important in the solar wind (low Ne) and in active regions (whenever the heating timescales are short).

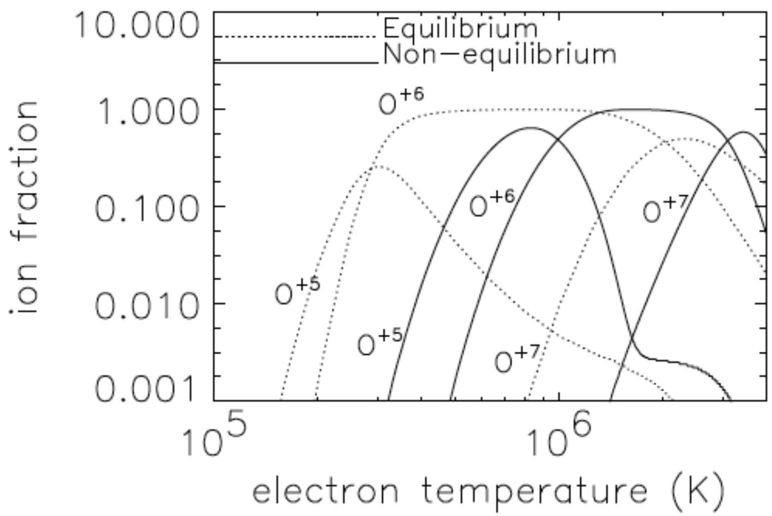


FIG. 5.—Oxygen ion fractions as a function of temperature for the equilibrium case (*dotted lines*) and when a constant flow speed of 30 km s$^{-1}$ is assumed (*solid lines*).

Esser+1998

Effects on spectral lines can be studied e.g. with the HYDRAD code (see examples in Bradshaw, Del Zanna & Mason (2003):

The radiative losses are calculated by solving the time-dependent ionization, including the advective term (the rate coefficients I and R are functions of temperature )

$$\frac{\partial}{\partial t}(N_r) + \frac{\partial}{\partial s}(N_r v) = N_{\rm e}(N_{r-1}S^e_{r-1} - N_r(S^e_r + R_r) + N_{r+1}R_{r+1}) \qquad N(X) = \sum_r N_r$$

# Ionization equilibrium with NMED

A fully self-consistent model is very complex and is not available. Approximations used within the KAPPA package show the effects for strong NMED:

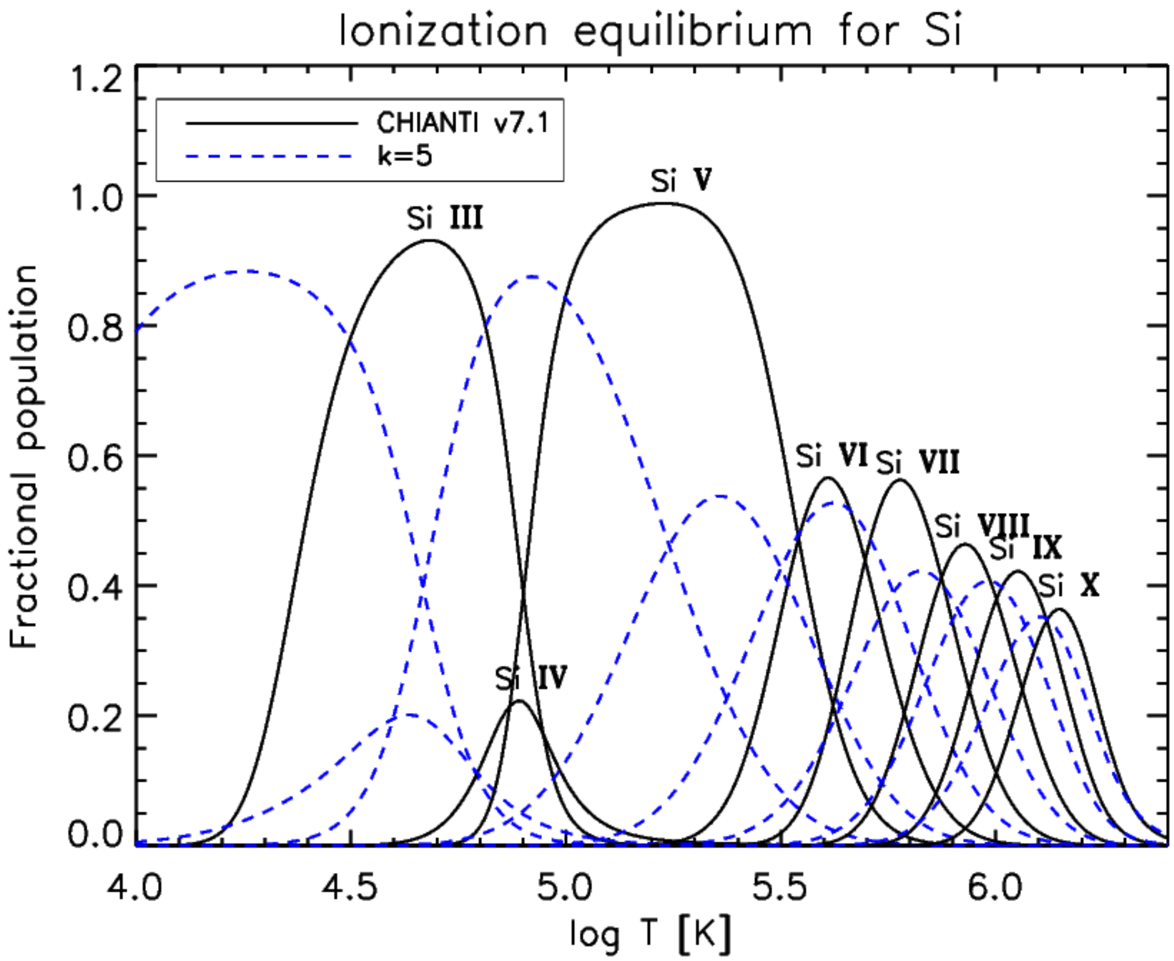

# DEM / EM

$$I(\lambda_{ji}) = \int_h N_e N_H A(X)\, G(N_e, T, \lambda_{j,i}) dh$$

If there is a continuous distribution of densities and temperatures along the line of sight, then we can define the column Differential Emission Measure (DEM) and total emission measure EM:

$$\mathrm{DEM}\ (\mathrm{T}) \equiv\ N_e N_H \frac{dh}{dT} \quad [\mathrm{cm}^{-5}\mathrm{K}^{-1}]$$
$$\mathrm{EM} \equiv \int_h N_e N_H dh = \int_T DEM(T)\ dT \qquad [\mathrm{cm}^{-5}]$$

$$I(\lambda_{ij}) = A(X) \int_T G(T)\, DEM(T)\, dT$$

The DEM(T) gives an indication of the amount of plasma along the line of sight that is emitting the radiation observed and has a temperature between T and T+dT. It is also used for measuring chemical abundances. Note that in the literature many different definitions of DEM, EM, and approximations can be found, for example:

$$\mathrm{DEM(T)} = \mathrm{N}_e^2 (dT/dh)^{-1}.$$
$$\mathrm{EM} = \int N_e^2 dh = \int DEM(T) dT$$

# Effective Te (Del Zanna & Mason 2014)

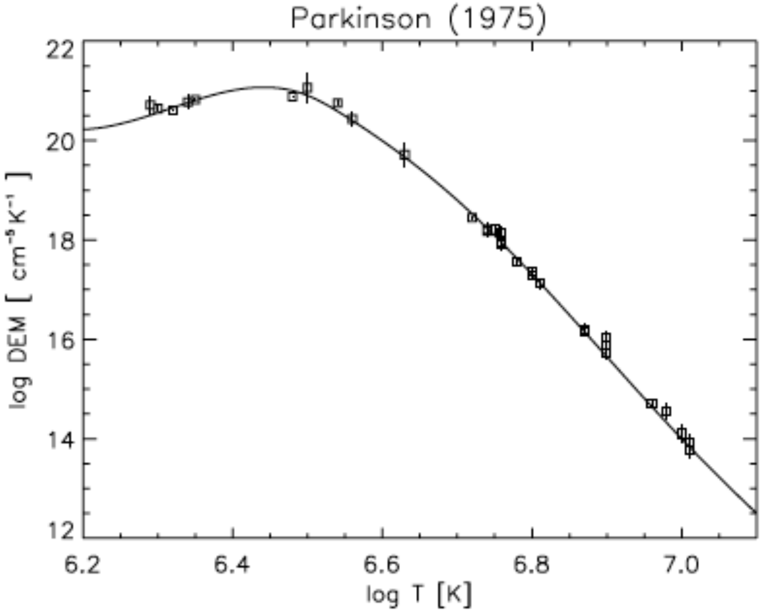


| $\lambda_{obs}$ | $I_{obs}$ | $T_{max}$ | $T_{eff}$ | $R$ | Ion |
|---|---|---|---|---|---|
| 13.55 | 0.163 | 6.98 | 6.47 | 0.59 | Ne IX |
| 13.70 | 0.334 | 6.56 | 6.47 | 0.92 | Ne IX |
| 13.82 | 0.174 | 6.80 | 6.51 | 1.01 | Fe XVII |
| 14.21 | 0.098 | 6.90 | 6.57 | 0.85 | Fe XVIII |
| | | | | | Fe XVIII |
| 16.78 | 1.9 | 6.74 | 6.50 | 1.15 | Fe XVII |

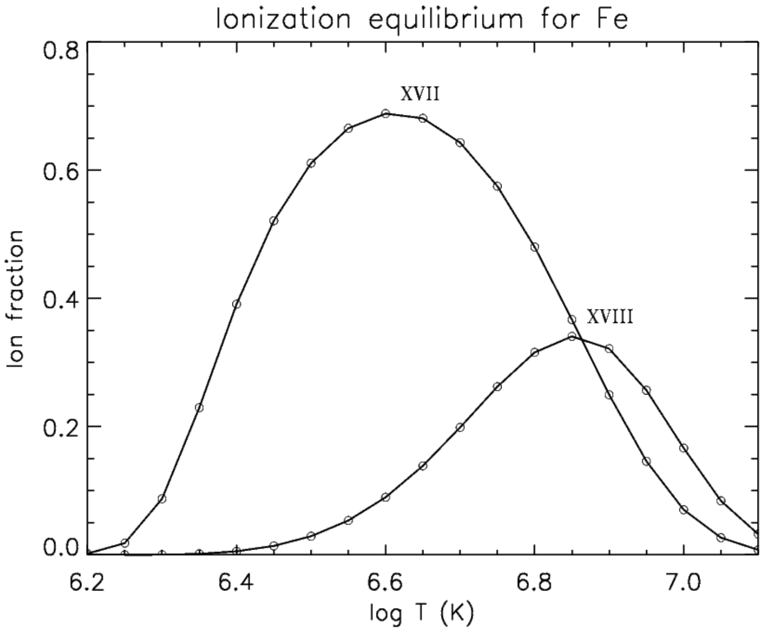


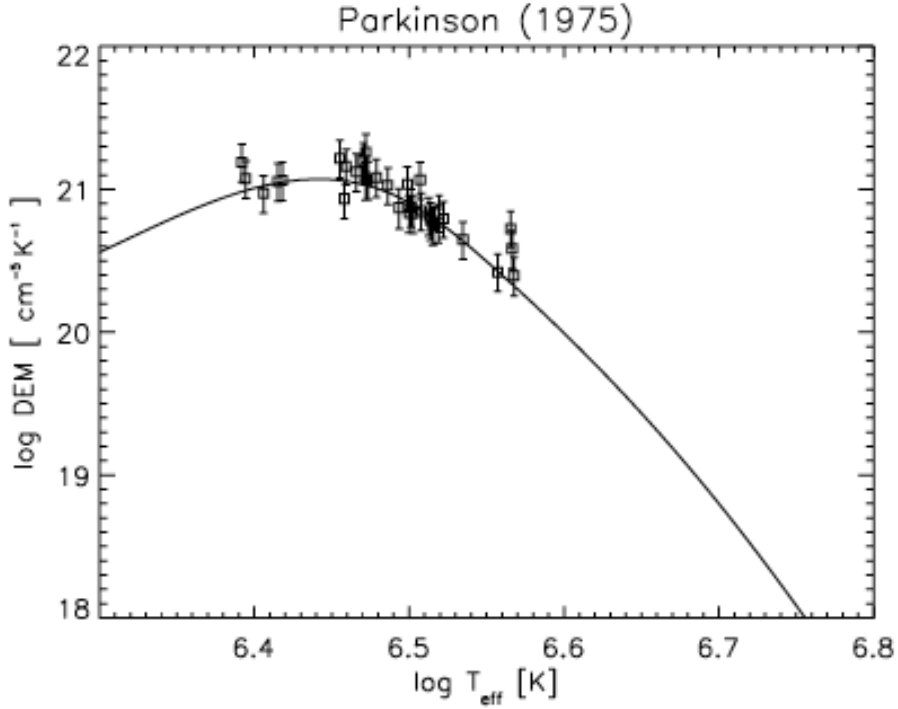


$$T_{\rm eff} = \int G(T)\,{\rm DEM}(T)\,T\,{\rm d}T \Big/ \int G(T)\,{\rm DEM}(T)\,{\rm d}T$$

# Spectroscopic filling factors

If one assumes an homogeneous slab of plasma of thickness dh, once elemental abundances are known, and a line intensity measured, one can obtain an average $\langle EM \rangle = \langle N_e^2 \rangle$ dh from which the path length dh can be estimated once $N_e$ is measured from e.g. a line ratio. Dere et al.(1987) used HRTS transition region C IV intensities and O IV densities form a line ratio to obtain path lengths of 0.1-10 km, much smaller than the observed sizes of the spicular structures (2400 km).

In other words, average $\langle N_e^2 \rangle$ obtained from the measured EM and estimated dh are much smaller than expected from the averaged densities obtained from line ratios.

$$f = \frac{\langle N_\mathrm{e}^2 \rangle}{\langle N_\mathrm{e} \rangle^2} = \frac{\langle EM \rangle}{\langle N_\mathrm{e} \rangle^2 \, \Delta h}$$

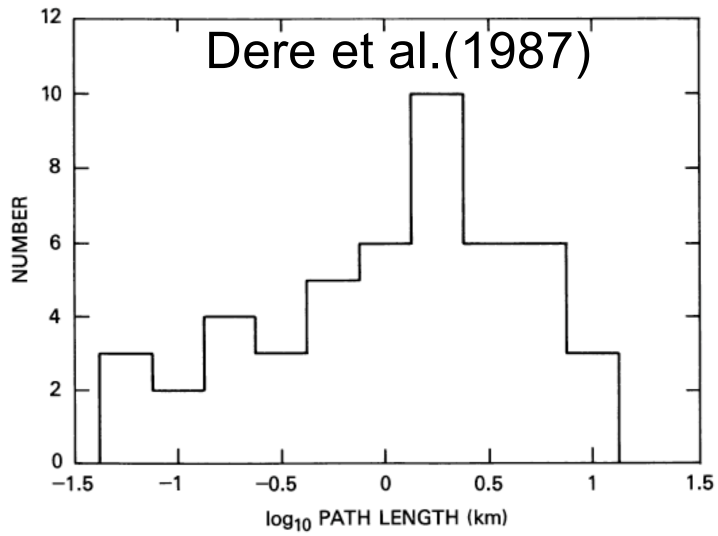


For coronal loops is close to 1 (SOHO/CDS: Del Zanna 2003, Del Zanna & Mason 2003; Hinode/EIS: Tripathi et al. 2009)

# EM loci

$$I_{ji} = \int f \; Ab(Y)\; G_{ji}(T_e)\; N_e^{\,2}\; dh \cong$$

$$Ab(Y) \int \; G_{ji}(T_e)\, dT < \int \; N_e^{\,2}\; dh / dT >$$

$$EM = \int N_e(h)^2\, dh \qquad \frac{Iobs}{Ab(Y)\; Gji(Te)}$$

Del Zanna (2003) re-introduced the EM loci method (Strong 1978) to AR loops. Isothermal !

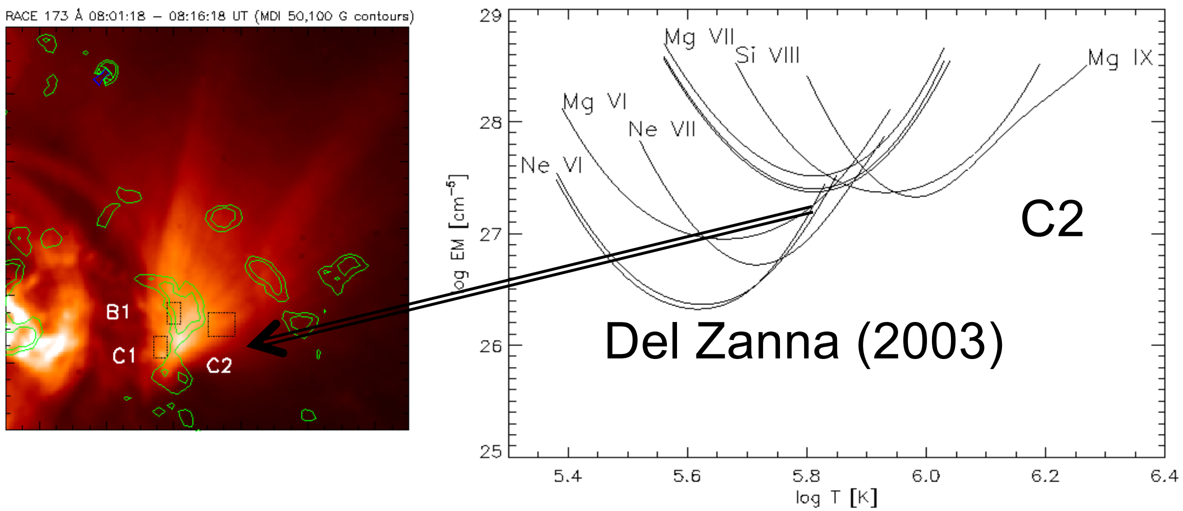


For each line and temperature $T_i$ the value $I_{ob}$ / $G(T_i)$ represents an upper limit to the value of the emission measure at that temperature, assuming that all the observed emission $I_{ob}$ is produced by an isothermal plasma at the temperature $T_i$.

# Anomalous ions

Lines from Li-like and Na-like ions are stronger (factors of 2-5) than predicted. These lines are the strongest in the UV !
**Si IV and C IV**

$$I_{ji} = \int Ab(X)\, G_{ji}(T_e)\, N_e^2\, dh$$

$$EM = \int N_e(h)^2\, dh$$

$$EMLoci = \frac{Iobs}{Ab(X)\; Gji(Te)}$$

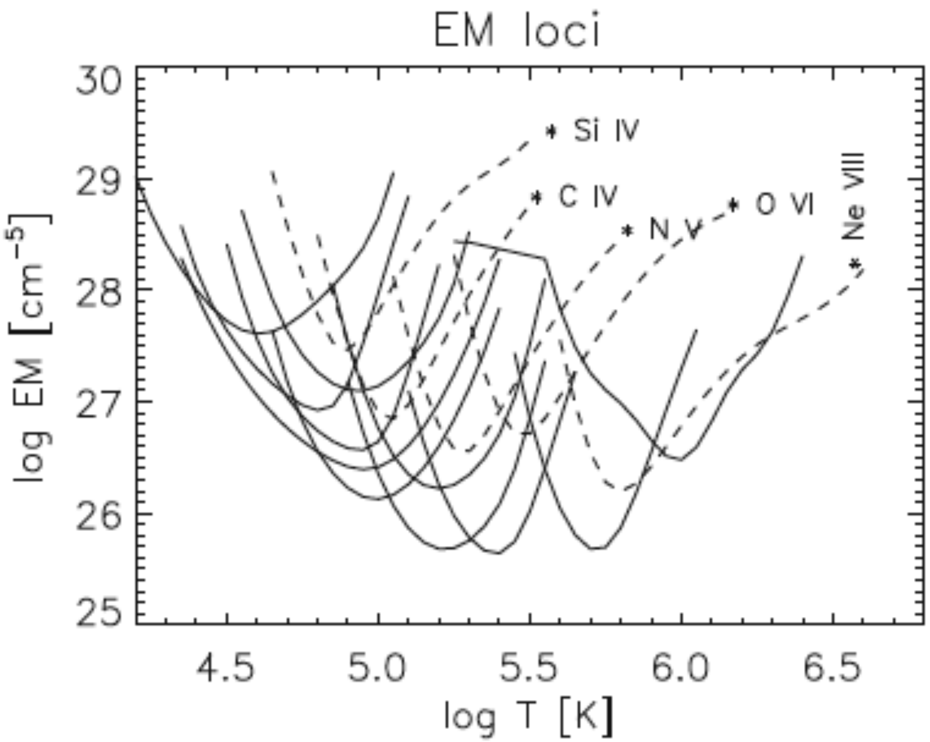


Sun-as-a-Star (Judge+1995, Del Zanna& Mason)

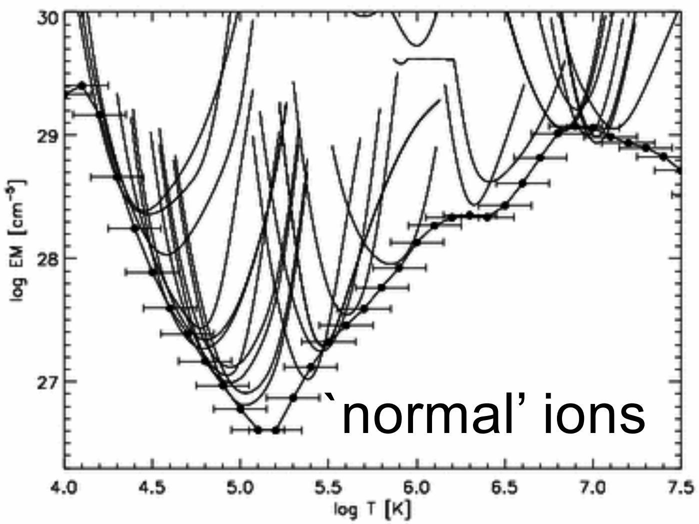


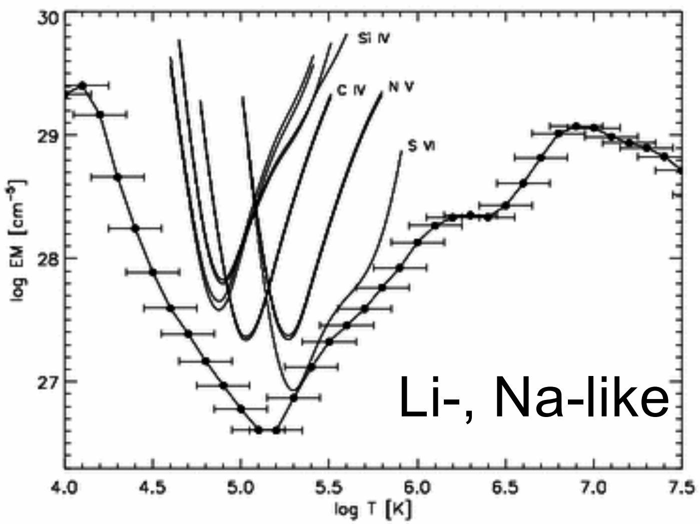


Del Zanna+(2002): first to show that the problem is present also in UV stellar observations

# Chemical abundances

- EM Loci or EM, DEM curves have been used since 1963 to measure the relative abundances in the corona, which are different than photospheric. There is a correlation with the FIP, indicating that the process occurs in the chromosphere (hard to model !), see one of the possible explanations in Laming, Sol. Phys. Living Review.

- Abundances relative to H can be measured using the continuum.

- For a review of key results see our Living Review, as many in the literature are incorrect for various reasons, one related to how the plasma is distributed in temperature.

# Chemical abundances in CH plumes

The Widing and Feldman (1989) approximation imposes a continuous distribution of the values $DEM_L$ plotted at the temperature of maximum ion abundance.

Incorrect abundances (by a factor of 10) can be obtained when plasma is isothermal as in CH plumes.

Plumes in coronal holes

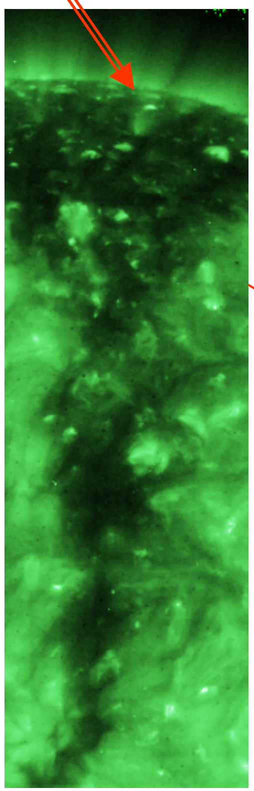

$$\mathrm{DEM_L} \equiv \frac{I_{\mathrm{ob}}}{Ab(X) \int_T C(T)dT}$$

FIP=10

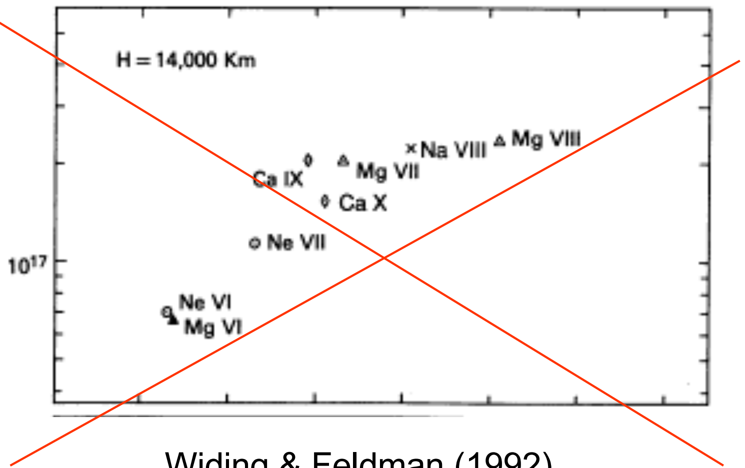


Widing & Feldman (1992)

FIP=0

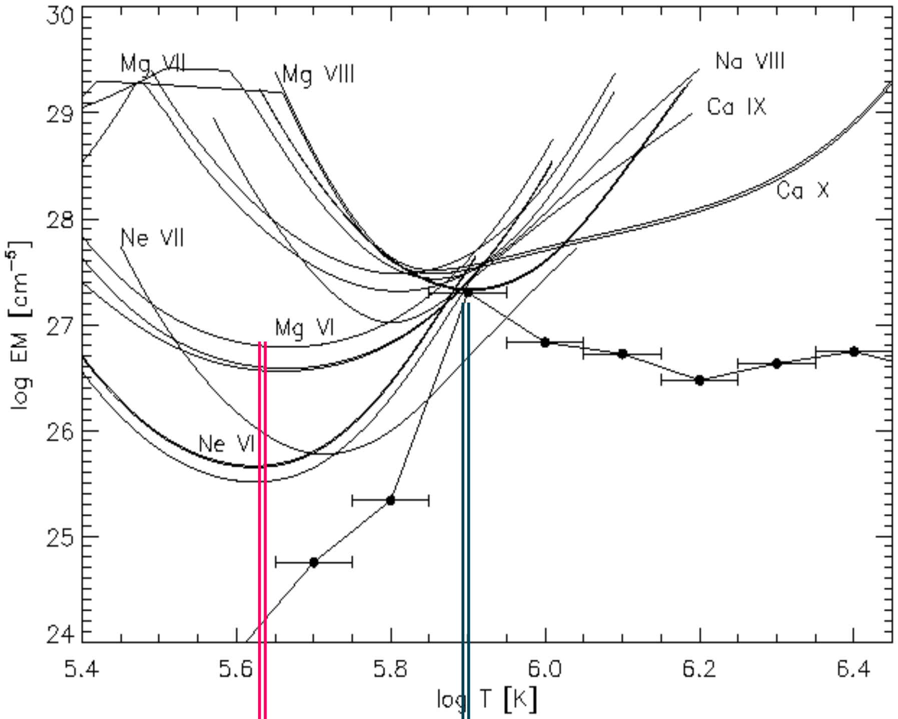


Te of maximum emissivity in ionization equilibrium

Actual Te

Del Zanna et al. (2003)

G. Del Zanna - Solarnet school - Jan 2021

# FIP BIAS in AR loops (Skylab)

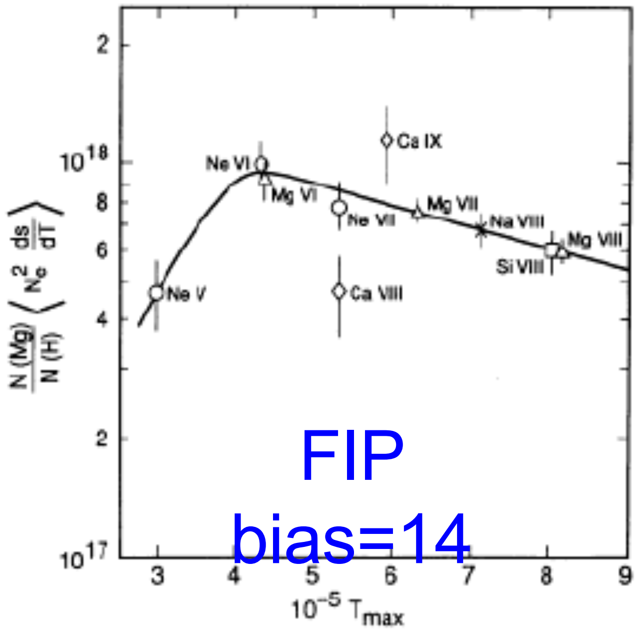


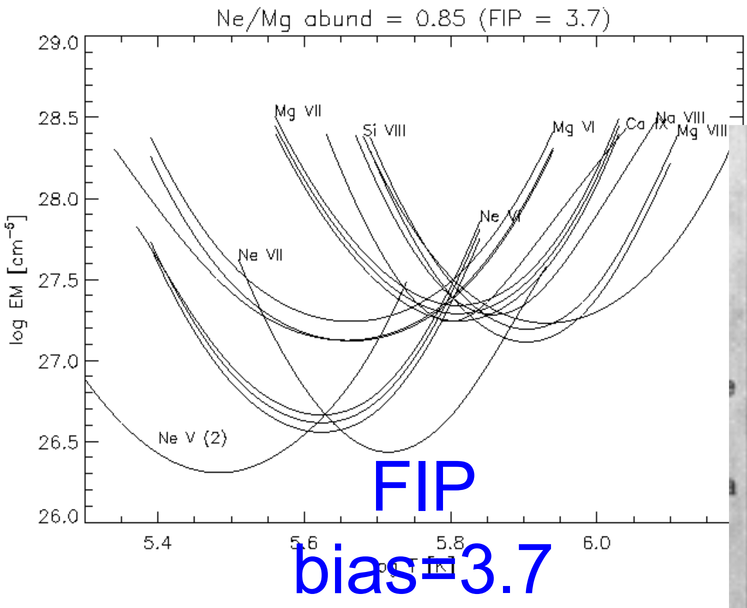


Mg VI,
Ne VI

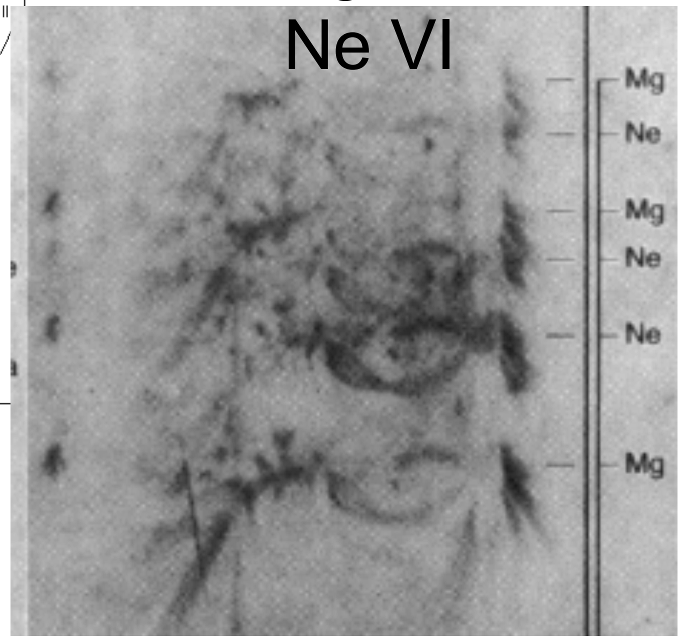


The EM Loci curves are consistent with an FIP

bias present but 4 times lower !
(Del Zanna 2003)

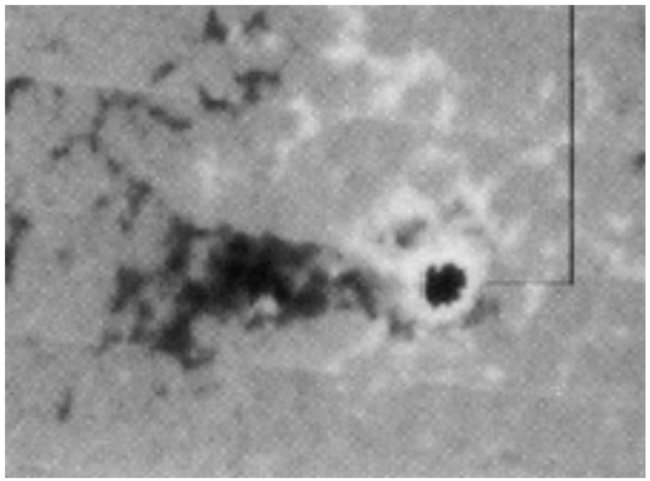

Sheely (1996)

# Continuum

Free-free (f-f) produce a continuum of photons with energies E=0-1/2 $mv^2$)

Free-bound (f-b) produces photons at energies 1/2 $mv^2 - E_f$

with $E_f$ the final energy of the atomic state. F-b depends on the chemical abundances.

Continuum is present at all wavelengths

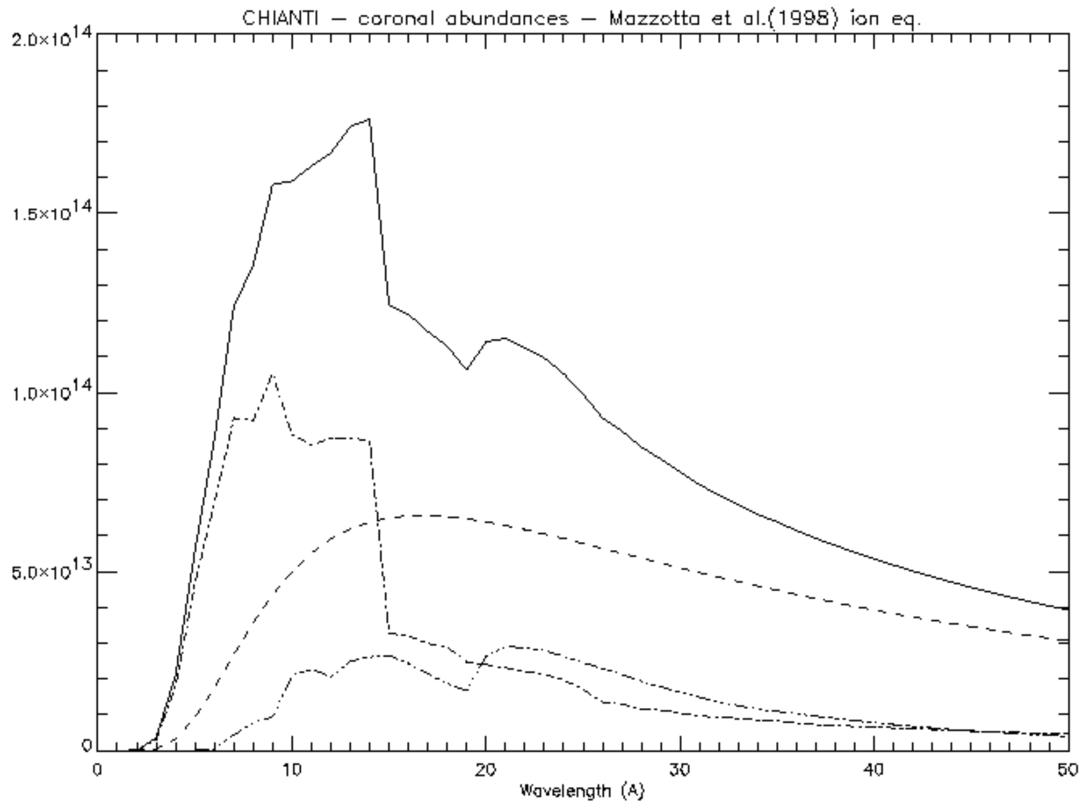


Note that the expressions found in the literature for the f-f and f-b normally assume Maxwellian electron distributions.

# END

Thank you